Design of a sliding mode controller with model-based switching functions applied to robotic systems

by

Charles FALLAHA

MANUSCRIPT-BASED THESIS PRESENTED TO ÉCOLE DE TECHNOLOGIE SUPÉRIEURE
IN PARTIAL FULFILLMENT FOR THE DEGREE OF
DOCTOR OF PHILOSOPHY
Ph.D.

MONTREAL, MAY 7, 2021

ÉCOLE DE TECHNOLOGIE SUPÉRIEURE
UNIVERSITÉ DU QUÉBEC

BOARD OF EXAMINERS

THIS THESIS HAS BEEN EVALUATED

BY THE FOLLOWING BOARD OF EXAMINERS

M. Maarouf Saad, Thesis supervisor
Departement of electrical engineering, École de technologie supérieure

M. Guy Gauthier, President of the board of examiners
Department of systems engineering, École de technologie supérieure

M. Vahé Nerguizian, Member of the jury
Department of electrical engineering, École de technologie supérieure

M. Wael Suleiman, External examiner
Department of computer and electrical engineering, Université de Sherbrooke

M. Jawhar Ghommam,
Department of computer and electrical engineering, Sultan Quaboos University

THIS THESIS WAS PRESENTED AND DEFENDED

IN THE PRESENCE OF A BOARD OF EXAMINERS AND THE PUBLIC

ON APRIL 28, 2021

AT ÉCOLE DE TECHNOLOGIE SUPÉRIEURE

FOREWORD

Control development of complex dynamic systems such as multi-joint robot arms is a considerable challenge. Conventional linear control strategies present performance limitations for high speed and acceleration displacements. Therefore it becomes mandatory to transition to robust nonlinear control techniques in order to ensure satisfactory performance. This thesis explores a particular type of nonlinear control applied to robotic systems, namely sliding mode control. This control technique features inherent robust properties and is applicable to many physical systems, including robotic systems.

The main purpose of this thesis is to propose and formalize a novel design of nonlinear sliding functions based on the dynamic model of robotic systems that will allow the asymptotic convergence of the system towards the reference trajectory when the sliding mode is reached. The design of such functions allows for an important simplification of the torques input control law, while preserving the inherent robustness properties and tracking performance of conventional sliding mode control. This simplification ensures a complete decoupling of the chattering effect of the torque inputs, which then leads as well to overall chattering reduction on all joint axes. From a practical standpoint, the simplification of the torques control law prevents against premature failures of actuating components in the system, and avoids unaccounted for fast dynamics behaviour in the closed-loop system.

ACKNOWLEDGEMENTS

My thanks go first to Professor Maarouf Saad, my PhD supervisor, who has supported my work and provided me with invaluable guidance and recommendations to improve the quality of my research.

I would also like to thank the members of the jury who have accepted to read and evaluate my work, and Professor Jawhar Ghommam for his recommendations on some technical aspects of my research.

Special thanks go to Dr. Yassine Kali, who has provided a great amount of help and collaboration with the experimental validation of my work and with my journal papers.

My extended gratitude goes to Professor Lama Seoud and Mr. Joe Sfeir for their precious help and support during the last stretch of my work.

Finally, I want to thank my parents and my wife for their unconditional support and encouragements, and without whom I would have never been able to reach this achievement.

Conception d'une commande par modes glissants à surfaces non-linéaires appliquée à des systèmes robotisés

Charles FALLAHA

RÉSUMÉ

Cette thèse présente un travail sur l'approfondissement de l'étude de la commande non-linéaire par modes glissants sur les systèmes électromécaniques dont le modèle dynamique peut être formalisé selon la structure mathématique standard des bras robotisés manipulateurs. Plus particulièrement, ce travail de recherche porte sur une conception novatrice de surfaces de glissements non-linéaires basées sur le modèle dynamique des systèmes robotisés. La conception des surfaces non-linéaires basées sur le modèle consiste à simplifier les termes non-linéaires de la commande en couples incluant les matrices d'inertie, d'accélération et de gravité en les utilisant dans les surfaces de glissement même. Ainsi, par rapport à la conception typique des surfaces de glissement linéaires, la loi de commande en couples résultante est considérablement simplifiée, et devient linéaire en fonction des vecteurs d'erreur de position et de vitesse. Cette simplification entraîne ainsi une réduction des contraintes dynamiques transitoires et des niveaux de bruits numériques et analogiques provenant des signaux des capteurs faisant partie du système de contrôle en boucle fermée du système robotisé. De plus, la compensation de la matrice d'inertie dans les surfaces de glissement assure un découplage total des niveaux de commutations haute-fréquence du terme discontinu sur la loi des couples. Ce découplage induit à son tour une réduction générale des commutations haute-fréquence sur tous les axes. Par ailleurs, la conception des surfaces de glissement basées sur le modèle engendre également une étude complémentaire sur la matrice de gravité du système robotisé. En effet, cette étude complémentaire a permis de caractériser certaines propriétés algébriques novatrices liées à la matrice de gravité qui servent à établir des critères de compensation de cette dernière dans la conception même des surfaces de glissement. Il est également possible d'utiliser les caractéristiques de la matrice de gravité afin de valider mathématiquement cette dernière, ce qui fournit donc un moyen de complémenter la validation mathématique traditionnelle des matrices d'inertie et d'accélérations du modèle du robot. Afin de valider expérimentalement l'approche de conception des surfaces de glissement basées sur le modèle du robot, un banc de test d'un prototype d'un bras exosquelette à 7 degrés de liberté a été utilisé dans un premier temps. Comparée à l'approche conventionnelle, l'approche proposée démontre une réduction importante des contraintes dynamiques ainsi que des commutations haute-fréquence sur les couples d'entrées, tout en assurant un très bon suivi de trajectoire. Afin de démontrer par la suite la généralisation de l'approche sur d'autres systèmes robotisés, une application expérimentale a par ailleurs été validée sur un drone commercial de type quadri-rotor. Finalement, la revue de littérature situe notre travail de recherche par rapport aux publications scientifiques récentes, et prouve l'originalité de l'approche proposée, puisqu'au meilleur de nos connaissances, aucune méthode semblable utilisant la conception des surfaces de glissements basées sur le modèle du robot n'a été développée à ce jour.

Mots-clés: Modes glissants, Exosquelette, Robot, Fonctions de glissement basées sur le modèle, Commutations haute-fréquence, Contrôle Robuste, Quadri-rotor

Design of a sliding mode controller with model-based switching functions applied to robotic systems

Charles FALLAHA

ABSTRACT

This thesis presents an in-depth study sliding mode control applied on electromechanical systems which dynamic model can be formalized according to the standard mathematical structure of robotic manipulator arms. More specifically, this research work focuses on an innovative design of nonlinear sliding surfaces based on the dynamic model of robotic systems. The design of the nonlinear model-based surfaces consists in simplifying the nonlinear terms of the torque control input including the inertia, accelerations and gravity matrices by using them in the sliding surfaces themselves. Thus, compared to the typical design of linear sliding surfaces, the resulting torque control law is considerably simplified, and becomes linear as a function of the position and velocity error vectors. This simplification thus leads to a reduction in transient dynamic constraints and in digital and analog noise levels originating from the signals of the sensors that are part of the closed-loop control system. In addition, the compensation of the inertia matrix in the sliding surfaces ensures a total decoupling of the high-frequency chattering phenomenon originating from the discontinuous term of the torques control law. This decoupling in turn induces a general reduction in the chattering levels on all axes. In addition, the design of model-based sliding surfaces also generates a complementary study on the gravity matrix of the robotic system. Indeed, this complementary study makes it possible to characterize novel algebraic properties linked to the gravity matrix which serve to establish a compensation criterion for the latter in the very design of sliding surfaces. It is also possible to use the characteristics of the gravity matrix to mathematically validate the latter, thus providing a way to complement the traditional mathematical validation of the inertia and acceleration matrices of the robot model. In order to experimentally validate the model-based sliding surface design approach, a test bench including a prototype of an exoskeleton arm with 7 degrees of freedom is first used. Compared to the conventional approach, the proposed approach demonstrates a significant reduction in dynamic constraints as well as in the chattering levels on the torque inputs of the exoskeleton, while ensuring very good trajectory tracking performance. In order to subsequently demonstrate the generalization of the approach on other robotic systems, an experimental application has also been validated on a commercial quad copter drone. Lastly, the literature review positions our research work with relation to recent scientific publications, and proves the originality of the proposed approach, since to the best of our knowledge, no similar method using the design of model-based sliding surfaces on robotic systems has been developed to date.

Keywords: Sliding mode, Exoskeleton, Robot, Model-Based Switching Functions, Chattering, Robust Control, Quadcopter

TABLE OF CONTENTS

LIST OF TABLES

Page

LIST OF FIGURES

Page

LIST OF ABBREVIATIONS

ETS	École de Technologie Supérieure
TSMC	Terminal Sliding Mode Control
SISO	Single Input Single Output
MIMO	Multi Input Multi Output
IEEE	Institute of Electrical and Electronics Engineers
ASME	American Society of Mechanical Engineers
ETS-MARSE	Motion Assistive Robotic-Exoskeleton for Superior Extremity
HOSM	Higher Order Sliding Mode
STSMC	Super-Twisting Sliding Mode Control
DOF	Degree of Freedom
EIG	Eigenvalue
UAV	Unmanned Aerial Vehicule
CPU	Central Processing Unit
SMC	Sliding Mode Control
IMU	Inertial Measurement Unit
RMS	Root Mean Square
VR	Virtual Reality
AR	Augmented Reality
EMG	Electromyography

MPC	Model Predictive Control
STA	Super Twisting Algorithm
ERL	Exponential Reaching Law
DH	Denavit-Hartenberg
FPGA	Field Programmable Gate Array
HMI	Human Machine Interface
NI	National Instruments
PI	Proportional and Integral
DC	Direct Current

LIST OF SYMBOLS AND UNITS OF MEASUREMENTS

Sat	Saturation function
Sign	Signum function
K	Gain in the discontinuous term part of the sliding mode control law
S	Sliding function
u_{eq}	Equivalent term part of the sliding mode control law
u_{disc}	Discontinuous term part of the sliding mode control law
τ	Torques input vector applied on the robot arm (Newtons N)
θ	Joints angular/linear displacement vector of the robot arm (radians rad/ meter m)
θ_R	Reference joints angular/linear displacement vector of the robot arm (radians rad/ meter m)
$M(\theta)$	Inertia Matrix term of the robot arm
$V_m(\theta, \dot{\theta})$	Accelerations Matrix term of the robot arm
$G(\theta)$	Gravity vector term of the robot arm
σ	Anti-symmetric matrix resulting from the relationship binding the inertia and accelerations matrices
J_G	Jacobean matrix resulting from the gravity vector term of the robot arm.
Ψ_G	Symmetric matrix resulting from the gravity vector term of the robot arm
g	Gravity constant (Newtons per Kilogram N/Kg)

INTRODUCTION

The present decade has seen a considerable diversification of robotic systems in several fields of application. Traditionally linked to the industrial field, robotics has recently shown significant progress in the commercial and social fields, mainly due to the accessibility of available hardware and software technologies. This robotic era therefore implies the arrival on the market of new complex and atypical topologies of mobile and fixed robots. The study of these new robotic systems requires engineers to develop new simulation models and to optimize and simplify control laws. On the one hand, the validation of these new models becomes a central element in the robotic design phases. On the other hand, the development of new powerful and robust control algorithms is also becoming necessary to meet the growing needs of robotic applications.

It is in this context that this thesis focuses on the study of nonlinear sliding mode control applied to robotic electromechanical systems. Among the nonlinear control approaches, sliding mode control belongs to the family of variable structure controllers that were formalized in the early 1950s in the Soviet Union by scientists such as Emelyanov (1967), Filippov (1988) and Tsypkin (1984). The sliding mode control was subsequently introduced in the Western world by Utkin (1981), and then experienced a considerable expansion within the community of automation engineers. Several research and synthesis works were subsequently carried out, in particular by Slotine et al. (1987), Spurgeon (2008) and DeCarlo et al. (1988). The sliding mode control finds its application in several fields of engineering, including robotic systems, namely by Hashimoto, Maruyama and Harashima (1987) and Utkin et al. (1999). The sliding mode control applies to both single and multi-variable systems. The implementation of sliding mode control on these systems has proven to be considerably simpler than other nonlinear control techniques, allowing rapid implementation on complex systems. On the other hand, the variable structure of this command provides an intrinsic robustness property which, in practice, applies to uncertain systems without having to add adaptive correction loops (Slotine and Li, 1991). However, this property of robustness comes in particular from a term of discontinuous nature which appears in

the control law, and which has the disadvantage of creating uncontrolled high frequency switching on the control signal, known as chattering. Several strategies for reducing or eliminating the chattering phenomenon have been proposed in the scientific literature (Levant, 1993; Bartolini et al., 2000; Hamerlain et al., 2007; Parra-Vega and Hirzinger, 2001). Some of these strategies will be briefly presented in the literature review section. Therefore, given the amount of work and solutions proposed to address the common problem of chattering on sliding mode control signals, this thesis does not focus on this point, but rather focuses on the study of the design of nonlinear sliding surfaces based on the robot model, with a view to simplifying and reducing the constraints on the resulting control law. As an experimental prototype, an exoskeleton robot with 7 degrees of freedom will be chosen to test and validate the design. Exoskeleton robots are currently the subject of several studies and research for rehabilitation and physiotherapy applications (Tsagarakis and Caldwell, 2003). These studies involve, among other things, haptic control as shown by Frisoli et al. (2009) and Gupta and O'Malley (2006), control using measured biological signals (Lucas et al., 2004), or control by active movement of subjects (Kawasaki et al., 2007).

This research thesis is therefore structured as follows: A literature review will first be presented in order to position our research with respect to recent developments on sliding mode control. Then, Chapter 2 presents a summary of the model-based sliding functions approach by taking up the key notions of the journal articles that we published for this purpose, and which are covered in Chapters 3, 4 and 5. In addition, the contributions made by this research will be highlighted. Chapter 3 presents the article that was published in the journal *International Journal of Measurement Identification and Control* and which contains the development of model-based sliding functions for the setpoint convergence problem. In order to demonstrate that the proposed approach can be applied to electromechanical systems which are not only exclusive to manipulator robots, Chapter 4 presents the article which was published in the journal *International Journal of Automation and Control* and which demonstrates the application of the

proposed approach on a four-rotor type flying drone. Finally, Chapter 5 presents a generalization of the approach proposed for trajectory monitoring, the content of which has been published in the journal *IEEE Transactions on Mechatronics*. Finally, a synthesis as well as several recommendations will be presented by way of conclusion of this thesis report.

CHAPTER 1

LITERATURE REVIEW

In this section, a literature review is proposed in order to properly position the research work presented in this document. First, a general review of some well-known nonlinear control methods is presented. This review is then followed by a more detailed review of the sliding mode control, which focuses on the work undertaken to date on the reduction of the high-frequency chattering problem, as well as on the study of nonlinear sliding functions. A focus will then be made on robotic applications, and more particularly on manipulator robots, which will put into context our research work.

1.1 General overview

The exponential evolution of numerical computation tools currently allows an efficient implementation of complex real-time control algorithms. Among these algorithms, nonlinear digital controllers are increasingly used for the regulation of complex systems. Several works on nonlinear systems represent exhaustive references, especially by Khalil (2002), Isidori (1995), Slotine and Li (1991), and Krstic et al. (1995). Applications involving these nonlinear regulators are increasingly used both in industry and in research. These controllers can also include intelligent algorithms that rely on the use of artificial neural networks (Narendra, 1996) or on the use of fuzzy logic principles (Thomas and Armstrong-Helouvry, 1995).

Among classical nonlinear control techniques, feedback linearization control (Slotine and Li, 1991) is an approach well known in the scientific literature. This approach consists of linearizing the system by compensation and applying to the new linearized system a classic linear feedback control. In robotic applications, this approach takes a special form, known as the partitioned law (or computed torque approach) (Khosla and Kanade, 1989). In real applications, the feedback linearization approach is implemented with some parameter adaptation methods (Akhrif and Blankenship, 1988) in order to make it robust to modeling disturbances and uncertainties. This

method can even be combined with smart approaches to ensure its robustness (Park and Cho, 2007).

The backstepping control method is another well-known nonlinear approach. This approach is based on the progressive construction of Lyapunov functions formed from tracking errors (Yang et al., 2004; Pranayanuntana and Vanchai, 2000). This method is however applicable for systems with triangularizable structure, and the calculations of the control law become more complex with the order increase of the studied system. In scientific literature, this approach is often implemented with adaptive methods (Shieh and Hsu, 2008), as well as with intelligent observers and state estimators (Lin and Hsu, 2005).

1.2 Literature review on sliding mode control

Among the methods mentioned above, sliding mode control therefore remains an interesting nonlinear control approach to explore, given its simplicity of implementation and its natural robustness with respect to disturbances and modeling uncertainties. Similar to previous methods, sliding mode control can also be paired with smart approaches to improve expected performance, as presented in Liang et al. (2008), Fnaiech et al. (2009) and Orlowska-Kowalska et al. (2009). The following sub-section consists in exploring the literature review around sliding mode control, and positioning our research work.

1.2.1 Control of chattering levels

The main problem brought by sliding mode control is the high-frequency chattering phenomenon appearing on the control signals, and is characteristic of this control approach. Chattering is caused by a discontinuous term included in the sliding mode control law. In a practical (numerical) implementation, the commutations created by the discontinuous term do not occur instantaneously, which therefore leads to chattering. The other element which also favors chattering is that in practice, the sliding surface is never rigorously reached. Chattering is generally undesirable because it can excite undesirable dynamics on the system. However, in

certain applications such as in power electronics, Chattering does not necessarily have an adverse effect, as suggested by Slotine and Li (1991).

In the scientific literature involving sliding mode control, the main research focus is aimed on the reduction and/or elimination of the chattering phenomenon on the control inputs. Many methods have been developed in that sense to contain or eliminate chattering. Among the best known techniques, a method of softening the discontinuous term in the control law is mentioned by Slotine and Li (1991) and consists in substituting the discontinuous term of the control law $ksign(S)$ with the term $k \cdot sat(S/\Phi)$. The sat function is defined as follows :

$$sat\,(S/\Phi) = \begin{cases} 1 for S/\Phi > 1 \\ \frac{S}{\Phi} for -1 \leq S/\Phi \leq 1 \\ -1 elsewhere \end{cases} \tag{1.1}$$

With this approach, chattering on the control input is eliminated. The convergence of the error however remains in a neighborhood of the sliding surface, the amplitude of which is directly dependent on the chosen value of Φ. Tracking performance is therefore affected. In general, other functions which approximate the sign function have also been investigated in the literature. for example, Camacho et al. (1999) proposed the use of a sigmoid function instead of the sign function.

Another approach introduced by Levant (1993), and subsequently applied by numerous researchers (Floquet et al., 2003), consists in increasing the degree of the sliding functions from 1 to a certain degree r >1, by using the virtual time derivative of order r-1 of the control law. Choosing then this time derivative to be discontinuous, the actual control law is constructed by a series of integrals, and is therefore of continuous nature. It is also proven that this approach guaranties $S = \dot{S} = \ \ldots = S^{(r-1)}$. This approach has been applied by Hamerlain et al. (2007) on a robot trajectory tracking problem. Bartolini et al. (2000) and Parra-Vega and Hirzinger (2001) have focused on the second order in order to eliminate chattering on the control input. Higher order sliding mode control requires however the construction of S, $\dot{S}$, $\ldots$, $S^{(r-1)}$, which then implies the need for observers. A variant of this method applied only to sliding functions of

order 2 was introduced by Moreno and Osorio (2008), and known as 'Super-Twisting'. This method has been shown to eliminate chattering without having to use $\dot{S}$ in the expression of the control law.

Other approaches proposed in literature consist of reducing chattering by modifying the conventional reaching law. Gao and Hung (1993) have designed nonlinear reaching laws which allow a dynamic adaptation of a gain of the control law as a function of the variation of the sliding function. Thus, the further the state vector is from the sliding surface, the greater this gain is and tends to bring the vector back to the surface, and vice versa. Therefore, it is theoretically possible to reduce high frequency switching in steady state, without affecting the convergence time or even the system tracking error. Gao and Hung therefore proposed in particular two possible reaching laws to reduce chattering.

The first reaching law contains a term proportional to the sliding function which allows the system to reach the sliding surface more quickly when it is far from it. In addition, the proportional term reduces the effort required by the discontinuous part $sign(S)$ and therefore allows the reduction of the chattering levels on the control input. This reaching law is given by :

$$\dot{S} = -k \cdot sign\,(S) - Q \cdot S \tag{1.2}$$

In the second proposed reaching law there is a fractional power of the sliding function which multiplies the sign of this one, as follows:

$$\dot{S} = -k \cdot |S|^{\alpha}\, sign\,(S) \tag{1.3}$$

where α is real and strictly included between 0 and 1. It is also shown that the reaching law (1.3) generates a finite reaching time of the sliding surface.

Otherwise, an approach which proposes an exponentially varying reaching law has recently been studied in (Fallaha et al., 2011). This reaching law is given as follows :

$$\dot{S} = -\frac{k}{N\,(S)} sign\,(S)\,; N\,(S) = \delta_0 + (1-\delta_0)\,exp(-\alpha\,|S|^p) \tag{1.4}$$

with $\alpha \geq 0$, δ_0 is a strictly positive offset less than 1 and p a strictly positive integer. The choice of parameters k, δ_0 and α depends on several elements, namely the dynamics of the system, the extent of the uncertainties and the level of disturbances exerted on the system. When the sliding function S reaches 0, then $N(S)$ reaches 1. Therefore gain $\frac{k}{N(S)}$ reaches k but does not go to 0, as opposed to reaching law (1.3). It is therefore expected that with this approach a more robust behavior of the system will be observed with the reaching law (1.4). If on the other hand S increases, then $N(S)$ reaches δ_0 and $\frac{k}{N(S)}$ reaches $\frac{k}{\delta_0}$, which is a bounded value. Hence, $k \leq \frac{k}{N(S)} \leq \frac{k}{\delta_0}$ and $-\frac{k}{\delta_0}\,|S| \leq S\dot{S} \leq -k\,|S| \leq 0$, and therefore the system remains stable in the Lyapunov sense.

1.2.2 Nonlinear sliding functions

In contrast to studies of reduction or elimination of chattering in sliding mode control, much less work is present in the literature regarding the study of nonlinear sliding functions. Among the works on nonlinear functions, Choi et al. (1994) have explored sliding functions with variation of the parameters over time in order to improve the robustness and the transient performance of the control. More recently, a focus on Terminal Sliding Mode Control (TSMC) (Yu et al., 2005; Cao et al., 2015), in which nonlinear sliding functions are designed to ensure a rapid convergence of the tracking error towards 0 in a finite time. The TSMC has been introduced by Venkataraman and Gulati (1991). The initial version of this approach is based upon the design of nonlinear sliding functions which have the following form for second-order systems:

$$\dot{S} = \lambda \cdot x^p + \dot{x},\ p > 0 \tag{1.5}$$

The choice of the value of p must verify certain particular conditions and has an impact on the convergence performance of the system when on the sliding surface. Several variants of this method have subsequently evolved, such as the fast terminal sliding mode (Yu and Zhihong, 2002).In robotics, the terminal sliding mode control is interesting because it provides a greater precision of convergence to the movement of the robot (Tang, 1998; Wang et al., 2009; Jin et al., 2009).

However, all of the above mentioned methods involving nonlinear sliding functions design do not include any model-based compensation term in their expression.

In summary, this literature review positions our research work with regards to the existing research work in scientific journals. Therefore, the model-based sliding functions design approach seems to represent a genuine contribution to the sliding mode control field, as it has not been explored before. To be noted that the model-based sliding functions design approach can be easily combined with the existing chattering reduction techniques for optimal performance. It would even seem conceivable to combine the design of model-based sliding functions with the terminal sliding mode control to ensure an exact convergence of the error system towards 0, and in a finite time. These latter points, while interesting to explore, are not part of the present research work, which will focus only on the design of sliding functions based on the dynamic model of the robot.

CHAPTER 2

MODEL-BASED SLIDING FUNCTIONS DESIGN REVIEW AND THEORETICAL CONTRIBUTIONS

This chapter puts into context our research subject by first stating the problem encountered with conventional sliding mode controllers applied to robotic systems and using typically linear sliding surfaces. The conventional use of linear sliding surfaces simplifies the dynamics of the closed loop system, but at the cost of a complex, nonlinear, and considerably coupled resulting control law. From a practical point of view, the implementation of such a control law could generate undesirable effects, such as premature failures of actuators, secondary effects of couplings, or even the appearance of high-frequency dynamics on the closed-loop system. The main contribution of the research subject consists in the design of nonlinear sliding surfaces based on the dynamic model of the robot, and which also ensure an asymptotic convergence of the system with a controlled dynamics. This leads to a considerable simplification of the torque control law, with the possibility of a complete decoupling of the chattering phenomenon on each of the robot axes. The secondary contribution that results from the design of the model-based switching functions is the characterization of the gravity term of the robot model. This characterization leads to the formulation of a condition on the proportional matrix of the controller in order to ensure an asymptotic convergence of the system towards the desired trajectory. This characterization of the term of gravity also makes it possible to push further the overall validation of the dynamic model of the robot.

2.1 Conventional Sliding Mode Control Review

Sliding mode control is a nonlinear control approach that is relatively simple to implement and is applicable to several kinds of single and multivariate system structures as presented by Utkin et al. (1999).This approach has inherent robustness properties which are attributed to the structure of the control law which contains a discontinuous term. Moreover, this discontinuous term is responsible for the high-frequency chattering phenomenon that is characteristic of the conventional approach. Before stating some of the issues related to conventional sliding

mode control, it would be appropriate at this point to briefly introduce the basic concepts of conventional sliding mode control as well as its application on robot arms.

The sliding mode control forces the states of the closed-loop controlled system to stay or "slide" on a surface or hyper-plane defined in state space. In the traditional case, the hyper-plane S = 0 is characterized by a function S which represents a linear relationship between state errors and their successive derivatives:

$$S = \sum_{i=0}^{n-1} C_i * e^{(i)} \tag{2.1}$$

n represents the order of the controlled system. Matrix constants C_i are chosen in such a way as to obtain an asymptotic convergence of state errors towards 0, while following specific criteria of dynamic performance. In order to ensure the condition $S = 0$, the control law must therefore be designed accordingly. To describe this process, consider the example of the following second-order nonlinear single input/single output (SISO) system:

$$\ddot{x} = f(x, \dot{x}) + b(x, \dot{x}) \cdot u \tag{2.2}$$

Where f and b are both nonlinear functions in terms of x and $\dot{x}$, and b is invertible. Let x_d be the reference trajectory and $e = x - x_d$ the tracking error which converges to zero. The first step consists of choosing the switching function S as per (2.1) for $n = 2$, namely:

$$S = \lambda e + \dot{e}, \lambda > 0 \tag{2.3}$$

The second step consists of ensuring that the sliding surface $S = 0$ is reached through the proper design of the control law $u(t)$. In order to achieve this, the time derivative of S is typically chosen to meet the following relationship, often referred to as reaching law:

$$\dot{S} = -k \cdot sign(S), k > 0 \tag{2.4}$$

Reaching law (2.4) implies that the condition $S \cdot \dot{S} < 0$ at any time t, therefore guaranteeing that S will converge to 0 over time.

Forming the time derivative of S by using (2.3) and considering (2.2), then (2.4) can be written as:

$$\lambda \dot{e} + (f(x, \dot{x}) + b(x, \dot{x}) \cdot u - \ddot{x}_d) = -k \cdot sign(S) \tag{2.5}$$

Solving for u in (2.5) gives the expression of following control law:

$$u(t) = \underbrace{b^{-1}(\ddot{x}_d - \lambda \dot{e} - f(x, \dot{x}))}_{u_{eq}} - \underbrace{b^{-1} k(x)\, sign(S)}_{u_{disc}} \tag{2.6}$$

The control law (2.6) is formed of two terms of different nature. u_{eq} is the equivalent control of continuous nature, and includes the system's dynamic model terms $f(x, \dot{x})$ and $b(x, \dot{x})$. This compensation keeps the closed-loop system on the sliding surface. The second term, u_{disc}, is of discontinuous nature, and allows the state error vector to reach the sliding surface. This term also makes it possible to ensure the robustness of the closed-loop system against external disturbances or potential modeling errors. This term is also responsible for the typical high frequency chattering phenomenon on control signals. Figure 2.1 illustrates the process described in the phase plane for the particular case of the second order system, where the state error vector reaches the linear surface and progresses on the latter to asymptotically reach the equilibrium point 0 (Fallaha et al., 2011).

In the case of complex MIMO systems such as multi-joint manipulator robots, the expression of u_{eq} and u_{disc} becomes considerably complex and strongly nonlinear. This complexity can add constraints on the torque inputs control law in transient and steady-state regimes. The general dynamic equation of multi-joint manipulator robots without friction and without external constraints is well established in the literature (Craig, 2005) and can be expressed as a second order nonlinear differential equation in joint vector space, as follows:

$$\tau = M(\theta)\, \ddot{\theta} + V_m\left(\theta, \dot{\theta}\right) \dot{\theta} + G(\theta) \tag{2.7}$$

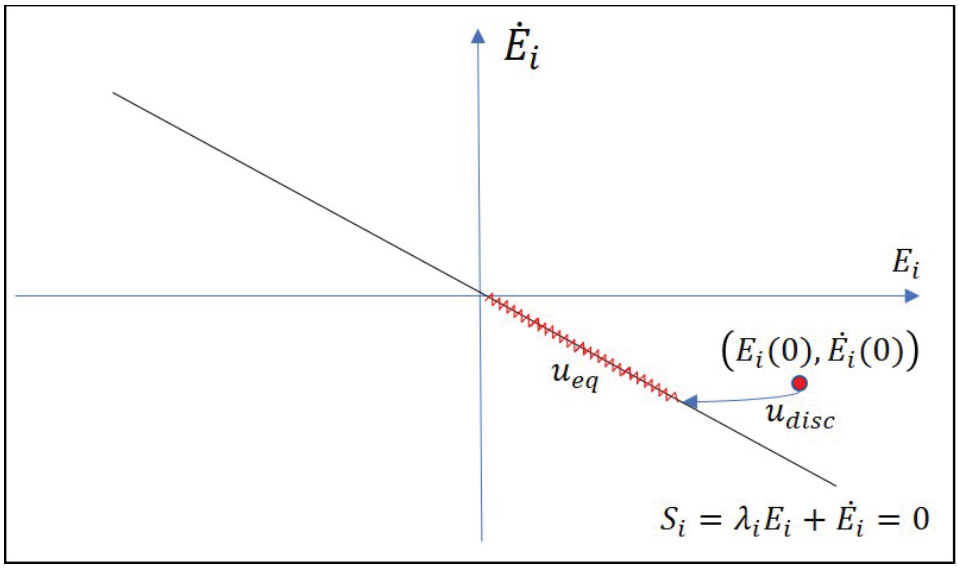

Figure 2.1 Convergence in the phase plane with linear sliding surface

τ is the torque inputs vector, θ is the joint angles and displacements vector, $M(\theta)$ is the inertia matrix and is symmetrical and positive definite, $V_m(\theta, \dot{\theta})$ is the centrifugal and Coriolis accelerations matrix, $G(\theta)$ is the gravity vector term.

By applying the sliding mode control method on second order MIMO systems, a first order linear vector sliding function is then chosen based on the tracking error term and its time derivative as follows:

$$S = \Lambda E + \dot{E}, \Lambda = diag(\lambda_i), \ \lambda_i > 0 \tag{2.8}$$

$E = \theta - \theta_R$ is the tracking error vector between the measured angles and displacements vector θ and the reference angles and displacements vector θ_R. Following the design procedure associated with sliding mode control and similarly to the SISO example above, the input torque control law is then designed to force the vector E to reach the surface $S = 0$. As per (2.8), condition $S = 0$ then forms a first-order linear differential equation as a function of E whose asymptotic convergence towards 0 is ensured by an appropriate choice of values λ_i. To ensure that surface $S = 0$ is reached,the control law is designed to ensure the following reaching law put into a

matrix format:

$$\dot{S} = -K \cdot sign(S), K = diag\left(k_i\right), \quad k_i > 0 \tag{2.9}$$

Relationship (2.9) allows here again to reach the surface S = 0 in a finite time which depends on the chosen values k_i. Using relationships (2.7), (2.8) and (2.9), it follows that the torque inputs control law takes the following form (Fallaha et al., 2011):

$$\tau = \underbrace{V_m\left(\theta, \dot{\theta}\right)\dot{\theta} + G\left(\theta\right) - M\left(\theta\right) * \left(\Lambda\dot{E} - \ddot{\theta}_R\right)}_{u_{eq}} - \underbrace{M\left(\theta\right) K \cdot sign(S)}_{u_{disc}} \tag{2.10}$$

Relationship (2.10) shows a structure similar to that described in equation (2.6), including the equivalent term u_{eq} and the discontinuous term u_{disc}.

2.2 Problem Statement

The torque inputs control law (2.10) is complex and strongly nonlinear in the general case. This complexity also increases with the number of degrees of freedom of the robot. The term u_{eq} includes the matrices and vectors forming the robot model. In the case of fast trajectories tracking, this has the effect of increasing the transient constraints on the overall control law. It is even possible that the steady state is also affected if this nonlinear dependence on the joint angles and displacements leads to an amplification of the analog or digital noises inherent to the measurement methodologies adopted. The discontinuous term for its part also includes the inertia matrix which multiplies the term $sign(S)$. The inertia matrix is non-diagonal in the general case. This therefore leads to the coupling the high-frequency chattering phenomenon on the input torques, the amplitude of which also depends on the variations of the elements of the inertia matrix.

2.3 Model-Based switching functions design applied to robotic arms

The solution presented in this research which addresses the above problem statement focuses on the design of nonlinear sliding functions based on the robot model. These sliding functions

aim to absorb the problematic terms of the torques control law. In contrast to the expression of conventional linear sliding functions given by (2.8), the resulting functions $S(\theta, \theta_R)$ are based on the robot's model, and thus are in the general case nonlinear and mutually coupled. Figure 2.2 presents the concept of using model-based nonlinear sliding functions by showing an example in the phase plane in which the sliding surface is nonlinear, but nonetheless ensures asymptomatic convergence of the system towards the equilibrium point. The approach therefore

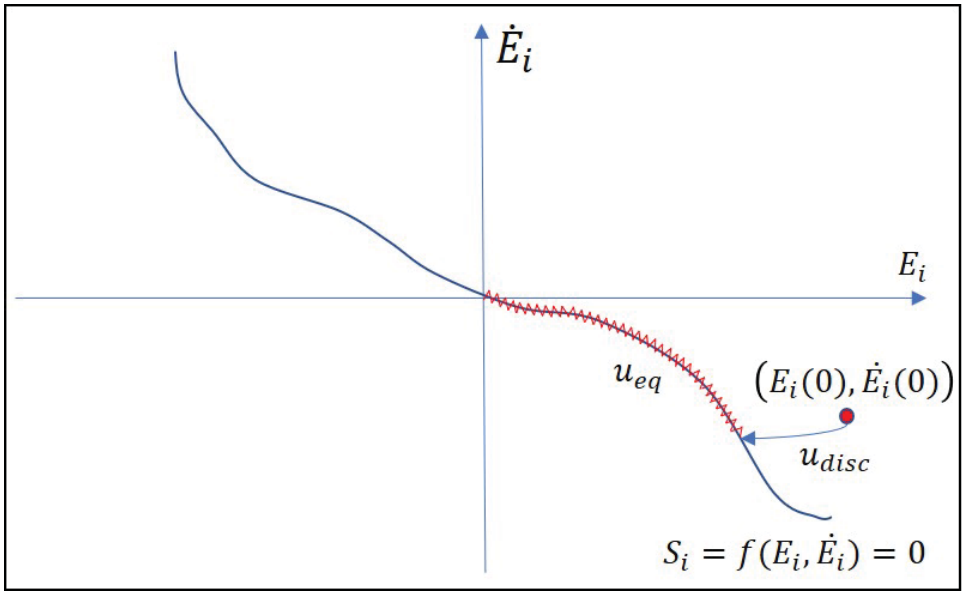

Figure 2.2 Convergence in the phase plane with the model-based nonlinear sliding surfaces

consists of moving towards a complexification and coupling of the sliding functions, with the aim of leading in return to a simplification and decoupling of the input torques control law. The difficulty in this case is obviously the design of the functions $S(\theta, \theta_R)$ which will allow the adequate simplification of the torque inputs, while ensuring the asymptotic convergence of the state error vector towards 0.

2.3.1 Model-Based switching functions design for the setpoint problem

This section summarizes the approach which is presented in more detail in the article of Chapter 3 published in the journal *International Journal of Measurement Identification and Control*

and which consists in designing sliding functions based on the robot's model for a setpoint convergence problem.

Returning to the description of the design of the sliding functions based on the model in the problem statement section, the idea is to design sliding functions which can absorb the nonlinear terms forming the compensation part of the control law . These sliding functions are first designed for the setpoint convergence problem. In our case, the setpoint equilibrium point is set to 0. The linear sliding functions typically chosen for the setpoint 0 can be deduced from (2.8) and are given by:

$$S = \Lambda\theta + \dot{\theta} \tag{2.11}$$

The first step is to see if the inertia matrix $M(\theta)$ can be removed from the discontinuous term of the law (2.10) by transferring it to the function (2.11). Intuitively, given that $M(\theta)$ is positive definite, the following nonlinear function is expected to provide asymptotic convergence of θ towards 0 when $S = 0$:

$$S = M(\theta)\dot{\theta} + \Gamma\theta \tag{2.12}$$

With Γ a constant symmetric and positive definite matrix. The proof of asymptotic stability can indeed be easily established using the following Lyapunov function:

$$V = \frac{1}{2} \cdot \theta^T \Gamma \theta \tag{2.13}$$

Indeed, the time derivative of V is then given by:

$$\dot{V} = \dot{\theta}^T \Gamma \theta \tag{2.14}$$

When the sliding surface is reached (i.e. $S = 0$), then from (2.12) it comes that:

$$M(\theta)\dot{\theta} = -\Gamma\theta \tag{2.15}$$

Using then (2.15) in (2.14) leads to the following expression of $\dot{V}$:

$$\dot{V} = -\dot{\theta}^T M(\theta)\dot{\theta} \tag{2.16}$$

Equation (2.16) shows that $\dot{V}$ is negative semi-definite. However, when the sliding surface is reached, $\dot{\theta} = 0$ implies that $\theta = 0$ as well. Therefore this establishes that the sliding surface $S = 0$ ensures the asymptotic convergence of θ towards 0.

On the other hand, using the switching function (2.12) in the reaching law (2.9) leads to the following:

$$M(\theta)\ddot{\theta} + \dot{M}(\theta)\dot{\theta} + \Gamma\dot{\theta} = -K \cdot sign(S) \tag{2.17}$$

Using (2.7) in (2.17) gives the following

$$\tau - V_m\left(\theta, \dot{\theta}\right)\dot{\theta} - G\left(\theta\right) + \dot{M}(\theta)\dot{\theta} + \Gamma\dot{\theta} = -K \cdot sign(S) \tag{2.18}$$

And then solving for the torque vector, the inputs control law becomes:

$$\tau = -V_m\left(\theta, \dot{\theta}\right)\dot{\theta} + G\left(\theta\right) - K \cdot sign\left(S\right) - \left(\Gamma + \sigma\left(\theta, \dot{\theta}\right)\right)\dot{\theta} \tag{2.19}$$

$\sigma\left(\theta, \dot{\theta}\right)$ is a skew-symmetric matrix which satisfies the following known relationship between the inertia matrix and the accelerations matrix (Spong et al., 2005) :

$$\sigma\left(\theta, \dot{\theta}\right) = \dot{M}\left(\theta\right) - 2V_m\left(\theta, \dot{\theta}\right) \tag{2.20}$$

Compared to (2.10), the torque inputs control law (2.19) shows that the inertia matrix $M\left(\theta\right)$ is not present anymore in the discontinuous term $K \cdot sign\left(\Sigma\right)$. This implies a decoupling of chattering effect between the torque input vector's elements by choosing K diagonal.

The second step consists of evaluating the potential compensation of the term $-\left(\sigma\left(\theta, \dot{\theta}\right) + V_m\left(\theta, \dot{\theta}\right)\right)\dot{\theta}$ which is present in (2.19) by transferring it as well within the sliding function S. Since the torque vector τ manifests through a first order time differentiation of S, the latter function should

therefore include the time integral of the term $-\left(\sigma\left(\theta,\dot{\theta}\right)+V_m\left(\theta,\dot{\theta}\right)\right)\dot{\theta}$ as follows :

$$S = M\left(\theta\right)\dot{\theta}+\Gamma\theta+\Delta\int\theta dt-\int\left(\sigma\left(\theta,\dot{\theta}\right)+V_m\left(\theta,\dot{\theta}\right)\right)\dot{\theta}dt \tag{2.21}$$

The term $\Delta\int\theta dt$, in which Δ is a symmetric and positive definite constant matrix, is a necessary term that ensures the asymptotic convergence towards 0.

Note that the time derivative of $S(\theta,\dot{\theta})$ can be deduced from (2.21):

$$\dot{S}(\theta,\dot{\theta}) = M(\theta)\ddot{\theta}+\dot{M}(\theta)\dot{\theta}+\Gamma\dot{\theta}+\Delta\theta-\left(\sigma(\theta,\dot{\theta})+V_m(\theta,\dot{\theta})\right)\dot{\theta} \tag{2.22}$$

Which simplifies into the following:

$$\dot{S}(\theta,\dot{\theta}) = M(\theta)\ddot{\theta}+V_m(\theta,\dot{\theta})\dot{\theta}+\Gamma\dot{\theta}+\Delta\theta \tag{2.23}$$

Using (2.7) in (2.23):

$$\dot{S}(\theta,\dot{\theta}) = \tau+\Gamma\dot{\theta}+\Delta\theta-G(\theta) \tag{2.24}$$

Using therefore (2.24) in reaching law (2.9), and solving for τ gives the following control law:

$$\tau = -\Gamma\dot{\theta}-\Delta\theta+G\left(\theta\right)-Ksign\left(S\right) \tag{2.25}$$

In order to prove the asymptotic stability of θ towards 0 when $S = 0$, consider the following Lyapunov function:

$$V = \frac{1}{2}\dot{\theta}^T M\dot{\theta}+\frac{1}{2}\theta^T\Delta\theta \tag{2.26}$$

The time derivative of V is:

$$\dot{V} = \frac{1}{2}\dot{\theta}^T\dot{M}\dot{\theta}+\dot{\theta}^T M\ddot{\theta}+\dot{\theta}^T\Delta\theta \tag{2.27}$$

(2.27) can also be written as:

$$\dot{V} = \frac{1}{2}\dot{\theta}^T\dot{M}\dot{\theta}+\dot{\theta}^T(\tau-V_m-G)+\dot{\theta}^T\Delta\theta \tag{2.28}$$

Using the expression (2.25) of τ in (2.28) gives:

$$\dot{V} = \frac{1}{2}\dot{\theta}^T(\dot{M} - 2V_m)\dot{\theta} - \dot{\theta}^T\Gamma\dot{\theta} - \dot{\theta}^T Ksign(S) \tag{2.29}$$

Since $\dot{M} - 2V_m$ is skew-symmetric, this leads to:

$$\dot{V} = -\dot{\theta}^T\Gamma\dot{\theta} - \dot{\theta}^T Ksign(S) \tag{2.30}$$

Therefore, when the sliding surface $S = 0$ is reached, then:

$$\dot{V} = -\dot{\theta}^T\Gamma\dot{\theta} \tag{2.31}$$

Therefore $\dot{V}$ is negative semi-definite, and therefore the proof of convergence of θ to 0 is very straitforward.

As a final step, in order to simplify further the control law (2.25) it is possible to compensate the gravity term $G(\theta)$ with the following sliding function:

$$S\left(\theta,\dot{\theta}\right) = M\left(\theta\right)\dot{\theta} + \Gamma\theta + \Delta\int\theta dt - \int\left(\sigma\left(\theta,\dot{\theta}\right) + V_m\left(\theta,\dot{\theta}\right)\right)\dot{\theta}dt + \int\left(G\left(\theta\right) - G\left(0\right)\right)dt \tag{2.32}$$

The choice of the sliding function (2.32) ultimately leads to the following simplified torque inputs control law:

$$\tau = \underbrace{-\Gamma\dot{\theta} - \Delta\theta + G\left(0\right)}_{u_{eq}}\underbrace{-Ksign\left(S\right)}_{u_{disc}} \tag{2.33}$$

Therefore, the law (2.33) shows a simplified relation of the torque inputs control law, which becomes linear in terms of the angles and speeds of joints. To be also noted that choosing a diagonal gain matrix K leads to a decoupled chattering effect on all joint axes. The proof of asymptotic convergence of θ towards 0 when the sliding surface $S\left(\theta,\dot{\theta}\right) = 0$ is reached uses the

following constraint on the eigenvalues of the matrix Δ:

$$Min_i\left(Eig_i\Delta\right) > Max_i\left(Eig_i\Psi_G\right) \tag{2.34}$$

Ψ_G is a matrix of symmetric nature that is constructed upon the gravity matrix $G(\theta)$ as follows:

$$\Psi_G\left(\theta\right) = -\left(\int_0^1 J_G\left(h\cdot\theta\right)dh\right), J_G = \left[\frac{\partial G_i}{\partial\theta_j}\right] \tag{2.35}$$

Moreover, it can be shown that

$$G(\theta) - G(0) = -\Psi_G\left(\theta\right)\cdot\theta \tag{2.36}$$

Indeed, relationship (2.34) implies that the difference $\Delta - \Psi_G(\theta)$ is positive definite.

Note that Appendix I provides additional explanation material to relationships (2.35) and (2.36) through a simple SISO example.

When the sliding surface $S(\theta,\dot{\theta}) = 0$ is reached, (2.33) becomes:

$$\tau = -\Gamma\dot{\theta} - \Delta\theta + G(0) \tag{2.37}$$

Consider now the following Lyapunov candidate function:

$$L(\theta,\dot{\theta}) = \frac{1}{2}\dot{\theta}^T M(\theta)\dot{\theta} + P(\theta) - P(0) \tag{2.38}$$

with P a scalar function defined as (Tomei, 1991):

$$P(\theta) = U(\theta) + \frac{1}{2}\theta^T\Delta\theta - \theta^T G(0) \tag{2.39}$$

U is the potential energy term from which is derived $G(\theta)$. Differentiating $P(\theta)$ with respect to θ and noting that $\dfrac{\partial U(\theta)}{\partial\theta} = G(\theta)$ (Spong et al., 2005), then using (2.36), the following relation

can be obtained:

$$\frac{\partial P(\theta)}{\partial \theta} = G(\theta) + \Delta\theta - G(0) = (\Delta - \Psi_G(\theta))\,\theta \tag{2.40}$$

Since $\Delta - \Psi_G(\theta)$ is positive definite, then $\frac{\partial P(\theta)}{\partial \theta} = 0$ only for $\theta = 0$, and therefore $P(\theta)$ is absolute minimum for $\theta = 0$ (Tomei, 1991), which implies $P(\theta) - P(0) > 0$ for $\theta \neq 0$. Thus, from (2.38) it can be deduced that $L(\theta, \dot{\theta})$ is a Lyapunov function. Differentiating $L(\theta, \dot{\theta})$ with respect to time gives:

$$\dot{L}(\theta, \dot{\theta}) = \dot{\theta}^T M(\theta)\ddot{\theta} + \frac{1}{2}\dot{\theta}^T \dot{M}(\theta)\dot{\theta} + \dot{\theta}^T G(\theta) + \dot{\theta}^T \Delta\theta - \dot{\theta}^T G(0) \tag{2.41}$$

The above equation can also be written as:

$$\dot{L}(\theta, \dot{\theta}) = \dot{\theta}^T \tau + \dot{\theta}^T \Delta\theta - \dot{\theta}^T G(0) \tag{2.42}$$

Using relationship (2.37), (2.42) simplifies into:

$$\dot{L}(\theta, \dot{\theta}) = -\dot{\theta}^T \Gamma \dot{\theta} \tag{2.43}$$

Therefore $\dot{L}(\theta, \dot{\theta})$ is negative semi-definite. Applying Barbalat's lemma (Slotine and Li, 1991), $\dot{\theta}$ converges to 0. Using (2.7) and (2.37) it comes that:

$$\Delta\theta + (G(\theta) - G(0)) = (\Delta - \Psi_G(\theta))\,\theta \underset{t}{\rightarrow} 0 \tag{2.44}$$

Since $\Delta - \Psi_G(\theta)$ is positive definite, this proves that θ converges to 0

2.3.2 Generalization of model-based sliding functions design for trajectory tracking applications

The design of model-based sliding functions for the trajectory tracking problem has been developed in the article presented in Chapter 5 and published in the journal *IEEE/ASME*

Transactions on Mechatronics. As per the design, the following sliding function is then chosen:

$$\Sigma = S\left(\theta, \dot{\theta}\right) - S\left(\theta_R, \dot{\theta}_R\right) \tag{2.45}$$

θ_R is the reference trajectory. It should then be noted that the sliding function (2.32) for the setpoint problem becomes a particular case of (2.45) for $\theta_R = \dot{\theta}_R = 0$.The other important point is that the generalization to trajectory tracking in this case is not trivial, given that the function $S(\theta, \dot{\theta})$ is nonlinear in the general case. Thus, it will be noted that:

$$\Sigma = S\left(\theta, \dot{\theta}\right) - S\left(\theta_R, \dot{\theta}_R\right) \neq S\left(\theta - \theta_R, \dot{\theta} - \dot{\theta}_R\right) \tag{2.46}$$

Note that the proof of asymptotic stability of $\Sigma = 0$ as developed in the paper of Chapter 5 goes through the construction of a Lyapunov-like function similar to (2.36). However, this Lyapunov-like function in this case can be negative, but with a negative bound. The usage of such Lyapunov-like function has been presented by Slotine and Li (1991) and leads to the same conclusion of global asymptotic stability.

The choice of the sliding function (2.45) for trajectory tracking leads to the following torque control law:

$$\tau = \underbrace{\tau_R - \Gamma\dot{E} - \Delta E}_{u_{eq}} \underbrace{-Ksign\left(\Sigma\right)}_{u_{disc}} \tag{2.47}$$

With $\tau_R = M\left(\theta_R\right)\ddot{\theta}_R + V_m\left(\theta_R, \dot{\theta}_R\right)\dot{\theta}_R + G\left(\theta_R\right)$, and $E = \theta - \theta_R$. To be noted that τ_R is exclusively formed of constructed terms and signals, and contains no measured or estimated terms or signals. Figure 2.3 depicts the general block diagram of the sliding mode control algorithm with model-based sliding functions: To be noted that the law (2.33) becomes a particular case of (2.47) for $\theta_R = \dot{\theta}_R = 0$. The new simplified torque inputs control law (2.47) shows linear behavior as a function of the error E and its time derivative. Another important point is the cancellation of matrix $M\left(\theta\right)$ in the discontinuous term u_{disc}. This result implies a complete decoupling of the chattering phenomenon on all joint axes, provided that matrix K is

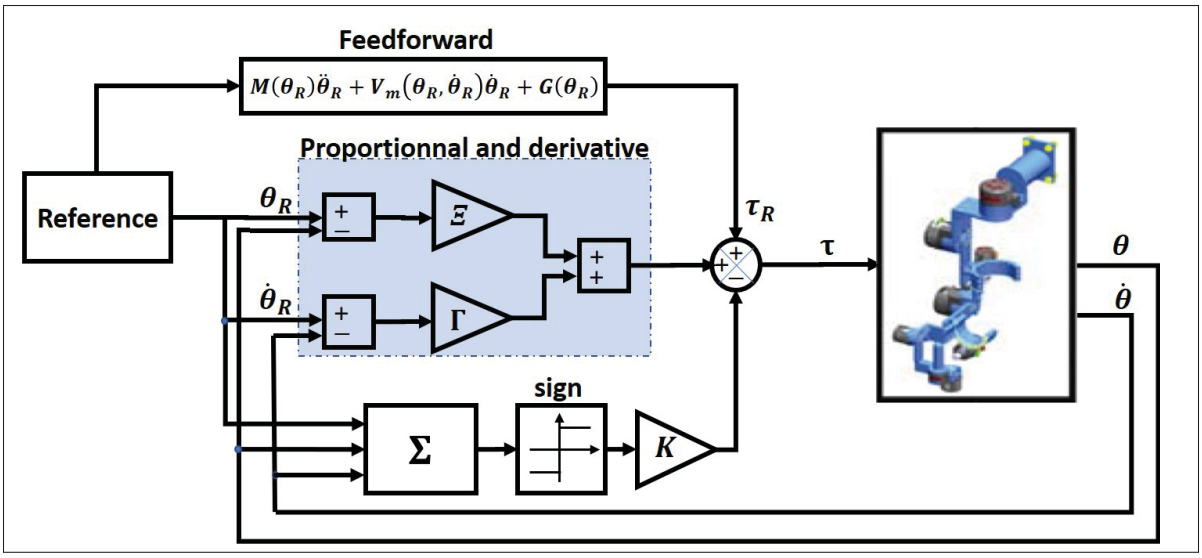

Figure 2.3 General block diagram of trajectory tracking sliding mode controller with model-based sliding functions

chosen to be diagonal. Finally, control law (2.47) can be considered as simple proportional and derivative controller with a discontinuous term providing robustness properties to the closed-loop system.

2.4 Experimental validation of the proposed approach to different robotic systems

The model-based sliding function design approach has been experimentally validated on different robotic systems. As shown in the article *IEEE/ASME Transactions on Mechatronics* in Chapter 5, the approach has been validated experimentally on a 7-DOF exoskeleton arm nicknamed ETS-MARSE, and which is presented in Figure 2.4: The experimental results recorded with the proposed approach are discussed in Chapter 5 and compared to the conventional sliding mode approach with linear surfaces. To visually illustrate the difference between these 2 approaches, Figure 2.5 below compares simulation results of asymptotic convergence in the phase plane of ETS-MARSE's axis 2 for a) the conventional approach with linear surfaces, and b) the proposed approach with model-based sliding surfaces. The part in blue represents the reaching phase, and the part in red represents the sliding phase on the surface. Note in b) the non-linearity of

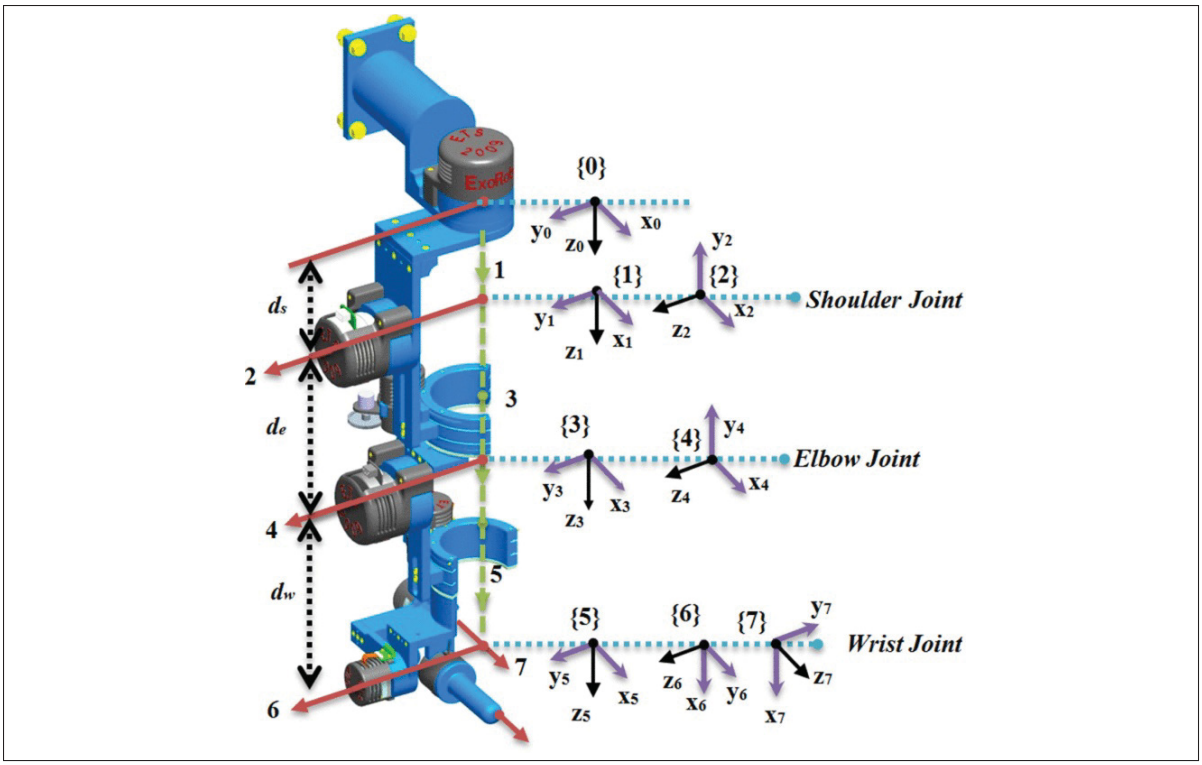

Figure 2.4 ETS-MARSE Structure and Reference Frames Assignation

the sliding surface with the proposed approach using model-based functions, in contrast to the conventional sliding surface design approach in a).

The proposed approach has also been experimentally applied to the inner control loop of a Parrot-type quad-copter drone, as presented in the article *International Journal of Automation and Control* of Chapter 5. Figure 2.6 shows the drone with the experimental setup environment. Thus, it is therefore demonstrated that the proposed model-based sliding function design approach can be applied to a large family of various robotic systems, whose dynamic model can be put into a typical form of mechanical dynamic equations of the second order.

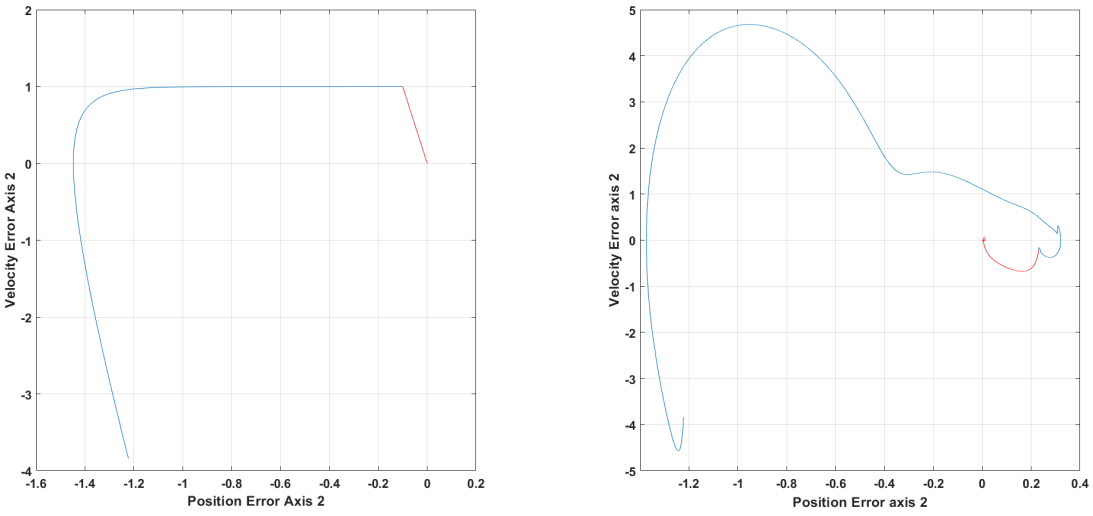

a) Convergence on a linear sliding surface b) Convergence on model-based sliding surface

Figure 2.5 Simulation results in the phase plane for ETS-MARSE's axis 2

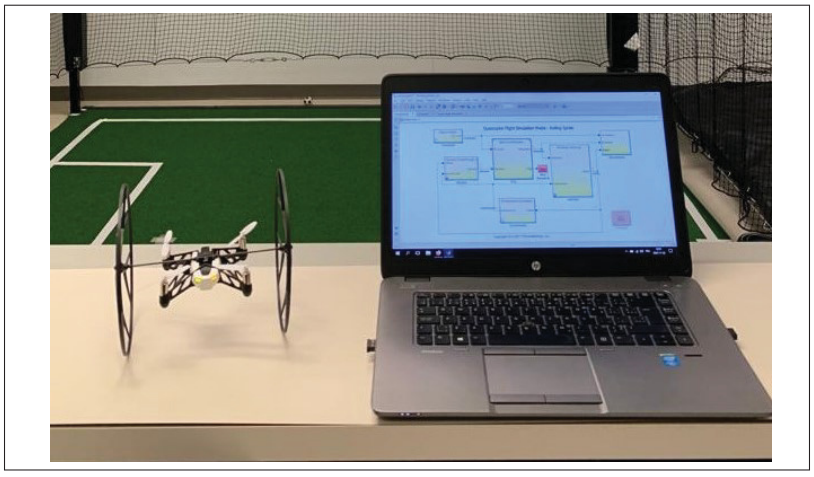

Figure 2.6 Quad-copter Parrot and experimental setup environment

2.5 Proposed approach's novelty claim and theoretical contributions

The design of model-based sliding functions is an innovative and original approach, since no publication or scientific research has yet addressed this subject, of what has been observed to date.

1. The main contribution of this approach is the substantial simplification of the torque control law. This simplification results in several advantages such as the reduction of transient constraints and noise levels on the torque signals, decoupling of the chattering effect on all joint axes, and ease of adjustment of the control parameters. This approach can also be combined with existing chattering reduction/elimination techniques for optimal operation.
2. The second related point of contribution consists in the study of the gravity term which was undertaken within the framework of the latter's compensation by the new sliding functions. This study led to a relationship derived from the model's gravity term, which not only serves to establish a compensation criterion for the latter, but also allows further validation of the mathematical dynamic model of the robot.

CHAPTER 3

MODEL BASED SLIDING FUNCTIONS DESIGN FOR SLIDING MODE ROBOT CONTROL

Charles Fallaha[1] , Maarouf Saad[1]

[1] Department of electrical engineering, École de Technologie Supérieure,
1100 Notre-Dame Ouest, Montréal, Québec, Canada H3C 1K3

Article published in the journal « International Journal of Modeling Identification and Control »
in July 2018.

3.1 Abstract

This paper introduces a novel manifold design for sliding mode control, applicable to second order mechanical systems which nonlinear dynamics can be formalized into that of robotic manipulators. The new approach shows that model based sliding manifold design simplifies substantially the torque control law, which ultimately becomes linear in terms of joint angles and rates. This approach allows additionally decoupling of the chattering effect on the torque inputs on each axis. A new property related the gravity term is introduced and is used for stability analysis and model validation purposes. Simulation results compare the introduced approach to the conventional linear manifold design. The results demonstrate that the new approach reduces transient constraints on torque input, and is more robust to matched uncertainties for low inertia robots.

Keywords: Sliding mode control, nonlinear control, robot control, nonlinear sliding manifolds, chattering.

3.2 Introduction

Nonlinear control has become more accessible over the years with the continuous increase in digital computing power, and can be found in numerous engineering applications. Cutting edge industries are also beginning to grasp the importance of nonlinear control, and their

application to their inherently nonlinear plants and processes, as this understandably provides a substantial improvement in performance. Among the most known modern nonlinear control techniques, sliding mode control has grown in popularity within the controls community, and its applications reach out to numerous fields, including robotics. Two main characteristics usually bring controls engineers to consider using sliding mode control, that is the simplicity of implementation, and the overall robustness of the closed loop system. These usually make the practical implementation of sliding mode control particularly simple and efficient. Most of the research papers found on sliding mode control are mainly focused on two major topics, namely chattering reduction on the control input and study of nonlinear sliding manifolds. The chattering phenomenon is originated from a discontinuous term in the control input which purpose is to absorb disturbances as well as matched or unmatched uncertainties, and therefore increase the robustness of the control. The problem with chattering is that it enforces on the control input uncontrolled high frequency commutations which could either alter physical components or excite high frequency dynamics on the closed loop system. Research efforts on this matter have attempted to treat or control chattering while compromising on or keeping the same level of robustness. A straightforward way to reduce chattering is to smoothen the discontinuous term by using a saturation function. This technique is known as the boundary layer approach (Slotine and Li, 1991). The disadvantage of such an approach is that the robustness of the control is reduced, and the system remains within a boundary of the sliding manifold. Gao and Hung (1993), Camacho et al. (1999) and Fallaha et al. (2011) explore nonlinear reaching laws in order to reduce the discontinuous gain and thus chattering when the sliding manifold is reached. Another approach to reduce chattering was introduced by Levant (1993) and consists of increasing the order of the system. This approach is also known as higher order sliding mode control (HOSM). A particular case of HOSM is second order sliding mode control. Hamerlain et al. (2007), Bartolini et al. (1998), Bartolini et al. (2000) and Parra-Vega and Hirzinger (2001) propose different applications of second order sliding mode control. However, the drawback of HOSM is that the stability proofs are mainly based on geometrical methods. In order to address this, Moreno and Osorio (2008) proposed a Lyapunov based approach for studying the stability of a particular type of a second order sliding mode controller, namely the super-twisting sliding

mode controller (STSMC). Floquet and Barbot (2007) and Gonzalez et al. (2012) have explored as well the STSMC approach. On the other hand, the study of nonlinear sliding manifolds is focused on two separate objectives that could be combined as well; first, improving the transient effects on the control input, and second, ensuring a finite convergence time of the sliding system on the manifold, which is not met by the typical linear manifold design. Choi et al. (1994) and Stepanenko and Su (1993) have explored the use of sliding functions with time-varying parameters to improve robustness and transient behaviour of the control input. More recently, research was focused on terminal sliding mode control, where nonlinear sliding functions are designed to ensure a fast and finite convergence time on the sliding surface (Feng et al., 2002; Yu et al., 2005; Tang, 1998).

This paper features a novel sliding manifold design approach based on the general dynamic model of robotic systems. It uses the inherent properties of the model matrices in order to ensure asymptotic stability to the system while in sliding mode. Finally, it provides considerable simplification of the torque vector expression, and offers as well a means of decoupling the chattering effect on the robot axes. The paper introduces as well a new property applied on the gravity term, which is used for stability analysis and model validation purposes (Fallaha and Saad, 2016). The presented methodology is kept as general as possible, and is applicable to all second order mechanical systems which dynamics can be formalized into that of the general model of robotic systems. To be noted that the paper is solely focused on the study of the asymptotic stability of the system towards the zero equilibrium point. Trajectory tracking study will be carried out in a separate paper material. This paper is organized as follows: Section II gives a brief overview of the conventional sliding mode control, and formulates the need to design model based sliding manifolds. Sections III and IV present the core of the theoretical development of the paper, and introduce model based sliding manifold design, for first order and higher order manifolds. Section V applies the model based sliding manifold design to two examples of 2-DOF robots and presents simulation results with analysis and discussions. Section V finally concludes the paper.

3.3 Problem Formulation and Motivation

This section presents an overview of a robot arm general dynamics and also gives a brief review of sliding mode control applied on the robot. It highlights the main limitations of using linear sliding manifolds and expresses the need to have additional freedom in designing more complex model-based manifolds. The general dynamics of a robot arm manipulator without any friction effect is very well established in the robotic literature, and is given by:

$$\tau = M(\theta)\ddot{\theta} + V_m(\theta, \dot{\theta})\dot{\theta} + G(\theta) \tag{3.1}$$

Where τ is the torque control input vector, θ is the robot joints angles vector, $M(\theta)$ is the inertia matrix, and is positive definite, $V_m(\theta, \dot{\theta})$ is the centrifugal and Coriolis matrix, $G(\theta)$ is the gravitational term vector. Moreover, matrices M and V_m are bounded by the following property (Spong et al., 2005):

$$S(\theta, \dot{\theta}) = \dot{M}(\theta) - 2V_m(\theta, \dot{\theta}) \tag{3.2}$$

Where S is a skew-symmetric matrix. In typical sliding mode, the sliding functions design is defined as a linear first order structure in terms of θ and $\dot{\theta}$, namely:

$$\Sigma = \Lambda\theta + \dot{\theta} \tag{3.3}$$

Where Σ is the sliding functions vector and $\Lambda = diag(\lambda_{ii}), \lambda_{ii} > 0$

The control law is designed to ensure that the sliding manifold is reached, which is equivalent to $\Sigma = 0$. In this case, vector θ will converge to the equilibrium point 0 following a first order behaviour, with a rate defined by matrix Λ. On the other hand, in order to achieve the sliding condition, the control law is designed such that the following relationship is always verified:

$$\dot{\Sigma} = -Ksign(\Sigma) \tag{3.4}$$

Where sign is the well-known signum function, and $K = diag(k_{ii}), k_{ii} > 0$.

The control law that allows for (3.4) is given by:

$$\tau = V_m\dot{\theta} + G(\theta) - M(\theta)Ksign(\Sigma) - M(\theta)\Lambda\dot{\theta} \tag{3.5}$$

Equation (3.5) shows that τ is formed of many terms, one of which is discontinuous, as it includes the signum function. This term is responsible for the chattering phenomenon widely observed and studied in sliding mode control. Equation (3.4) is also referred to as the reaching law, as it will force to reach 0 in a finite amount of time t_r . t_r is the reaching time, and is directly linked to K by the following relation:

$$K = \frac{|S\,(t=0)|}{t_r} \tag{3.6}$$

In order to meet a required reaching time and convergence speed, K is therefore bounded by relation (3.6). Note that K also plays a central role in disturbance and uncertainties rejection, and the higher the value of K, the higher the robustness of the sliding mode control, but the higher the chattering levels on the control input as well. Observing (3.5) again, the signum term is also a function of the inertia matrix, which then implies that the choice of K is dependent upon $M(\theta)$ as well. Since $M(\theta)$ is not diagonal in the general sense, this also implies a coupling effect of the chattering on the torque vector. In order to remove this dependency, a model-based nonlinear sliding manifold design is proposed in the next sections. The approach will be also aimed at simplifying and reducing transient constraints on the control inputs.

3.4 Model-Based First-Order Sliding Manifold Design

In this section, a nonlinear sliding function design including the inertia matrix of the robot is proposed. As opposed to the linear function defined by (3.3), consider the following model-based function:

$$\Sigma = M(\theta)\dot{\theta} + \Gamma\theta \tag{3.7}$$

where Γ is a positive definite matrix. As will be shown below, the inclusion of the inertia matrix will allow the decoupling of the chattering inputs, as well as break the dependency of K on $M(\theta)$. For the rest of the development, consider the following 2 cases:

Case 1: Γ is constant in time.

Case 2: $\Gamma = P\Phi P^T$, where P is the matrix formed by the eigenvectors of the inertia matrix, and Φ is a diagonal matrix with constant and strictly positive elements such that $\Phi = diag(\phi_{ii}), \phi_{ii} > 0$. Note that the following holds as well:

$$D = P^T M P \tag{3.8}$$

where D is a diagonal matrix which elements are the eigenvalues of the inertia matrix, $D = diag(d_{ii}), d_{ii} > 0$.

Proposition 1: For both case 1 and case 2, the sliding manifold $\Sigma = 0$, where Σ is given by (3.7), will ensure the asymptotic stability of θ to 0.

Proof 1: For case 1, choose the following Lyapunov candidate:

$$V = \frac{1}{2} \cdot \theta^T \Gamma \theta \tag{3.9}$$

Since Γ is constant, differentiating (3.9) gives:

$$\dot{V} = \dot{\theta}^T \Gamma \theta \tag{3.10}$$

When the sliding manifold is reached, $\Sigma = 0$. Therefore, from (3.7):

$$\Gamma\theta = -M(\theta)\dot{\theta} \tag{3.11}$$

Multiplying both sides of (3.11) by $\dot{\theta}^T$ to the left:

$$\dot{\theta}^T \Gamma \theta = -\dot{\theta}^T M(\theta)\dot{\theta} \tag{3.12}$$

Therefore,

$$\dot{V} = -\dot{\theta}^T M(\theta)\dot{\theta} \leq 0 \tag{3.13}$$

From (3.13), $\dot{V}$ is semi-negative definite. Assuming however that $\dot{V}$ is continuous, then Barbalat's lemma shows that $\dot{V}$ converges to 0 with time, which implies that $\dot{\theta}$ converges to 0 with time as well. Also using (3.11) finally implies that θ converges to 0 with time, which completes the proof for case 1. For case 2, consider the following variable change:

$$x = P^T \theta, \Xi = P^T \Sigma \tag{3.14}$$

Using this variable change in (3.7) gives:

$$P\Xi = M \cdot (\dot{P}x + P\dot{x}) + P\Phi P^T \cdot (Px) \tag{3.15}$$

Simplifying (3.15) and using the orthogonality properties of matrix P gives:

$$\Xi = P^T M P\dot{x} + (\Phi + P^T M\dot{P})x \tag{3.16}$$

Using (3.8) in (3.16):

$$\Xi = D\dot{x} + (\Phi + DP^T\dot{P})x \tag{3.17}$$

$\Sigma = 0$ implies that $\Xi = 0$ as per the variable change of (3.14). Therefore, using (3.17) gives:

$$D\dot{x} = (\Phi + DP^T\dot{P})x = 0 \tag{3.18}$$

Using the fact that D is invertible then implies:

$$\dot{x} = (D^{-1}\Phi + P^T\dot{P})x = 0 \tag{3.19}$$

Since D and Φ are both diagonal matrices:

$$D^{-1}\Phi = diag_i\left(\frac{\phi_{ii}}{d_{ii}}\right) \tag{3.20}$$

Using the orthogonality properties of matrix P again, it can be shown that $P^T P$ is skew-symmetric. Multiplying (3.19) by x^T to the left therefore yields:

$$x^T\dot{x} = x^T diag_i\left(\frac{\phi_{ii}}{d_{ii}}\right)x \tag{3.21}$$

Equation (3.21) shows that each x_i converges asymptotically to 0, which completes the proof for case 2. For both cases, the torque control law that will allow the reaching condition (3.4) to be met is given by:

$$\tau = -V_m(\theta,\dot{\theta}) + G(\theta) - K\cdot sign(\Sigma) - (\Gamma + S)\dot{\theta} - \dot{\Gamma}\theta \tag{3.22}$$

From (3.22), the signum term is now independent of the inertia matrix and the chattering effect is decoupled for all the torque inputs, which was the aim of the design. This also means that the choice of K remains independent of $M(\theta)$. For case 1, note that $\dot{\Gamma} = 0$ in (3.22).

3.5 Model-Based higher-order sliding manifold design

In the last section, the first-order sliding manifold design yielded a simplification of the control input by removing the inertia matrix term from the discontinuous control. In this section, a higher-order sliding manifold design is proposed, to which an integral term is added. This is intended to further simplify the torque control input. Two higher-order sliding manifolds are proposed; the first compensates only the centrifugal and Coriolis term and the other compensates both the centrifugal and Coriolis and the gravity terms with an additional constraint to meet.

3.5.1 Compensation of the centrifugal and Coriolis term in the control input

In this section, the following higher-order sliding function is considered:

$$\Sigma = M(\theta)\dot{\theta} + \Gamma\theta + \Delta \int \theta dt - \int (S + V_m)\dot{\theta} dt \tag{3.23}$$

Γ and Δ are constant positive definite matrices. In equation (3.23), integral terms are added to give more degrees of freedom in simplifying the torque control input and completely remove the dependency on the inertia matrix and the centrifugal and Coriolis term.

Proposition 2: The sliding manifold $\Sigma = 0$, where Σ is given by (3.23), will ensure the asymptotic stability of θ to 0.

Proof 2: Choose the following Lyapunov candidate:

$$V = \frac{1}{2}\dot{\theta}^T M\dot{\theta} + \frac{1}{2}\theta^T \Delta\theta \tag{3.24}$$

Differentiating (3.24) gives:

$$\dot{V} = \frac{1}{2}\dot{\theta}^T \dot{M}\dot{\theta} + \dot{\theta}^T M\ddot{\theta} + \dot{\theta}^T \Delta\theta \tag{3.25}$$

When the sliding manifold $\Sigma = 0$ is reached, $\dot{\Sigma} = 0$ as well. Therefore:

$$\dot{M}\dot{\theta} + M\ddot{\theta} + \Gamma\dot{\theta} + \Delta\theta - (S + V_m)\dot{\theta} = 0 \tag{3.26}$$

(3.26) can also be written as:

$$\left(\frac{1}{2}\dot{M}\dot{\theta} - V_m\dot{\theta}\right) + \frac{1}{2}\dot{M}\dot{\theta} + M\ddot{\theta} + \Gamma\dot{\theta} - S\dot{\theta} + \Delta\theta = 0 \tag{3.27}$$

Multiplying (3.27) by $\dot{\theta}^T$ to the left and noticing that S and $\frac{1}{2}\dot{M} - V_m$ which is equal to $\frac{1}{2}S$ is also skew-symmetric gives:

$$\frac{1}{2}\dot{\theta}^T\dot{M}\dot{\theta} + \dot{\theta}^T M\ddot{\theta} + \dot{\theta}^T\Gamma\dot{\theta} + \dot{\theta}^T\Delta\theta = 0 \tag{3.28}$$

Using (3.28) in (3.25) finally gives:

$$\dot{V} = -\dot{\theta}^T\Gamma\dot{\theta} \leq 0 \tag{3.29}$$

Using again Barbalat's lemma, $\dot{V}$ converges to 0 with time, which implies that $\dot{\theta}$ converges to 0 with time. Using also (3.26) finally implies that θ converges to 0 with time, which completes the proof.

The torque control input that allows Σ given by (3.23) to converge to 0 is given by:

$$\tau = G(\theta) - K \cdot sign(\Sigma) - \Gamma\dot{\theta} - \Delta\theta \tag{3.30}$$

In (3.30), it can now be seen that the dependence of the torque control input to $M(\theta)$ and $V_m\dot{\theta}$ is completely removed. Compared now to (3.5), the control law of (3.30) is simpler and transient constraints are expected therefore to have less impact on the control input. It remains also obvious that the latter carries additionally the same advantages mentioned in section 3.4, with regards to decoupled chattering effect on torque inputs, and the independency of K to $M(\theta)$.

3.5.2 Compensation of the gravity term in the control input

In this section, the following higher order sliding function is considered:

$$\Sigma = M(\theta)\dot{\theta} + \Gamma\theta + \Delta\int\theta dt - \int(S + V_m)\dot{\theta}dt + \int(G(\theta) - G(0))dt \tag{3.31}$$

With Γ and Δ are constant positive definite matrices. Compared to (3.23), (3.31) includes an additional integral term which purpose is to compensate for the gravity term in the torque

control law. Proposition 3 below proves that the corresponding manifold will allow asymptotic convergence if an additional constraint is verified by Δ.

Proposition 3: the sliding manifold $\Sigma = 0$, where Σ is given by (3.31), will ensure the asymptotic stability of θ to 0 provided that the eigenvalues of matrix Δ verify the following constraint:

$$Min_i\,(Eig_i\Delta) > Max_i\,(Eig_i\Psi_G) \tag{3.32}$$

Where $\Psi_G(\theta)$is a symmetric matrix defined in proof 3 below. Note that since $\Psi_G(\theta)$ is symmetric, it is diagonalizable, and all its eigenvalues are real values.

Proof 3: Consider the following Lyapunov candidate function:

$$V = \frac{1}{2}\dot{\theta}^T M\dot{\theta} + \frac{1}{2}\theta^T\Delta\theta + U - \theta^T G(0) \tag{3.33}$$

Where U is the potential energy term from which is derived $G(\theta)$. U is chosen such that $U - \theta^T G(0) > 0$. This choice is valid under the assumption that the initial value of θ is bounded. Differentiating (3.33) and noticing that $\frac{dU}{dt} = \dot{\theta}^T G(\theta)$, (Spong et al., 2005):

$$\dot{V} = \frac{1}{2}\dot{\theta}^T\dot{M}\dot{\theta} + \dot{\theta}^T M\ddot{\theta} + \dot{\theta}^T\Delta\theta + \dot{\theta}^T G(\theta) - \dot{\theta}^T G(0) \tag{3.34}$$

Lemma 1 in appendix based on the mean value theorem (Fallaha and Saad, 2016) applied to differentiable vector functions, proves the following property that $G(\theta) - G(0)$ can be written as:

$$G(\theta) - G(0) = -\Psi_G(\theta)\cdot\theta \tag{3.35}$$

Where $\Psi_G(\theta)$ is a symmetric matrix, and can be deduced from the jacobian of $G(\theta)$ by using relation (A-2) in appendix A. Therefore (3.34) can be written as:

$$\dot{V} = \frac{1}{2}\dot{\theta}^T\dot{M}\dot{\theta} + \dot{\theta}^T M\ddot{\theta} + \dot{\theta}^T\Delta\theta - \dot{\theta}^T\Psi_G(\theta)\theta \tag{3.36}$$

When the sliding manifold $\Sigma = 0$ is reached, $\dot{\Sigma} = 0$ as well. Therefore:

$$\dot{M}(\theta)\dot{\theta} + M(\theta)\ddot{\theta} + \Gamma\dot{\theta} + \Delta\theta - (S + V_m)\dot{\theta} - \Psi_G(\theta) \cdot \theta = 0 \tag{3.37}$$

(3.37) can be also written as follows:

$$\left(\frac{1}{2}\dot{M}(\theta)\dot{\theta} - V_m\dot{\theta}\right) + \frac{1}{2}\dot{M}(\theta)\dot{\theta} + M(\theta)\ddot{\theta} + \Gamma\dot{\theta} - S\dot{\theta} + \Delta\theta - \Psi_G(\theta) \cdot \theta = 0 \tag{3.38}$$

Multiplying (3.38) by $\dot{\theta}^T$ to the left, and noticing that S and $\frac{1}{2}\dot{M} - V_m$ which is equal to $\frac{1}{2}S$ is also skew-symmetric gives:

$$\frac{1}{2}\dot{\theta}^T\dot{M}(\theta)\dot{\theta} + \dot{\theta}^T M(\theta)\ddot{\theta} + \dot{\theta}^T\Gamma\dot{\theta} + \dot{\theta}^T\Delta\theta - \dot{\theta}^T\Psi_G(\theta) \cdot \theta = 0 \tag{3.39}$$

Using (3.39) in (3.36) gives:

$$\dot{V} = -\dot{\theta}^T\Gamma\dot{\theta} \leq 0 \tag{3.40}$$

Using here again Barbalat implies that $\dot{\theta}$ converges to 0 with time. Using (3.37) shows therefore that:

$$(\Delta - \Psi_G(\theta)) \cdot \theta \underset{t}{\rightarrow} 0 \tag{3.41}$$

Lemma 2 in the appendix A shows that constraint (3.32) implies that $\Delta - \Psi_G(\theta)$ is positive definite. From (3.41) it comes that θ converges to 0 with time, which completes the proof. The torque control input that allows Σ given by (3.31) to converge to 0 is given by:

$$\tau = G(0) - K \cdot sign(\Sigma) - \Gamma\dot{\theta} - \Delta\theta \tag{3.42}$$

The control law (3.42) is now in its simplest form, as $G(\theta)$ is now replaced by G(0) . Compared to the initial control law (3.5), (3.42) has a much less complex expression, and is now fully linear in terms of θ and $\dot{\theta}$. It is also possible to force a complete decoupling of the axes by choosing for instance Γ and Δ to be diagonal matrices.

Matrix $\Psi_G(\theta)$ has therefore a central role in the compensation of the gravity vector in the control law, and its eigenvalues can be used to form an asymptotic convergence condition by imposing a constraint on matrix Δ, as per (3.32). The symmetry property of $\Psi_G(\theta)$ and its eigenvalues can be used as well to study and validate the gravity vector model.

The following application example shows the computation and study of matrix $\Psi_G(\theta)$ and its eigenvalues for a 2 DOF robot manipulator.

Example

In this example, a method for computing $\Psi_G(\theta)$ is given for a 2 DOF robot example depicted in Figure 3.1. The structure of $\Psi_G(\theta)$ is validated and its eigenvalues functions are formed to study the asymptotic stability constraint applied on matrix Δ. Figure 3.1 shows the 2 DOF robot

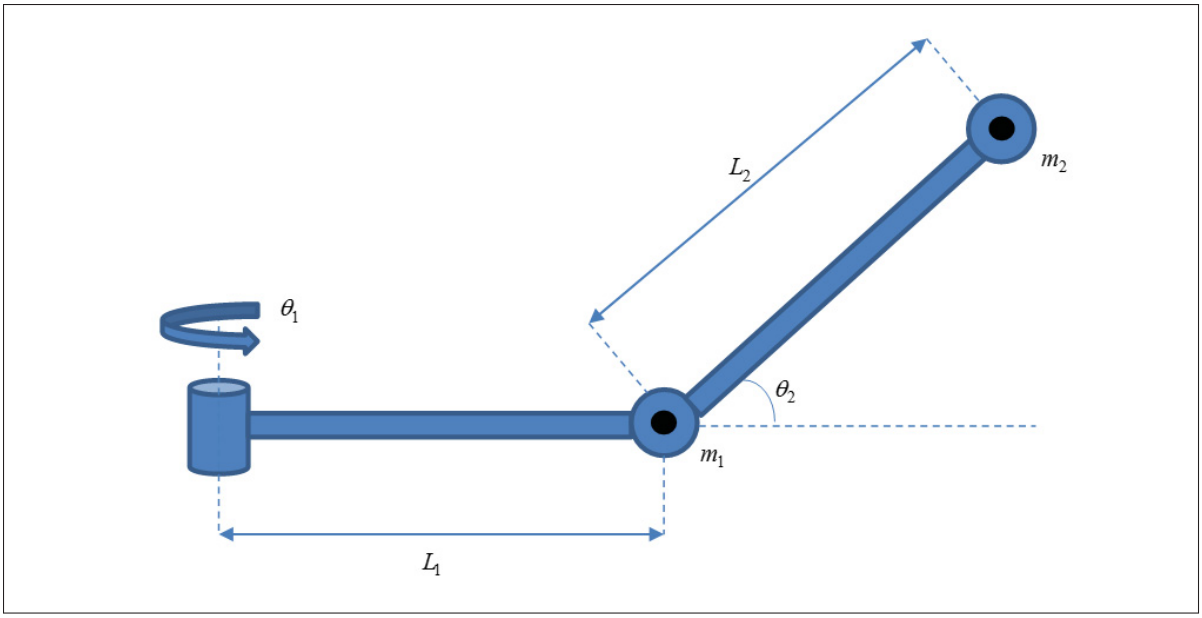

Figure 3.1 RR Manipulator

arm with two perpendicular rotational axes. Both joint masses are assumed located at distal points as represented in the figure. The dynamic model of the robot has already been studied in

(Craig (2005)) and the following matrices can be derived:

$$M(\theta) = \begin{bmatrix} m_1 L_1^2 + m_2 (L_1 + L_2 c_2)^2 & 0 \\ 0 & m_2 L_2^2 \end{bmatrix} \tag{3.43}$$

$$V(\theta, \dot{\theta}) = \begin{bmatrix} -2(L_1 + L_2 c_2) m_2 L_2 s_2 \dot{\theta}_1 \dot{\theta}_2 \\ (L_1 + L_2 c_2) m_2 L_2 s_2 \dot{\theta}_1^2 \end{bmatrix} \tag{3.44}$$

$$G(\theta) = \begin{bmatrix} 0 \\ m_2 g L_2 c_2 \end{bmatrix} \tag{3.45}$$

The working envelope of the robot is given by the following intervals defined in the joint space variables:

$$\theta_1 \in \left[-\frac{\pi}{2}, \frac{\pi}{2}\right], \theta_2 \in \left[-\frac{\pi}{2}, \frac{\pi}{2}\right] \tag{3.46}$$

Using the expression of $G(\theta)$ in (3.45), the jacobian matrix of $G(\theta)$ can be deduced by applying relation (3.69) given in appendix A:

$$J_G = \begin{bmatrix} 0 & 0 \\ 0 & -m_2 L_2 g s_2 \end{bmatrix} \tag{3.47}$$

It is now possible to compute matrix $\Psi_G(\theta)$ as defined in lemma 1 of appendix A.

$$\Psi_G(\theta) = -\left(\int_0^1 J_G\,(h \cdot \theta) dh\right) = -\begin{bmatrix} [0]_0^1 & [0]_0^1 \\ [0]_0^1 & \left[\frac{m_2 L_2 g \cdot c(h\theta_2)}{\theta_2}\right]_0^1 \end{bmatrix} \tag{3.48}$$

Which therefore yields the following expression of matrix $\Psi_G(\theta)$:

$$\Psi_G\,(\theta) = \begin{bmatrix} 0 & 0 \\ 0 & \frac{m_2 g L_2}{\theta_2}\,(1 - cos\,(\theta_2)\,) \end{bmatrix} \tag{3.49}$$

As expected, $\Psi_G(\theta)$ is symmetric, and provides therefore a validation of the structure of the gravity vector (θ) . Note that in this particular case $\Psi_G(\theta)$ is diagonal, resulting from the structure of the robot, as gravity acts exclusively on its second joint.

In order to verify (3.35), compute $\Psi_G(\theta) \cdot \theta$:

$$\Psi_G(\theta) \cdot \theta = \begin{bmatrix} 0 & 0 \\ 0 & \frac{m_2 g L_2}{\theta_2}(1 - cos(\theta_2)) \end{bmatrix} \cdot \begin{bmatrix} \theta_1 \\ \theta_2 \end{bmatrix} = \begin{bmatrix} 0 \\ m_2 g L_2 (1 - cos(\theta_2)) \end{bmatrix} \tag{3.50}$$

Computing on the other hand $G(\theta) - G(0)$ gives:

$$G(\theta) - G(0) = \begin{bmatrix} 0 \\ m_2 g L_2 c_2 \end{bmatrix} - \begin{bmatrix} 0 \\ m_2 g L_2 \end{bmatrix} = \begin{bmatrix} 0 \\ m_2 g L_2 (cos(\theta_2) - 1) \end{bmatrix} \tag{3.51}$$

It can therefore be deduced from (3.50) and (3.51) that $G(\theta) - G(0) = -\Psi_G(\theta)\theta$, which verifies relation (3.35).

From (3.49), the eigenvalues of $\Psi_G(\theta)$ can be easily deduced:

$$\lambda_1 = 0; \lambda_2 = \frac{m_2 g L_2}{\theta_2}(1 - cos(\theta_2)) \tag{3.52}$$

From (3.52), λ_2 is only function of θ_2 as gravity acts only on the second joint. It can be shown that λ_2 is strictly monotonous, as it increases with θ_2. Since θ_2 varies in the $\left[-\frac{\pi}{2}, \frac{\pi}{2}\right]$ interval, then

$$\lambda_{2max} = \frac{2 \cdot m_2 g L_2}{\pi} \tag{3.53}$$

In order to insure asymptotic stability with the control law (3.42), the eigenvalues of matrix Δ must all be greater than λ_{2max}, as per (3.32). Figure 3.2 below shows the variation of λ_2 in the joint space with the following numerical values of the robot's parameters:

$m_1 = 0.5kg; m_2 = 0.5kg; l_1 = 0.2m; l_2 = 0.2m; g = 9.81N/kg$

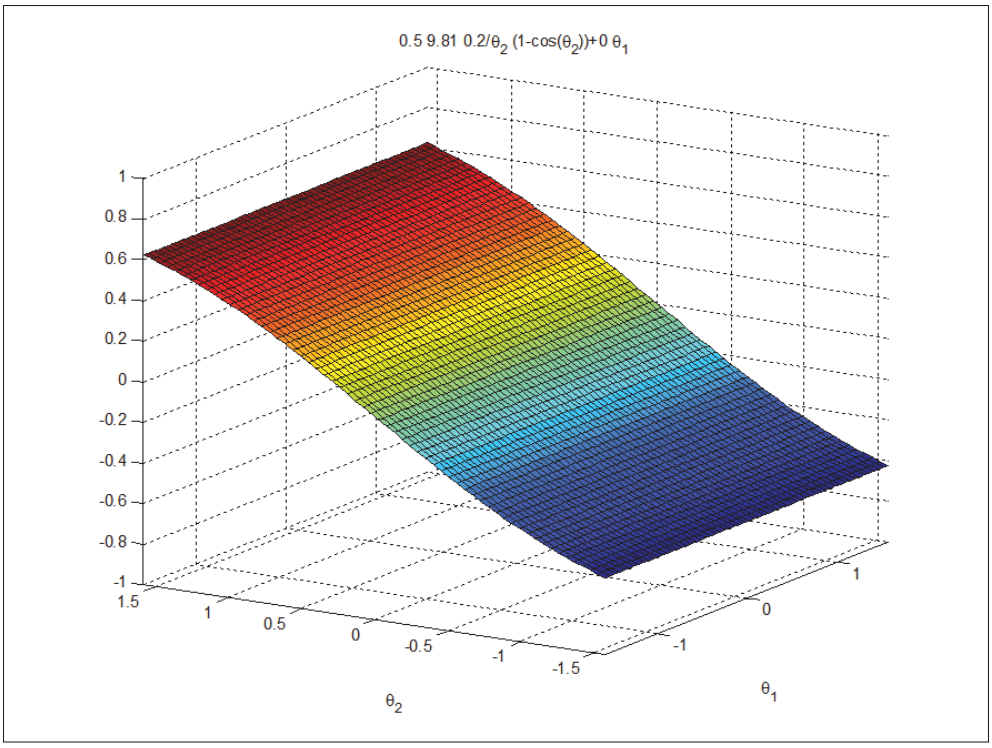

Figure 3.2 RR Manipulator Eigenvalue 2 Function in Joint Space

3.6 Case Studies on 2 DOF Planar Robots

This section studies the application of model based nonlinear sliding manifolds on two examples of 2-DOF planar robots through simulations. In the first example, a robot with a relatively higher inertia, Coriolis and centrifugal terms compared to the second example is chosen. In the second example, the robot is considered with matched uncertainties on the gravity term. In both examples, the model based sliding function of (3.31) is used, which therefore yields to the simplified control law of (3.42). The simulation results for both examples are compared to conventional sliding manifold design.

3.6.1 2 DOF Planar Robot with Higher Inertia, Coriolis and Centrifugal forces

This example studies a 2-DOF planar robot that has a rotational and prismatic joints (PR), and with relatively high inertia, Coriolis and centrifugal effects. This is done by choosing adequate

dynamic parameters and operating the robot at relatively high joint rates. The objective of this study is to show that with model based sliding manifold design, the resulting transient constraints on the torques control input are reduced compared to the baseline case of linear sliding manifold design. As presented in the theoretical development above, this shows that by using model based sliding manifold design, additional degrees of freedom can be used to simplify the control input. The robot used in this example is depicted in Figure 3.3. θ_1 and d_2 are the joints angle and

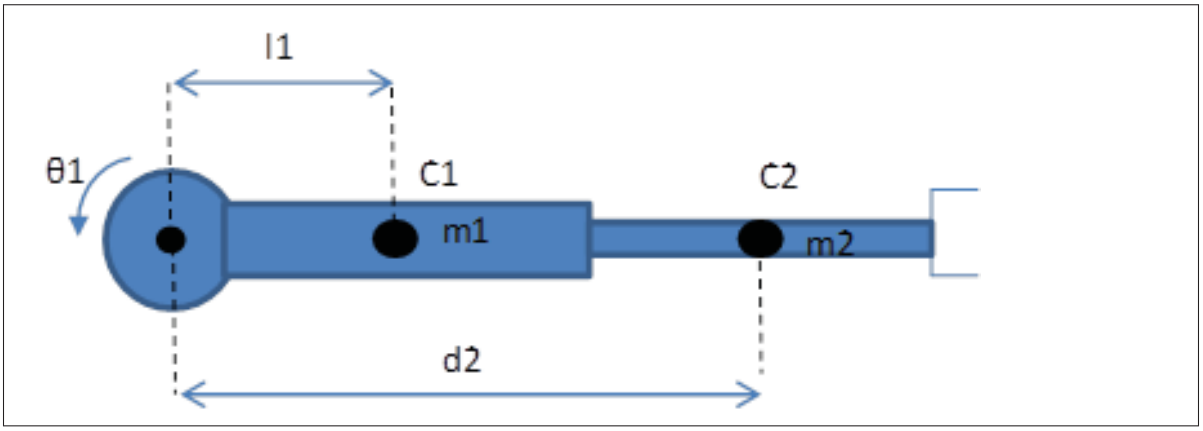

Figure 3.3 RP Manipulator

displacement respectively for axes 1 and 2, and vary respectively within $[0, 2\pi]$ and $[0, 2]$. m_1 and m_2 are respectively the masses of links 1 and 2, located at the centers of masses C_1 and C_2. The inertia tensors of links 1 and 2 at the center of masses are given by:

$$ {}^{C_1}I_1 = \begin{bmatrix} I_{xx1} & 0 & 0 \\ 0 & I_{yy1} & 0 \\ 0 & 0 & I_{zz1} \end{bmatrix} {}^{C_2}I_2 = \begin{bmatrix} I_{xx2} & 0 & 0 \\ 0 & I_{yy2} & 0 \\ 0 & 0 & I_{zz2} \end{bmatrix} $$

The dynamic model has been already studied in (Craig, 2005) and the following matrices were derived:

$$ M(\theta) = \begin{bmatrix} \left(m_1 l_1^2 + I_{zz1} + I_{zz2} + m_2 d_2^2\right) & 0 \\ 0 & m_2 \end{bmatrix} \tag{3.54} $$

$$ V(\theta, \dot{\theta}) = \begin{bmatrix} m_2 d_2 \dot{d}_2 & m_2 d_2 \dot{\theta}_1 \\ -m_2 d_2 \dot{\theta}_1 & 0 \end{bmatrix} \tag{3.55} $$

$$G(\theta) = \begin{bmatrix} (m_1 l_1 + m_2 d_2)\, g c_1 \\ m_2 g s_1 \end{bmatrix} \tag{3.56}$$

Note that in this particular case $M(\theta)$ is diagonal. The following numerical values of the parameters were used in simulation: $m_1 = 0.1kg; m_2 = 0.2kg; l_1 = 1m; I_{zz1} = 0; I_{zz2} = 0; g = 9.81N/kg$

As mentioned above, it is proposed to apply the model based sliding function design in (3.31) with the gravity term compensation. In order to assess the performance of the model based sliding function, a baseline using conventional linear higher order sliding manifold design is used for the exercise. Equation (3.57) is the typical choice in this case:

$$\Sigma = \dot{\theta} + \Lambda\theta + C \int \theta dt \tag{3.57}$$

Where Λ and C are chosen to be positive definite diagonal matrices. In order to have a high convergence speed, assume a double pole placement of -20 in (3.57). This gives the following numerical values for matrices Λ and C:

$$\Lambda = \begin{bmatrix} 40 & 0 \\ 0 & 40 \end{bmatrix}, C = \begin{bmatrix} 400 & 0 \\ 0 & 400 \end{bmatrix} \tag{3.58}$$

Gain K was chosen to be equal to $K = \begin{bmatrix} 5 & 0 \\ 0 & 2.5 \end{bmatrix}$. in order now to have similar dynamics on the model-based sliding manifold, the following Γ and Δ are chosen:

$$\Gamma = 40 * M(0); \Delta = 400 * M(0); M(0) = \begin{bmatrix} 0.1 & 0 \\ 0 & 0.2 \end{bmatrix} \tag{3.59}$$

Choosing $M(0)$ in the design of Γ and Δ as per (3.59) actually yields to lower values for the latter matrices, as the values of $M(\theta)$ are actually the lowest for $\theta = 0$ in this particular example. This therefore translates into a lower convergence rate at the beginning, but reaches progressively

the same convergence rate with time. A possible ponderation between the maximum and the minimum values of $M(\theta)$ could be used as well.

Note that since higher order sliding manifolds are used for both conventional and model based sliding functions design, it is possible to completely remove the reaching phase by choosing the proper initial condition for the integral term.

For this example, $\Psi_G(\theta)$ is computed in the appendix and given by equation (3.75). Analysis of the eigenvalues of $\Psi_G(\theta)$ was done in Matlab, and shows that in this case, both eigenvalues are lower than 4 for the defined working envelope of the robot. From (3.48), it can be deduced that the eigenvalues of Δ are 40 and 80. Therefore constraint (3.32) is respected and the sliding function (3.31) can be used in this case.

In order to have the same chattering level as with the baseline, matrix K was tuned as follows: $K = \begin{bmatrix} 0.5 & 0 \\ 0 & 0.5 \end{bmatrix}$.

The comparison of baseline and model based-sliding function approach was done in Simulink with the above numerical values of the sliding functions. Figure 3.4 features the comparison results of the movement of the robot from an initial condition of $(\theta_{10} = 0.5rd/s, d_{20} = 1m)$ to the convergence point (0,0). The simulation results show that using the model based sliding manifold approach leads to constraints reduction on the control input, while keeping similar tracking performance on the joint angles. With the model based sliding manifold approach, the initial torque input for axis 1 is set at about -20 Nm, whereas it is set around -60 Nm with the baseline approach. This difference comes mainly from the initial condition on the inertia matrix that still appears in the baseline torque control law. The peak value of torque input for axis 1 reaches approximately 8 Nm with the model based sliding manifold design, whereas it reaches approximately 12 Nm with the baseline design. This difference comes mainly from the Coriolis and Centrifugal terms that are compensated for in the model based approach. Transient differences on the torque control input for axis 2 is not as apparent, but still show that transient effort remains lower with the proposed approach.

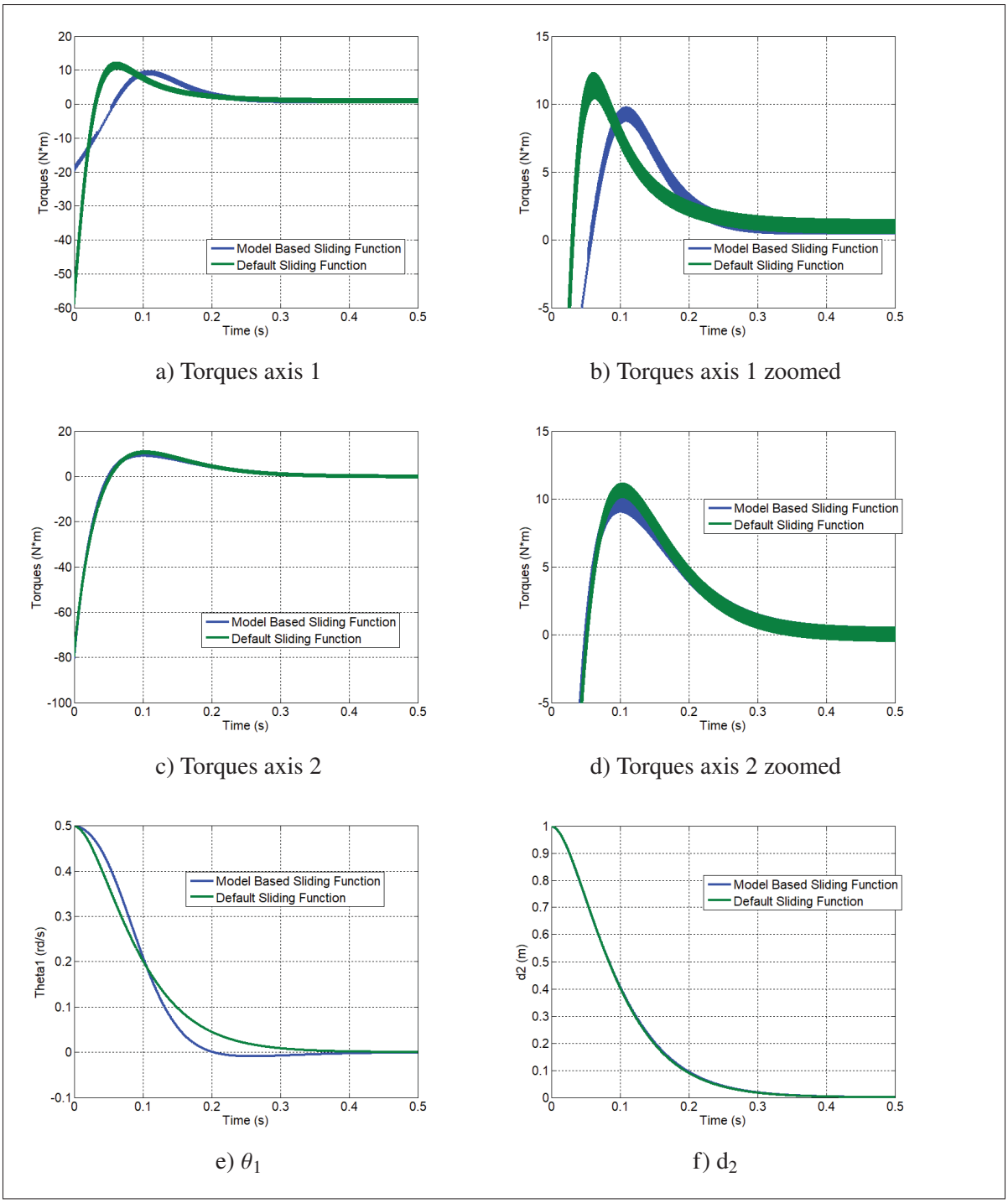

a) Torques axis 1

b) Torques axis 1 zoomed

c) Torques axis 2

d) Torques axis 2 zoomed

e) θ_1

f) d_2

Figure 3.4 Model-Based Versus Default Sliding Function Design for RP Manipulator

3.6.2 2-DOF Planar Robot with Lower Inertia under Matched Uncertainties

In this example, another 2-DOF planar robot is considered that has two rotational joints (RR). The objective of this example is therefore to show that the lower inertia of the robot combined with matched uncertainties introduced in the model will force an increase of the discontinuous gain K in the conventional linear sliding manifold design in order to absorb the uncertainties. With the model based sliding manifold design approach, since the independence of the inertia is established, there is no need to increase the equivalent discontinuous gain. In this particular case, it is therefore shown that the model based sliding manifold design offers a more robust behaviour of the closed loop system.

The studied robot in this example has two rotational joints and is depicted in Figure 5. The parameters of the robot are chosen here such that the inertia matrix compared to the previous example has considerably less impact. θ_1 and θ_2 are the joints angle respectively for axes 1 and

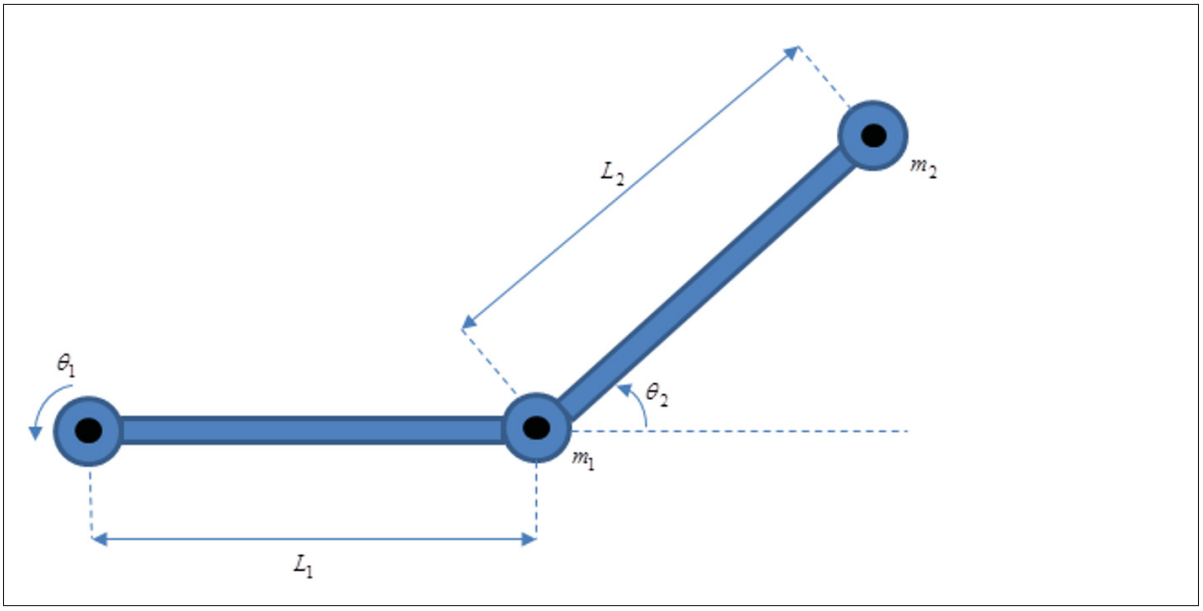

Figure 3.5 RR manipulator

2. The two-link manipulator is also considered to have two point masses m_1 and m_2 at distal point of each link. Joint angles of axes 1 and 2 vary respectively within $\left[0, \frac{\pi}{2}\right]$ and $\left[-\frac{\pi}{2}, \frac{\pi}{2}\right]$. The

dynamic model is also studied in (Craig, 2005) and the dynamic matrices are given below:

$$M(\theta) = \begin{bmatrix} l_2^2 m_2 + 2 l_1 l_2 m_2 c_2 + l_1^2 (m_1 + m_2) & l_2^2 m_2 + l_1 l_2 m_2 c_2 \\ l_2^2 m_2 + l_1 l_2 m_2 c_2 & l_2^2 m_2 \end{bmatrix} \tag{3.60}$$

$$V_m(\theta, \dot{\theta}) = \begin{bmatrix} -m_2 l_1 l_2 \dot{\theta}_2 s_2 & -m_2 l_1 l_2 s_2 (\dot{\theta}_1 + \dot{\theta}_2) \\ m_2 l_1 l_2 s_2 \dot{\theta}_1 & 0 \end{bmatrix} \tag{3.61}$$

$$G(\theta) = \begin{bmatrix} m_2 l_2 g c_{12} + (m_1 + m_2) l_1 g c_1 \\ m_2 l_2 g c_{12} \end{bmatrix} \tag{3.62}$$

As per the first example above, the same sliding manifolds with the same notations are used for both the baseline and the model-based design. In this case, a double pole placement of -30 is chosen, which gives the following numerical values for matrices Λ and C:

$$\Lambda = \begin{bmatrix} 60 & 0 \\ 0 & 60 \end{bmatrix}, C = \begin{bmatrix} 900 & 0 \\ 0 & 900 \end{bmatrix} \tag{3.63}$$

Gain K was chosen to be equal to $K = \begin{bmatrix} 50 & 0 \\ 0 & 50 \end{bmatrix}$. Similarly to before, Γ and Δ are chosen:

$$\Gamma = 60 * M(0); \Delta = 900 * M(0); M(0) = \begin{bmatrix} 0.02 & 0.008 \\ 0.008 & 0.004 \end{bmatrix} \tag{3.64}$$

In this particular case, choosing $M(0)$ in the design of Γ and Δ as per (3.64) actually yields to higher values for the latter matrices, as the values of $M(\theta)$ are actually the highest for $\theta = 0$ in this particular example. This therefore translates into a higher convergence rate at the beginning, but reaches progressively the same convergence rate with time. As mentioned in the previous example, a possible ponderation between the maximum and the minimum values of $M(\theta)$ could be used.

For this example, $\Psi_G(\theta)$ is computed in appendix A and given by equation (3.80). Analysis of the eigenvalues of $\Psi_G(\theta)$ was done in Matlab, and shows that in this case, both eigenvalues are lower than 0.3 for the defined working envelope of the robot. From (3.64), it can be deduced that the eigenvalues of Δ are 0.61 and 20.98. Therefore constraint (3.32) is respected and the sliding function (3.31) can be also used in this case.In order to have the same chattering level as with the baseline, matrix K was tuned as follows: $K = \begin{bmatrix} 0.6 & 0 \\ 0 & 0.2 \end{bmatrix}$. The comparison of baseline and model-based sliding function approach was done in Simulink with the above numerical values of the sliding functions. An introduction of matched uncertainties on the gravity term of the robot model was introduced equally for both approaches. Figure 3.6 shows the comparison results of the movement of the robot from an initial condition of $(\theta_{10} = 0.5rd/s, \theta_{20} = -0.5rd/s)$ to the convergence point (0,0). The following numerical values of the parameters were used in simulation: $m_1 = 0.1kg; m_2 = 0.1kg; l_1 = 0.2m; l_2 = 0.2m; g = 9.81N/kg$

Simulation results show that the proposed approach is more robust to matched uncertainties, as for the same gain K, the control input is able to ensure asymptotic convergence of the joint angles. The baseline approach is not able to provide this, even with a multiplier factor of 4 on gain K. This comes from the fact that with the baseline approach, the robustness to matched uncertainties is function of the inertia matrix, whereas with the proposed approach this dependence is removed. Indeed, for matched uncertainties, the baseline approach yields the following reaching law:

$$\dot{\Sigma} = M^{-1} \cdot F_m - K \cdot sign(\Sigma) \tag{3.65}$$

Where F_m is the term containing all the matched uncertainties, whereas the mode-based approach yields:

$$\dot{\Sigma} = F_m - K \cdot Sign(\Sigma) \tag{3.66}$$

Equation (3.66) shows that the reaching law is now independent of the inertia matrix, which therefore makes the choice of K independent as well of M. Since in this particular case the inertia of the robot is relatively small, (3.65) implies that matched uncertainties will yield to higher values of K for the baseline approach, in order to ensure the robustness of the sliding

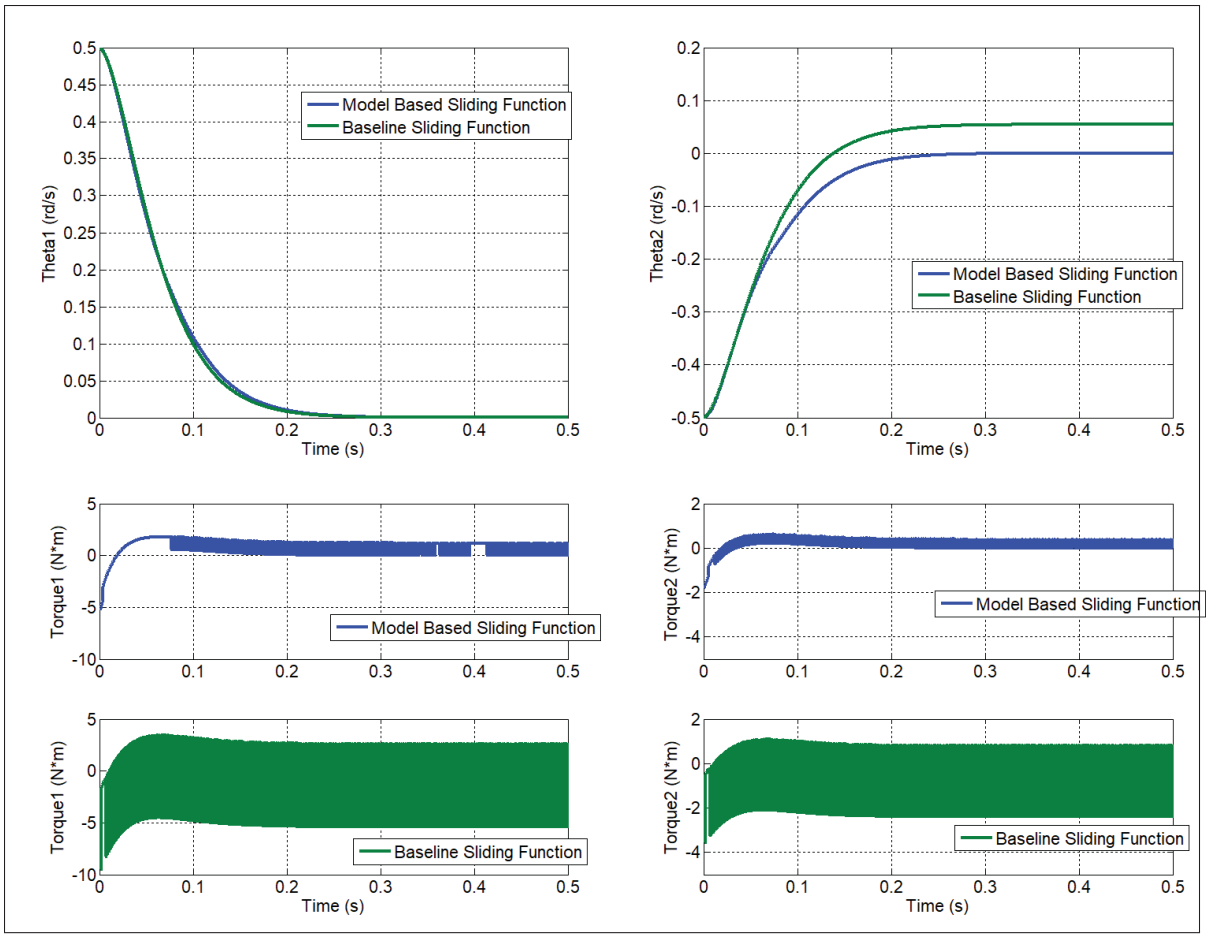

Figure 3.6 Model Based Versus Default Sliding Function Design for RR Manipulator Under Matched Uncertainties on the Gravitational Term

mode phase. Also note that with the baseline approach, the chattering effect is existent on both axes, even though only axis 1 reached the sliding mode phase. This corroborates the coupling effect of chattering with the baseline approach, for a non-diagonal inertia matrix.

3.7 Conclusion

This paper introduced a model based sliding manifold design methodology applied on robotic systems. It introduced as well a property related to the gravity term, that helped to compensate the latter in the control law. This property could be also used to verify the validity of the gravity term in the dynamic model of any robot. The theoretical development in the paper shows that the

model based sliding manifold approach offers a decoupling of the chattering effect on the torque inputs, and simplifies the control input by potentially removing the dependency on all model matrices and using them instead in the sliding manifold itself. This ultimately provides a linear control input in terms of the joint angles and rates. The advantage of such a simplification makes the control input less dependent to transient constraints for high dynamics effects, and the system more robust to matched uncertainties for low inertia effects, as presented in the simulation results. As mentioned previously, this paper was focused on the study of the asymptotic stability of the system towards the zero equilibrium point. Trajectory tracking study will be carried out in a separate paper material.

3.8 Appendix A. Supplementary Material

Lemma 1: The difference $G(\theta) - G(0)$ can be written as:

$$G(\theta) - G(0) = -\Psi_G(\theta) \cdot \theta \tag{3.67}$$

Where $\Psi_G(\theta)$ is a symmetric matrix

Proof of Lemma 1: Using the mean value theorem applied to differentiable vector functions, the following holds:

$$G(\theta) - G(0) = \left(\int_0^1 J_G(h \cdot \theta) dh \right) \cdot \theta \tag{3.68}$$

Where J_G is the square jacobian of G defined as follows:

$$J_G = \left[\frac{\partial G_i}{\partial \theta_j} \right] \tag{3.69}$$

Using the fact that G is derived from a potential energy U, namely:

$$G_i = \frac{\partial U}{\partial \theta_i} \tag{3.70}$$

Then the jacobian matrix can be written as:

$$J_G = \left[\frac{\partial}{\partial \theta_j} \frac{\partial}{\partial \theta_i} U \right] \tag{3.71}$$

Assuming that second partial derivatives of U are continuous and using Schwarz' theorem, the following holds:

$$\frac{\partial}{\partial \theta_j} \frac{\partial}{\partial \theta_i} U = \frac{\partial}{\partial \theta_i} \frac{\partial}{\partial \theta_j} U \tag{3.72}$$

Therefore J_G is symmetric. Noting $\Psi_G(\theta) = -\left(\int_0^1 J_G(h \cdot \theta) dh\right)$, $\Psi_G(\theta)$ will also be symmetric as it is the integral of a symmetric matrix, which completes the proof of Lemma 1. In order to validate the results of lemma 1, consider again the two 2-DOF robots studied in section 3.6.1.

3.8.1 Example A1: 2-DOF RP robot of section 3.6.1

Using the expression of $G(\theta)$ in (3.45) and applying (3.69) gives:

$$J_G = \begin{bmatrix} -(m_1 l_1 + m_2 d_2) g s_1 & m_2 g c_1 \\ m_2 g c_1 & 0 \end{bmatrix} \tag{3.73}$$

Note that as expected, J_G is symmetric. $\Psi_G(\theta)$ can now be derived as follows:

$$\Psi_G(\theta) = -\left(\int_0^1 J_G(h \cdot \theta) dh\right) = -\begin{bmatrix} \left[\frac{(m_1 l_1 + m_2 d_2 h) g c(h\theta_1)}{\theta_1} - \frac{m_2 d_2 g s(h\theta_1)}{{\theta_1}^2}\right]_0^1 & \left[\frac{m_2 g s(h\theta_1)}{\theta_1}\right]_0^1 \\ \left[\frac{m_2 g s(h\theta_1)}{\theta_1}\right]_0^1 & 0 \end{bmatrix} \tag{3.74}$$

Which therfore yields:

$$\Psi_G(\theta) = -\begin{bmatrix} \frac{(m_1 l_1 + m_2 d_2) g c_1 - m_1 l_1 g}{\theta_1} - \frac{m_2 d_2 g s_1}{{\theta_1}^2} & \frac{m_2 g s_1}{\theta_1} \\ \frac{m_2 g s_1}{\theta_1} & 0 \end{bmatrix} \tag{3.75}$$

In order to verify (3.35), form the following

$$\Psi_G(\theta)\,\theta = -\begin{bmatrix} \frac{(m_1 l_1 + m_2 d_2) g c_1 - m_1 l_1 g}{\theta_1} - \frac{m_2 d_2 g s_1}{\theta_1^2} & \frac{m_2 g s_1}{\theta_1} \\ \frac{m_2 g s_1}{\theta_1} & 0 \end{bmatrix} \begin{bmatrix} \theta_1 \\ d_2 \end{bmatrix} = -\begin{bmatrix} (m_1 l_1 + m_2 d_2)\, g c_1 - m_1 l_1 g \\ m_2 g s_1 \end{bmatrix} \tag{3.76}$$

Noticing that

$$G(0) = \begin{bmatrix} m_1 l_1 g \\ 0 \end{bmatrix} \tag{3.77}$$

It can be deduced then from (3.76) that $-\Psi_G(\theta)\theta = G(\theta) - G(0)$.

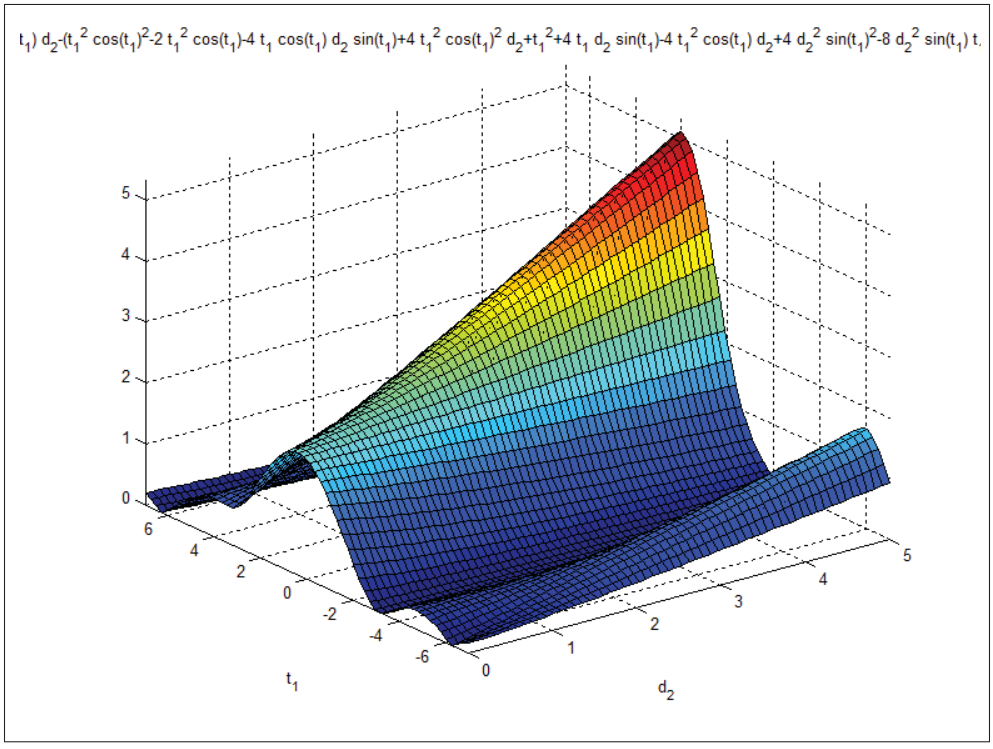

Figure 3.7 Eigenvalue 1 function of matrix $\Psi_G(\theta)$ for RP robot in section 3.6.1

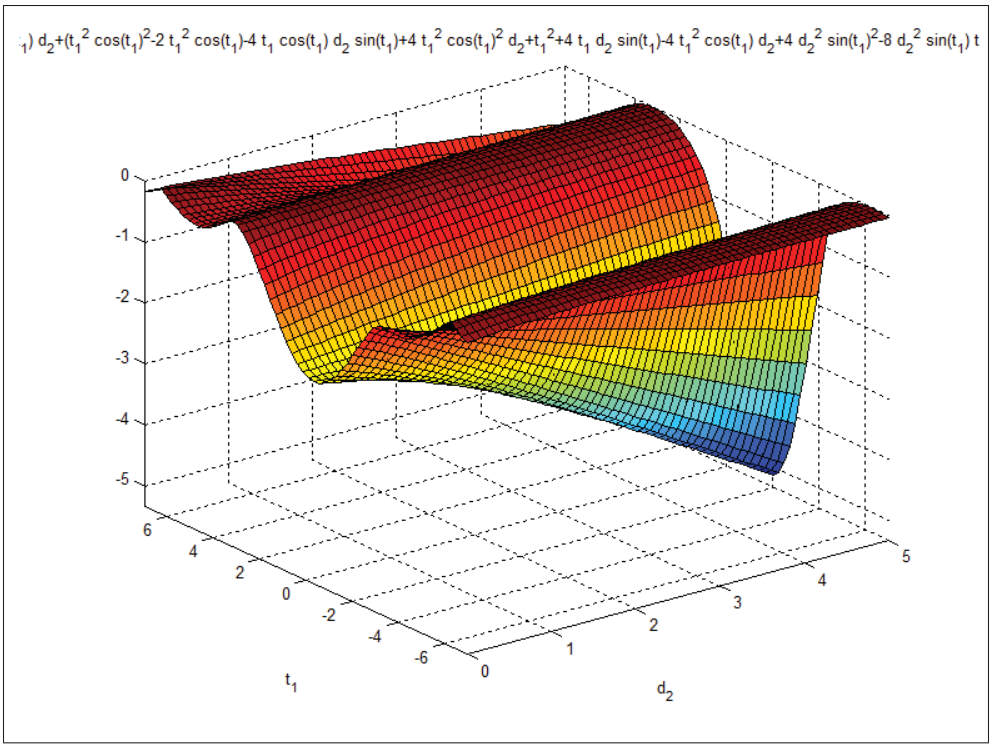

Figure 3.8 Eigenvalue 2 function of matrix $\Psi_G(\theta)$ for RP robot in section 3.6.1

3.8.2 Example A2: 2-DOF RR robot of section 3.6.2

Using the expression of $G(\theta)$ in (3.51) and applying (3.69) gives:

$$J_G = \begin{bmatrix} -m_2 l_2 g s_{12} - (m_1 + m_2)\, l_1 g s_1 & -m_2 l_2 g s_{12} \\ -m_2 l_2 g s_{12} & -m_2 l_2 g s_{12} \end{bmatrix} \tag{3.78}$$

Note that as expected, J_G is symmetric. $\Psi_G(\theta)$ can now be derived as follows:

$$\Psi_G(\theta) = -\left(\int_0^1 J_G(h\cdot\theta)dh\right) = -\begin{bmatrix} \left[\frac{m_2 l_2 g c(t(\theta_1+\theta_2))}{\theta_1+\theta_2}\right]_0^1 + \left[\frac{(m_1+m_2) l_1 g c(h\theta_1)}{\theta_1}\right]_0^1 & \left[\frac{m_2 l_2 g c(t(\theta_1+\theta_2))}{\theta_1+\theta_2}\right]_0^1 \\ \left[\frac{m_2 l_2 g c(t(\theta_1+\theta_2))}{\theta_1+\theta_2}\right]_0^1 & \left[\frac{m_2 l_2 g c(t(\theta_1+\theta_2))}{\theta_1+\theta_2}\right]_0^1 \end{bmatrix} \tag{3.79}$$

Which therefore yields:

$$\Psi_G(\theta) = -\begin{bmatrix} \frac{m_2 l_2 g c_{12} - m_2 l_2 g}{\theta_1+\theta_2} + \frac{(m_1+m_2) l_1 g c_1 - (m_1+m_2) l_1 g}{\theta_1} & \frac{m_2 l_2 g c_{12} - m_2 l_2 g}{\theta_1+\theta_2} \\ \frac{m_2 l_2 g c_{12} - m_2 l_2 g}{\theta_1+\theta_2} & \frac{m_2 l_2 g c_{12} - m_2 l_2 g}{\theta_1+\theta_2} \end{bmatrix} \tag{3.80}$$

In order to verify (3.35), form the following:

$$\begin{aligned} \Psi_G(\theta)\,\theta = -&\begin{bmatrix} \frac{m_2 l_2 g c_{12} - m_2 l_2 g}{\theta_1+\theta_2} + \frac{(m_1+m_2) l_1 g c_1 - (m_1+m_2) l_1 g}{\theta_1} & \frac{m_2 l_2 g c_{12} - m_2 l_2 g}{\theta_1+\theta_2} \\ \frac{m_2 l_2 g c_{12} - m_2 l_2 g}{\theta_1+\theta_2} & \frac{m_2 l_2 g c_{12} - m_2 l_2 g}{\theta_1+\theta_2} \end{bmatrix} \begin{bmatrix} \theta_1 \\ \theta_2 \end{bmatrix} = \\ -&\begin{bmatrix} (m_1+m_2)\, l_1 g c_1 + m_2 l_2 g c_{12} - m_2 l_2 g - (m_1+m_2)\, l_1 g \\ m_2 l_2 g c_{12} - m_2 l_2 g \end{bmatrix} \end{aligned} \tag{3.81}$$

Noticing that

$$G(0) = \begin{bmatrix} m_2 l_2 g + (m_1+m_2) l_1 g \\ m_2 l_2 g \end{bmatrix} \tag{3.82}$$

It can be deduced then from (3.81) that $-\Psi_G(\theta)\theta = G(\theta) - G(0)$.

Lemma 2: Constraint (3.32) implies that $\Delta - \Psi_G(\theta)$ is positive definite.

Proof of Lemma 2: (3.32) implies that there exists a real value v such that:

$$Min_i\,(Eig_i \Delta) > v > Max_i\,(Eig_i \Psi_G) \tag{3.83}$$

Consider now matrix V defined as:

$$V = vI \tag{3.84}$$

It can be therefore deduced that:

$$\Delta - \Psi_G(\theta) = \Delta - V + V - \Psi_G(\theta) = A + B \tag{3.85}$$

Where $A = \Delta - V$ and $B = V - \Psi_G(\theta)$.

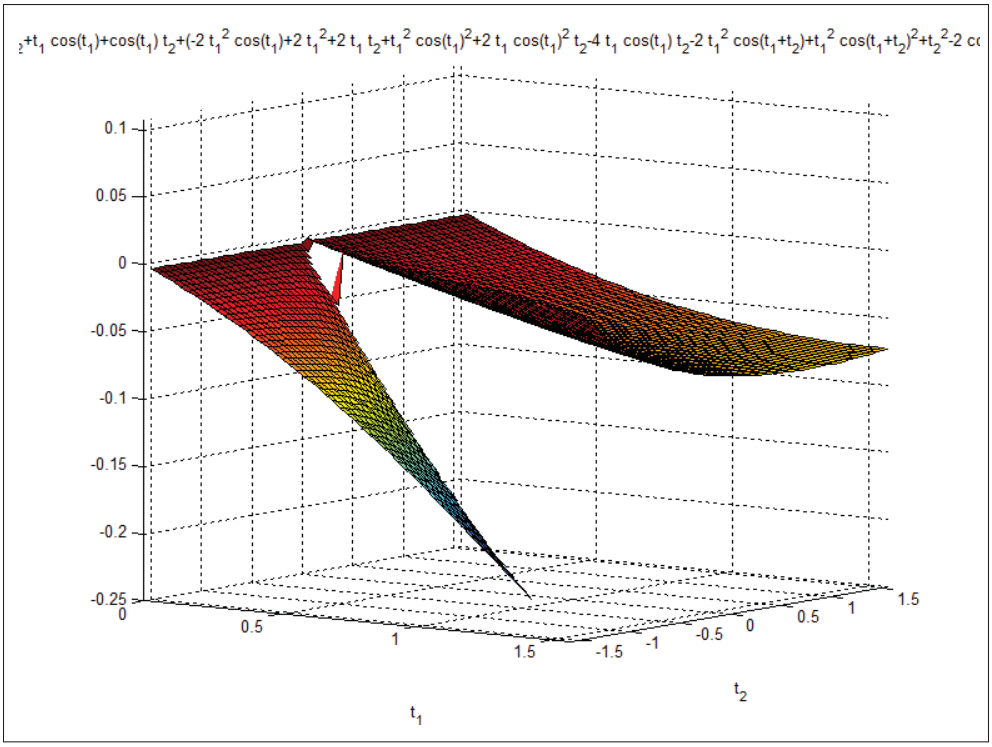

Figure 3.9 Eigenvalue 1 function of matrix $\Psi_G(\theta)$ for RR robot in section 3.6.2

Note that by construction, the eigenvalues of matrices A and B are respectively given by:

$$Eig_i A = Eig_i \Delta - v; Eig_i B = v - Eig_i \Psi_G \tag{3.86}$$

Using therefore relation (3.83), (3.86) implies that the eigenvalues of matrices A and B are all strictly positive, which also implies that A and B are positive definite, and therefore A+B is also positive definite. From (3.85), it comes that $\Delta - \Psi_G(\theta)$ is positive definite as well.

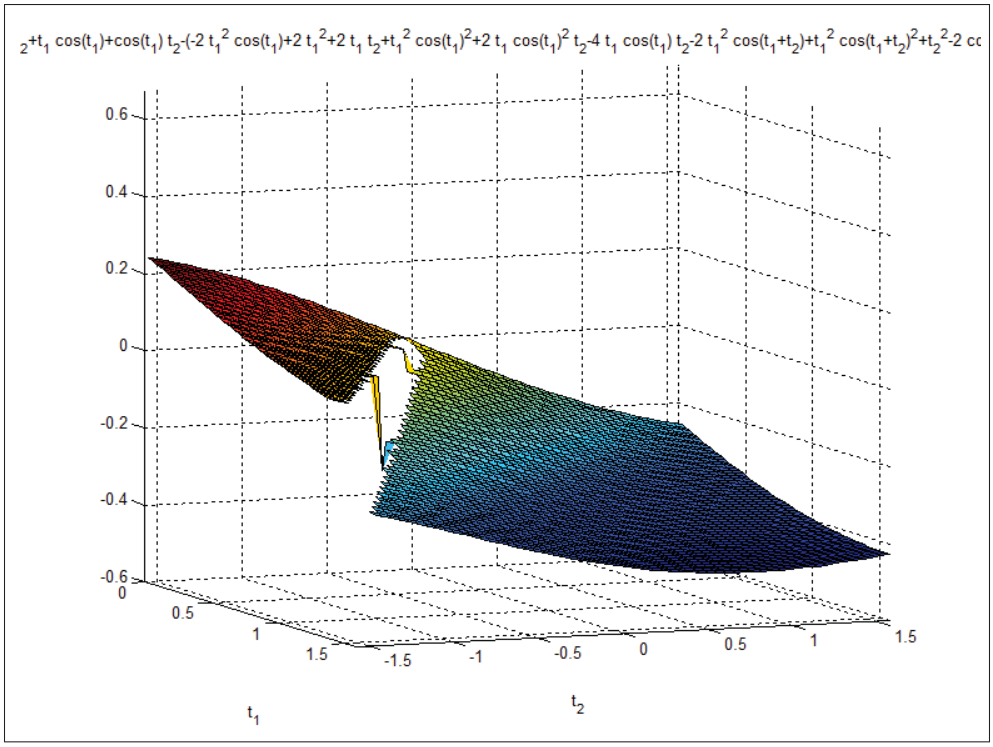

Figure 3.10 Eigenvalue 2 function of matrix $\Psi_G(\theta)$ for RR robot in section 3.6.2

CHAPTER 4

FIXED-TIME SLIDING MODE FLIGHT CONTROL WITH MODEL-BASED SWITCHING FUNCTIONS OF QUADROTOR UNMANNED AERIAL VEHICLES

Charles Fallaha[1] , Maarouf Saad[1] , Jawhar Ghommam[2] , Yassine Kali[1]

[1] Department of electrical engineering, École de Technologie Supérieure,
1100 Notre-Dame Ouest, Montréal, Québec, Canada H3C 1K3
[2] Department of computer and electrical engineering, Sultan Quaboos University
Muscat 123, Oman

Article published in the journal « International Journal of Automation and Control » in November 2020.

4.1 Abstract

This paper proposes the design of a new sliding mode controller of the attitude fast inner-loop of a drone quadrotor type system. The controller uses the novel model-based switching functions approach, which leads to important simplifications of the pitch, roll and yaw torques control inputs fed to the quadrotor. The model-based switching functions approach forces as well a complete chattering decoupling of these three torque inputs and enhances the robustness of the closed-loop system. The proposed approach is combined with the fixed-time sliding mode approach, and is experimentally implemented and successfully validated on a quadrotor system.

Keywords: Sliding Mode Control; Model-Based Switching Functions; Fixed-Time Sliding Mode; Quadrotor; UAV.

4.2 Introduction

The field of robotics has known an important progress and diversification in the last decade. This has been mainly supported by the development of technology and by the increase of affordability of robotic hardware and software systems. The increase in sensors accuracy and in CPU computing power has also contributed in the development of more sophisticated

controllers for fixed and mobile robotics. The global robotic market is anticipated to reach 87 billion dollars (Wolfgang et al., 2017) by the end of 2025. Within mobile robotics, unmanned aerial vehicles (UAVs), and specifically multi-rotor systems have become increasingly popular, and their multiple engineering applications include inspection, exploration, agriculture and transportation.

UAVs were initially deployed in the mid 1930's, and were mainly used for non-military applications up to the late 1980's (Valavanis and Vachtsevanos, 2015). UAVs can be mainly classified into two comprehensive categories, namely fixed and rotary wing structures (Nguyen et al., 2020). A hybrid mix between both structures can also be considered. Multi-rotor UAVs fall within the rotary wing structures category, and have recently known an important expansion in the mobile robotics market, thanks to their flexibility in flight properties, including hovering, maneuverability, speed and obstacles avoidance. On the other hand, multi-rotor UAVs are rather energy inefficient and consume considerable energy mainly in hovering applications. However, ongoing advances in battery technology and control systems techniques are helping to address this issue.

The controllers designed for multi-rotor UAVs are required to provide functional accuracy and robustness against outward and inward disturbances, including environmental and physical fluctuations. Nguyen et al. (2020) have provided a comprehensive study of controllers that are applied to multi-rotor UAVs, including linear and nonlinear controllers. Many research papers have tackled the control problem of multi-rotor UAVs and proposed several control algorithms. Among those controllers, feedback linearization (Al-Hiddabi, 2009; Voos, 2009; Abbasi et al., 2017), backstepping (Basri et al., 2015; Barikbin and Fakharian, 2019; Jiang et al., 2018), optimal control (Fessi and Bouallègue, 2019), intelligent control (Pratap and Purwar, 2019) and sliding mode control (SMC) (Modirrousta and Khodabandeh, 2017; Chen et al., 2019; Kali, Rodas, Gregor, Saad and Benjelloun, 2018) have been studied and applied to multi-rotor UAVs.

Among the nonlinear control techniques, SMC has been widely used for controlling nonlinear systems. SMC is an inherently robust approach that removes the need of adding adaptive

algorithms to the control loop (Slotine and Li, 1991) and can be applied to many SISO or MIMO systems. It has been recently applied on numerous robotic and mechatronic systems (Hosseinabadi and Abadi, 2019; Aboulem et al., 2019; Ardjal et al., 2019). However, the main downside of SMC in its practical implementation is the chattering phenomenon that occurs on the control input signals. This chattering effect is due to a discontinuous term used in the conventional construction of the control law input. However, numerous techniques presented in the literature have been successfully applied to reduce or eliminate the chattering phenomenon. The boundary layer approach introduced in (Slotine and Li, 1991) is a well-known technique that smoothens the discontinuous term by replacing the signum function with a saturation function. Nonlinear reaching laws have also been explored in (Gao and Hung, 1993; Camacho et al., 1999; Fallaha et al., 2011) in order to reduce the discontinuous gain when the system approaches the sliding surface. Higher-order sliding mode (HOSM) has been introduced by Levant (1993) and increases the order of the system. HOSM computes a discontinuous sliding mode control law that is the time derivative of the actual control law. This requires the implementation of higher order observers in its traditional implementation. A particular case of HOSM, namely second order sliding mode, has also been explored in literature, (Hamerlain et al., 2007; Bartolini et al., 2000; Parra-Vega and Hirzinger, 2001). Sivaramakrishnan et al. (2015) proposed a third order sliding mode control. More recently the super-twisting algorithm proposed by Moreno and Osorio (2008) has gained popularity and was further studied by Kali, Saad, Benjelloun and Khairallah (2018) and Gonzalez et al. (2012).

In this paper, SMC with the model-based switching functions approach (Fallaha and Saad, 2018) is experimentally applied to the setpoint stabilization problem of a quadcopter UAV's inner attitude control loop, whereby traditional linear switching functions are replaced by nonlinear model-based switching functions. The contribution of this paper is summarized into the following points:

1. Model-based switching functions substantially simplify the expression of the pitch, yaw and roll torque control inputs, while ensuring asymptotic convergence on the switching surface.

2. This simplification leads to the reduction of transient activity on the control input, as well as a complete chattering decoupling on the attitude angles torques.

The paper is therefore structured as follows: Section 2 presents the basics of the quadcopter drone mathematical modeling. Then, section 3 introduces the model-based switching functions approach with fixed-time and applies it to the quadcopter application, by underlining the advantages of the nonlinear model-based switching functions over the typical linear sliding functions design. Section 4 explores the experimental drone quadcopter setup and presents some experimental results comparison and analysis for the setpoint stabilization problem of the drone. Section 5 finally concludes the paper.

4.3 Quadrotor UAV Mathematical Modeling Development

The quadrotor UAVs typically include four independent electric motors mounted on a rigid cross structure as shown in Figure 4.1 (Castillo et al., 2004).

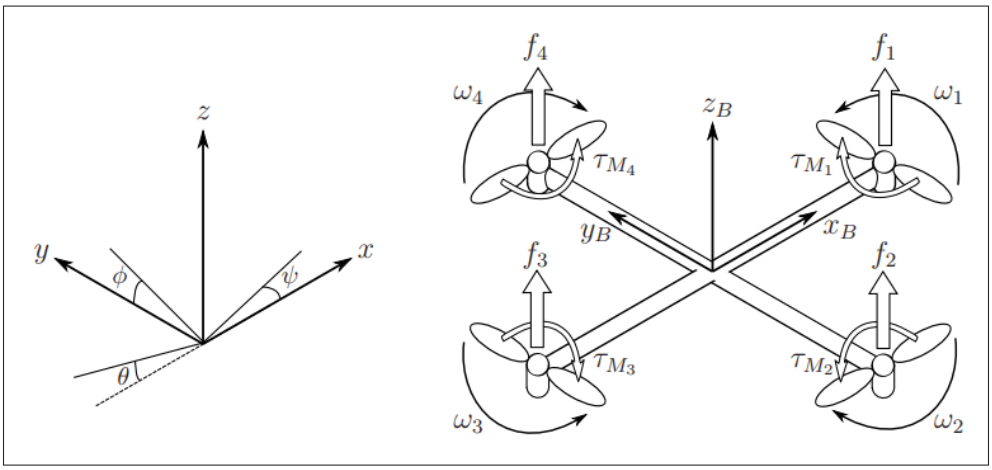

Figure 4.1 Quadcopter structure, frames and forces

4.3.1 Dynamics modeling of position and attitude

UAV systems can achieve up to 6-Degrees Of Freedom (DOF) formed by the position vector $P = [x, y, z]^T \in R^3$ that includes the altitude z and the Euler angles vector $\Theta = [\phi, \theta, \psi]^T \in R^3$ with ϕ represents the roll, θ represents the pitch and ψ represents the yaw.

The position dynamic model is given as in Castillo et al. (2004) by:

$$M \underbrace{\begin{bmatrix} \ddot{x} \\ \ddot{y} \\ \ddot{z} \end{bmatrix}}_{\ddot{P}} + \underbrace{\begin{bmatrix} K_x & 0 & 0 \\ 0 & K_y & 0 \\ 0 & 0 & K_z \end{bmatrix}}_{K} \underbrace{\begin{bmatrix} \dot{x} \\ \dot{y} \\ \dot{z} \end{bmatrix}}_{\dot{P}} = \underbrace{\begin{bmatrix} \tau_x \\ \tau_y \\ \tau_z \end{bmatrix}}_{\tau_P} \tag{4.1}$$

where K is the matrix of drag coefficients of translation, M denotes the quadrotor's mass, τ_x, τ_y and τ_z are virtual control inputs defined as follows:

$$\begin{aligned} \tau_x &= (\cos(\psi)\sin(\theta)\cos(\phi) + \sin(\psi)\sin(\phi))\, \tau_T \\ \tau_y &= (\sin(\psi)\sin(\theta)\cos(\phi) - \cos(\psi)\sin(\phi))\, \tau_T \\ \tau_z &= -Mg + \cos(\theta)\cos(\phi)\tau_T \end{aligned} \tag{4.2}$$

where g denotes the constant of gravity and τ_T is the thrust force, and acts vertically on the quadcopter. Note that the angles ϕ and θ are always assumed to be different from $\pm(\pi/2)$ in order to avoid singularity points in the control law.

As for the dynamic model of the attitude, it is represented as follows (Castillo et al., 2004):

$$\underbrace{\begin{bmatrix} J_{11} & J_{12} & J_{13} \\ J_{21} & J_{22} & J_{23} \\ J_{31} & J_{32} & J_{33} \end{bmatrix}}_{J(\Theta)} \underbrace{\begin{bmatrix} \ddot{\phi} \\ \ddot{\theta} \\ \ddot{\psi} \end{bmatrix}}_{\ddot{\Theta}} + \underbrace{\begin{bmatrix} B_{11} & B_{12} & B_{13} \\ B_{21} & B_{22} & B_{23} \\ B_{31} & B_{32} & B_{33} \end{bmatrix}}_{B(\Theta, \dot{\Theta})} \underbrace{\begin{bmatrix} \dot{\phi} \\ \dot{\theta} \\ \dot{\psi} \end{bmatrix}}_{\dot{\Theta}} = \underbrace{\begin{bmatrix} \tau_\phi \\ \tau_\theta \\ \tau_\psi \end{bmatrix}}_{\tau_\Theta} \tag{4.3}$$

where τ_ϕ, τ_θ and τ_ψ represent respectively the roll, pitch and yaw input torques, $J(\Theta)$ and $B(\Theta, \dot{\Theta})$ are respectively the inertia and the Coriolis matrices where their elements are defined as:

$$
\begin{aligned}
J_{11} =& I_x \\
J_{12} =& J_{21} = 0 \\
J_{13} =& J_{31} = -I_x \sin(\theta) \\
J_{22} =& I_y \cos^2(\phi) + I_z \sin^2(\phi) \\
J_{23} =& J_{32} = \left(I_y - I_z\right) \cos(\theta) \cos(\phi) \sin(\phi) \\
J_{33} =& I_x \sin^2(\theta) + \cos^2(\theta)\left(I_y \sin^2(\phi) + I_z \cos^2(\phi)\right) \\
B_{11} =& 0 \\
B_{12} =& \left(I_y - I_z\right)\left(\dot{\theta} \cos(\phi) \sin(\phi) + \dot{\psi} \cos(\theta)\left(\sin^2(\phi) - \cos^2(\phi)\right)\right) \\
& - I_x \dot{\psi} \cos(\theta) \\
B_{13} =& \left(I_z - I_y\right) \dot{\psi} \cos(\phi) \sin(\phi) \cos^2(\theta) \\
B_{21} =& \left(I_z - I_y\right)\left(\dot{\theta} \cos(\phi) \sin(\phi) + \dot{\psi} \cos(\theta)\left(\sin(\phi) - \cos^2(\phi)\right)\right) \\
& + I_x \dot{\psi} \cos(\theta) \\
B_{22} =& \left(I_z - I_y\right) \dot{\phi} \cos(\phi) \sin(\phi) \\
B_{23} =& \dot{\psi} \sin(\theta) \cos(\theta)\left(-I_x + I_y \sin^2(\phi) + I_z \cos^2(\phi)\right) \\
B_{31} =& \left(I_y - I_z\right) \dot{\psi} \cos(\phi) \sin(\phi) \cos^2(\theta) - I_x \dot{\theta} \cos(\theta) \\
B_{32} =& \left(I_z - I_y\right)\left(\dot{\theta} \sin(\theta) \cos(\phi) \sin(\phi) + \dot{\phi} \cos(\theta)\left(\sin^2(\phi) - \cos^2(\phi)\right)\right) \\
& + \dot{\psi} \cos(\theta) \sin(\theta)\left(I_x - I_y \sin^2(\phi) - I_z \cos^2(\phi)\right) \\
B_{33} =& \dot{\theta} \cos(\theta) \sin(\theta)\left(I_x - I_y \sin^2(\phi) - I_z \sin^2(\phi)\right) \\
& + \left(I_y - I_z\right) \dot{\phi} \sin(\phi) \cos(\phi) \sin^2(\theta)
\end{aligned}
\tag{4.4}
$$

where I_x, I_y and I_z are the moments of inertia. Moreover, the rotor speed w_r is defined by:

$$
w_r = w_1 - w_2 + w_3 - w_4 \tag{4.5}
$$

and is related to the input torques by:

$$\begin{bmatrix} \tau_T \\ \tau_\phi \\ \tau_\theta \\ \tau_\psi \end{bmatrix} = \begin{bmatrix} b & b & b & b \\ bl & -bl & -bl & bl \\ bl & bl & -bl & -bl \\ c & -c & c & -c \end{bmatrix} \begin{bmatrix} w_1^2 \\ w_2^2 \\ w_3^2 \\ w_4^2 \end{bmatrix} \tag{4.6}$$

where b, c and l are respectively the thrust coefficient, the drag coefficient, the distance that separates the rotor and the center of mass.

4.4 Model-Based Switching Functions with Fixed-Time SM Design

In this section, a nonlinear fixed-time sliding mode controller with model-based switching functions will be designed to ensure a robust flight for quadrotor system. For the design procedure, the following useful Lemma is presented:

Lemma 1. (Refer to Zuo (2015)) Consider a nonlinear system defined by:

$$\dot{S}(x) = -\mu_1 |S(x)|^{\nu_1} sign(S(x)) - \mu_2 |S(x)|^{\nu_2} sign(S(x)), \;\; S(0) = s_0 \tag{4.7}$$

where $\mu_1 > 0, \mu_2 > 0\, \nu_1 > 1$ and $\nu_2 \in (0, 1)$. Then, the considered system is practical fixed-time stable and the maximal required time to reach the equilibrium point is defined as follows:

$$T_{R_{max}} = \frac{1}{\mu_1(\nu_1 - 1)} + \frac{1}{\mu_2(1 - \nu_2)} \tag{4.8}$$

4.4.1 Position Controller Design

Let us design the position model-based sliding functions as follows:

$$\begin{aligned} S_P =& M\dot{E}_P + (K+\beta_1)E_P + \beta_2 \int_0^t E_P dt \\ =& M(\dot{P} - \dot{P}^d) + (K+\beta_1)(P - P^d) + \beta_2 \int_0^t (P - P^d)dt \end{aligned} \tag{4.9}$$

where $E_P = P - P^d \in R^3$ is the position tracking error vector with $P^d = \left[x^d, y^d, z^d\right]^T$ is the desired position vector and β_1 and β_2 are (3×3) diagonal matrices where the elements are strictly positive constants.

The aim of the proposed approach is to ensure robustness, fixed-time convergence of the model-based sliding functions to zero and to produce lower chattering. To this end, the following reaching law structure is selected:

$$\dot{S}_P = -K_1 \text{sig}^{\alpha_1}(S_P) - K_2 \text{sig}^{\alpha_2}(S_P) \tag{4.10}$$

where $K_1 = diag(K_{11}, K_{12}, K_{13})$ and $K_2 = diag(K_{21}, K_{22}, K_{23})$ are diagonal positive matrices, $\text{sig}^{\alpha_i}(S) = \left[|S_{P1}|^{\alpha_{i1}} \text{sign}(S_{P1}), \cdots, |E_{P3}|^{\alpha_{i3}} \text{sign}(S_{P3})\right]^T$ for $i = 1, 2$ with $\text{sign}(S_{Pj})$, α_{1j} and α_{2j} for $j = 1, 2, 3$ are defined by:

$$\text{sign}(S_{Pj}) = \begin{cases} 1, & if\ S_{Pj} > 0 \\ 0, & if\ S_{Pj} = 0 \\ -1, & if\ S_{Pj} < 0 \end{cases} \tag{4.11}$$

$$\alpha_{1j} = 0.5(\alpha_{1j}^* + 1) + 0.5(\alpha_{1j}^* - 1)\text{sign}(|S_{Pj}| - 1) \tag{4.12}$$

$$\alpha_{2j} = 0.5(1 + \alpha_{2j}^*) + 0.5(1 - \alpha_{2j}^*)\text{sign}(|S_{Pj}| - 1) \tag{4.13}$$

where $\alpha_{1j}^* > 1$ and $0.5 < \alpha_{2j}^* < 1$. To compute the expression of the position control law, let us compute $\dot{S}_P$ based on Equation (4.9) and using the dynamic model of the position given in (4.1)

as follows:

$$\begin{aligned}\dot{S}_P =& M\ddot{E}_P + (K+\beta_1)\dot{E}_P + \beta_2 E_P \\ =& M(\ddot{P} - \ddot{P}^d) + K(\dot{P} - \dot{P}^d) + \beta_1 \dot{E}_P + \beta_2 E_P \\ =& \tau_P - M\ddot{P}^d - K\dot{P}^d + \beta_1 \dot{E}_P + \beta_2 E_P\end{aligned} \tag{4.14}$$

Finally, the combination of the equations (4.10) and (4.14) leads to the following proposed fixed-time SM position control with model-based sliding functions:

$$\tau_P = M\ddot{P}^d + K\dot{P}^d - \beta_1 \dot{E}_P - \beta_2 E_P - K_1 \text{sig}^{\alpha_1}(S_P) - K_2 \text{sig}^{\alpha_2}(S_P) \tag{4.15}$$

Hence, the total force τ_T is obtained as follows:

$$\tau_T = \sqrt{\tau_x^2 + \tau_y^2 + (\tau_z + Mg)^2} \tag{4.16}$$

Theorem 1 Consider the position dynamic model of the quadrotor given in (4.1), the developed control law (4.15) ensures the convergence of the model-based sliding functions to zero in a fixed-time for $j = 1, 2, 3$ by:

$$T_{R_P,j} \leq \frac{1}{K_{1j}(\alpha_{1j} - 1)} + \frac{1}{K_{2j}(1 - \alpha_{2j})} \tag{4.17}$$

Proof. This demonstration presents the stability analysis of the overall system. Hence, a definite-positive Lyapunov function is selected and it's first time derivative is calculated as:

$$V_P = 0.5\, S_P^T\, S_p \tag{4.18}$$

$$\begin{aligned}\dot{V}_P &= S_P^T\, \dot{S}_p \\ &= S_P^T \left(\tau_P - M\ddot{P}^d - K\dot{P}^d + \beta_1 \dot{E}_P + \beta_2 E_P\right)\end{aligned} \tag{4.19}$$

Substituting τ_P by its expression (4.15) in the above equation gives:

$$\begin{aligned}\dot{V}_P &= S_P^T\big(-{K_1}^{\alpha_1}(S_P) - K_2\mathrm{sig}^{\alpha_2}(S_P)\big)\\ &= \sum_{j=1}^{3} S_{Pj}\big(-K_{1j}|S_{Pj}|^{\alpha_{1j}}\mathrm{sign}(S_{Pj}) - K_{2j}|S_{Pj}|^{\alpha_{2j}}\mathrm{sign}(S_{Pj})\big)\\ &= \sum_{j=1}^{3} -K_{1j}|S_{Pj}|^{1+\alpha_{1j}} - K_{2j}|S_{Pj}|^{1+\alpha_{2j}} \leq 0\end{aligned} \tag{4.20}$$

Hence, it is clear from the above equation that the closed-loop system is stable. Otherwise, based on equation (4.10) and **Lemma 1**, the used model-based sliding functions (4.9) are fixed-time stable. In other words, S_P converges to zero in a fixed-time that is independent of its initial value and depends only on the reaching law gains.

4.4.2 Attitude Controller Design

The objective here is to control the attitude states to their respective desired trajectories. The desired roll and pitch angles are generated from the virtual controllers (Alqaisi et al., 2020) as follows:

$$\begin{aligned}\phi_d &= \arctan\left(\cos(\theta_d)\left(\frac{\tau_x\sin(\psi_d) - \tau_y\cos(\psi_d)}{\tau_z + Mg}\right)\right)\\ \theta_d &= \arctan\left(\frac{\tau_x\cos(\psi_d) + \tau_y\sin(\psi_d)}{\tau_z + Mg}\right)\end{aligned} \tag{4.21}$$

In this part, the above used procedure will be adopted for the attitude tracking. The attitude model-based switching function is given as follows:

$$\begin{aligned}S_\Theta =& J(\Theta)\dot{E}_\Theta + \lambda_1 E_\Theta + \lambda_2\int_0^t E_\Theta dt - \int_0^t \left(F(\Theta,\dot{\Theta}) + B(\Theta,\dot{\Theta})\right)\dot{\Theta}dt\\ &+ \int_0^t \left(F(\Theta^d,\dot{\Theta}^d) + B(\Theta^d,\dot{\Theta}^d)\right)\dot{\Theta}^d dt\\ =& J(\Theta)(\dot{\Theta} - \dot{\Theta}^d) + \lambda_1 E_\Theta + \lambda_2\int_0^t E_\Theta dt - \int_0^t \left(F(\Theta,\dot{\Theta}) + B(\Theta,\dot{\Theta})\right)\dot{\Theta}dt\\ &+ \int_0^t \left(F(\Theta^d,\dot{\Theta}^d) + B(\Theta^d,\dot{\Theta}^d)\right)\dot{\Theta}^d dt\end{aligned} \tag{4.22}$$

where $E_\Theta = \Theta - \Theta^d \in R^3$ is the orientation tracking error vector with $\Theta^d = \left[\phi^d, \theta^d, \psi^d\right]^T$ is the desired Euler angles vector and λ_1 and λ_2 are (3×3) diagonal matrices where the elements are strictly positive constants and the matrix $F(\Theta, \dot{\Theta})$ is defined by:

$$F(\Theta, \dot{\Theta}) = \dot{J}(\Theta) - 2B(\Theta, \dot{\Theta}) \tag{4.23}$$

Hence, the derivative of S_Θ is computed as:

$$\begin{aligned}
\dot{S}_\Theta =& J(\Theta)\ddot{E}_\Theta + \dot{J}(\Theta)\dot{E}_\Theta + \lambda_1\dot{E}_\Theta + \lambda_2 E_\Theta - \left(F(\Theta, \dot{\Theta}) + B(\Theta, \dot{\Theta})\right)\dot{\Theta} \\
&+ \left(F(\Theta^d, \dot{\Theta}^d) + B(\Theta^d, \dot{\Theta}^d)\right)\dot{\Theta}^d \\
=& J(\Theta)(\ddot{\Theta} - \ddot{\Theta}^d) + \lambda_1\dot{E}_\Theta + \lambda_2 E_\Theta + B(\Theta, \dot{\Theta})\dot{\Theta} - B(\Theta^d, \dot{\Theta}^d)\dot{\Theta}^d \\
=& \tau_\Theta - J\ddot{\Theta}^d + \lambda_1\dot{E}_\Theta + \lambda_2 E_\Theta - B(\Theta^d, \dot{\Theta}^d)\dot{\Theta}^d
\end{aligned} \tag{4.24}$$

Otherwise, the selected fixed-time SM algorithm is given by:

$$\dot{S}_\Theta = -L_1 \mathrm{sig}^{\gamma_1}(S_\Theta) - L_2 \mathrm{sig}^{\gamma_2}(S_\Theta) \tag{4.25}$$

where $L_1 = diag(L_{11}, L_{12}, L_{13})$ and $L_2 = diag(L_{21}, L_{22}, L_{23})$ are diagonal positive matrices, $\mathrm{sig}^{\gamma_i}(S) = \left[|S_{\Theta 1}|^{\gamma_{i1}}\mathrm{sign}(S_{\Theta 1}), \cdots, |E_{\Theta 3}|^{\gamma_{i3}}\mathrm{sign}(S_{\Theta 3})\right]^T$ for $i = 1, 2$ with γ_{1j} and γ_{2j} for $j = 1, 2, 3$ are defined by:

$$\gamma_{1j} = 0.5(\gamma^*_{1j} + 1) + 0.5(\gamma^*_{1j} - 1)\mathrm{sign}(|S_{\Theta j}| - 1) \tag{4.26}$$

$$\gamma_{2j} = 0.5(1 + \gamma^*_{2j}) + 0.5(1 - \gamma^*_{2j})\mathrm{sign}(|S_{\Theta j}| - 1) \tag{4.27}$$

where $\gamma^*_{1j} > 1$ and $0.5 < \gamma^*_{2j} < 1$. Finally, combining equations (4.24) and (4.25) gives:

$$\tau_\Theta = J(\Theta)\ddot{\Theta}^d + B(\Theta^d, \dot{\Theta}^d)\dot{\Theta}^d - \lambda_1\dot{E}_\Theta - \lambda_2 E_\Theta - L_1 \mathrm{sig}^{\gamma_1}(S_\Theta) - L_2 \mathrm{sig}^{\gamma_2}(S_\Theta) \tag{4.28}$$

Theorem 2. Consider the attitude dynamic model of the quadrotor UAV system given in (4.3), the proposed control law (4.28) ensures the convergence of the model-based sliding functions to zero in a fixed-time given for $j = 1, 2, 3$ by:

$$T_{R\Theta,j} \leq \frac{1}{L_{1j}(\gamma_{1j} - 1)} + \frac{1}{L_{2j}(1 - \gamma_{2j})} \tag{4.29}$$

Proof. The proof of this theorem is similar to the one of position control. Hence, consider the following definite-positive Lyapunov function:

$$V_\Theta = 0.5\, S_\Theta^T\, S_\Theta \tag{4.30}$$

The derivative of the above function is computed as:

$$\begin{aligned} \dot{V}_\Theta &= S_\Theta^T\, \dot{S}_\Theta \\ &= S_\Theta^T \left(\tau_\Theta - J\ddot{\Theta}^d + \lambda_1 \dot{E}_\Theta + \lambda_2 E_\Theta - B(\Theta^d, \dot{\Theta}^d)\dot{\Theta}^d \right) \end{aligned} \tag{4.31}$$

Substituting τ_Θ by its expression (4.27) in the above equation gives:

$$\begin{aligned} \dot{V}_\Theta &= S_\Theta^T \big(- L_1{}^{\gamma_1}(S_\Theta) - L_2 \mathrm{sig}^{\gamma_2}(S_\Theta) \big) \\ &= \sum_{j=1}^{3} S_{\Theta j} \big(- L_{1j} |S_{\Theta j}|^{\gamma_{1j}} \mathrm{sign}(S_{\Theta j}) - L_{2j} |S_{\Theta j}|^{\gamma_{2j}} \mathrm{sign}(S_{\Theta j}) \big) \\ &= \sum_{j=1}^{3} -L_{1j} |S_{\Theta j}|^{1+\gamma_{1j}} - L_{2j} |S_{\Theta j}|^{1+\gamma_{2j}} \leq 0 \end{aligned} \tag{4.32}$$

Hence, above equation clearly demonstrates the stability of closed-loop system. Finally, the block diagram of the closed-loop system is represented in Figure 4.2.

4.5 Experimental Case Study

In this section, the performance of the developed fixed-time SM controller is experimentally validated. The used quadrotor is the Parrot rolling spider minidrone that has the physical

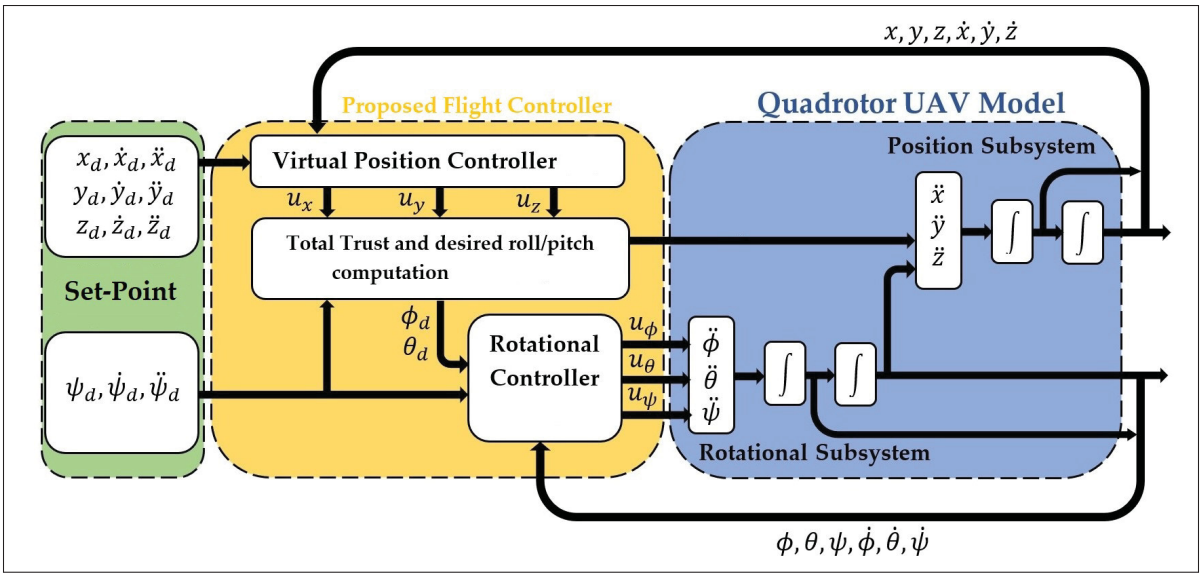

Figure 4.2 Closed-loop block diagram of the proposed flight control system

parameters given in Table 4.1 (Alqaisi et al., 2020) is equipped by an Inertial Measurement Unit (IMU) with a three-axis gyroscope, three-axis accelerometer, a compass, an altitude sonar and pressure sensors. The Parrot company and the Massachusetts Institute of Technology developed the used Simulink support package for PARROT minidrone. The latter makes the task of building and deploying flight control system easy following the implementation workflow depicted in Figure 4.3. Further details can be found in (Alqaisi et al., 2020). Notice that the drag coefficients K_x, K_y and K_z are not easily obtained in practical work. Hence, they form a bounded unknown dynamics. The experimental setup including the Parrot rolling spider minidrone and its work environement are depicted in Figure 4.4.

Table 4.1 Physical parameters of the studied quadcopter UAV

Parameter	**value**
mass: M	0.068 Kg
gravity: g	9.81 m/s^2
moment of inertia: I_x	0.068 10^{-3} Kg.m^2
moment of inertia: I_y	0.092 10^{-3} Kg.m^2
moment of inertia: I_z	0.136 10^{-3} Kg.m^2

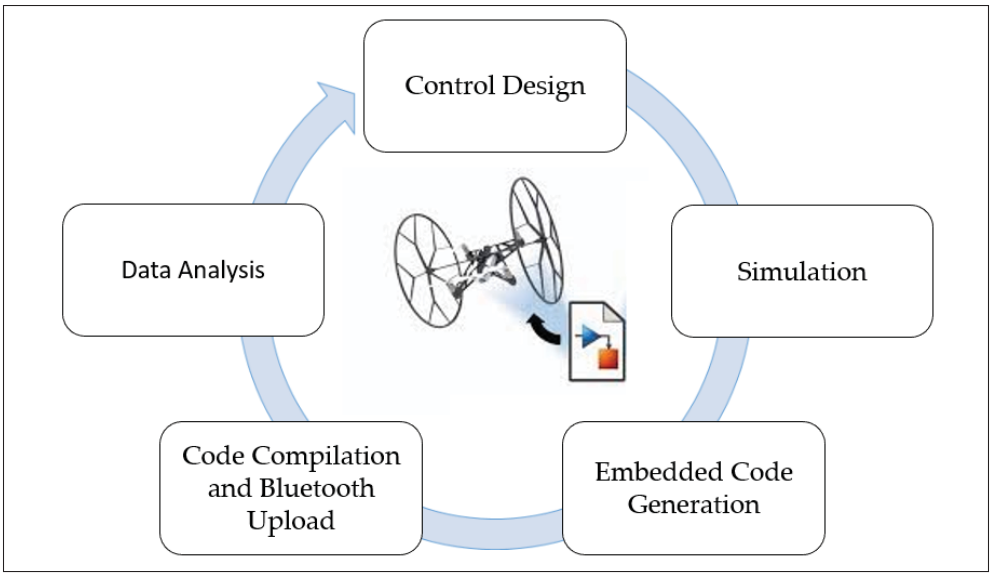

Figure 4.3 Implementation workflow

The purpose of this case study is to validate that the position and the heading of the quadcopter converge to the following setpoint references:

$$x_d = 0\text{ m},\ y_d = 0\text{ m},\ z_d = 1\text{ m},\ \psi_d = 0\text{ rad} \tag{4.33}$$

while the initial positions and angles are respectively $x(0) = y(0) = z(0) = 0$ m and $\phi(0) = \theta(0) = \psi(0) = 0$ rad. The above set-point references feature a typical hovering behavior at an altitude of 1 meter, with no displacement on the (x,y) plane, and all while keeping the drone's heading constant. During this scenario, the controller gains are tuned manually based on trial

Table 4.2 Controller gains

Gain	Selected value	Gain	Selected value
β_1	$diag(3,3,5)$	λ_1	$diag(.2,.2,.2)$
β_2	0.8	λ_2	$diag(.01,.01,.01)$
α^*_{1j}	$1.8 for\ j = 1,2,3$	γ^*_{1j}	$3 for\ j = 1,2,3$
α^*_{2j}	$0.85 for\ j = 1,2,3$	γ^*_{2j}	$0.85 for\ j = 1,2,3$
K_1	$diag(1,1,.1)$	L_1	$diag(.01,.01,.01)$
K_2	$diag(1,1,.5)$	L_2	$diag(.1,.1,.6)$

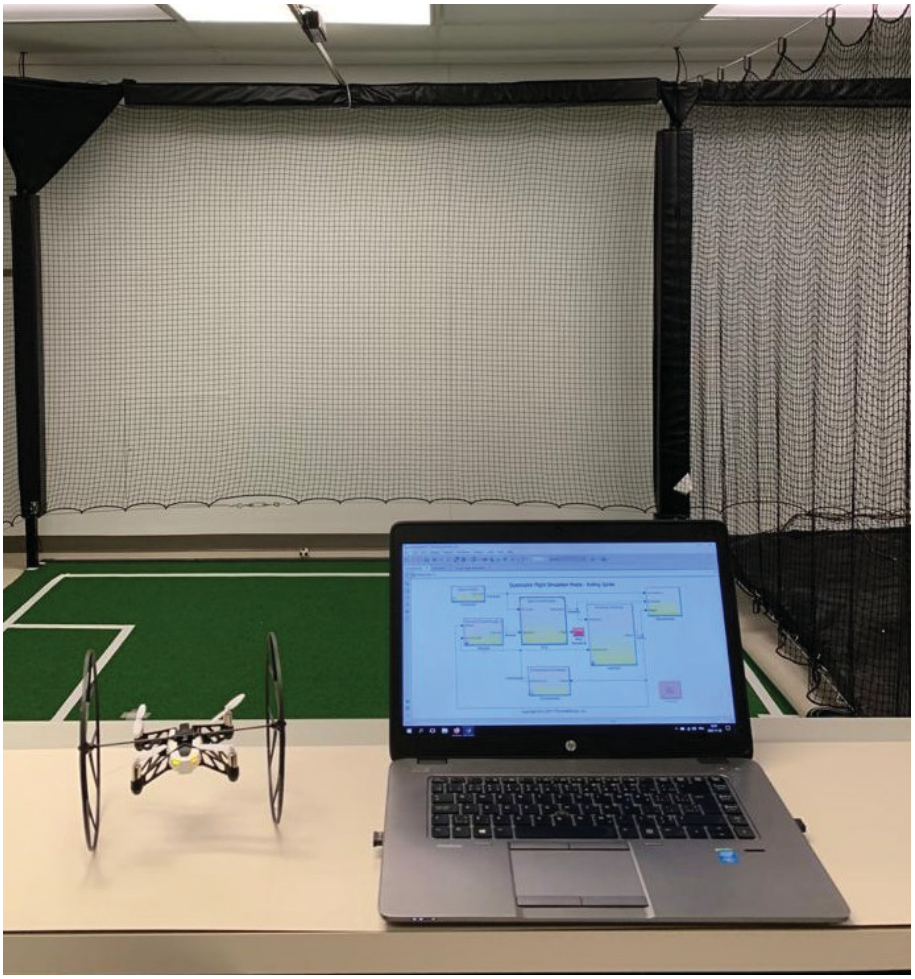

Figure 4.4 Experimental Setup

and error method while ensuring the stability conditions and then fixed as in Table 4.2. Moreover, the quadcopter feedback for the control system is managed as: the minidrone's IMU which ensures the measurement of the translational accelerations in the body frame $\ddot{P}_B = [\ddot{x}_B, \ddot{y}_B, \ddot{z}_B]^T$. The translational acceleration $\ddot{P} = [\ddot{x}, \ddot{y}, \ddot{z}]^T$, velocity $\dot{P} = [\dot{x}, \dot{y}, \dot{z}]^T$ and position $P = [x, y, z]^T$ defined in the inertial frame are computed as follows:

$$\ddot{P} = R\,\ddot{P}_B, \quad \dot{P} = R\left[\int_a^b \frac{1}{M}F + \dot{P}_B + \Omega\right], \quad P = \frac{0.01\tau}{z-1}\dot{P} \tag{4.34}$$

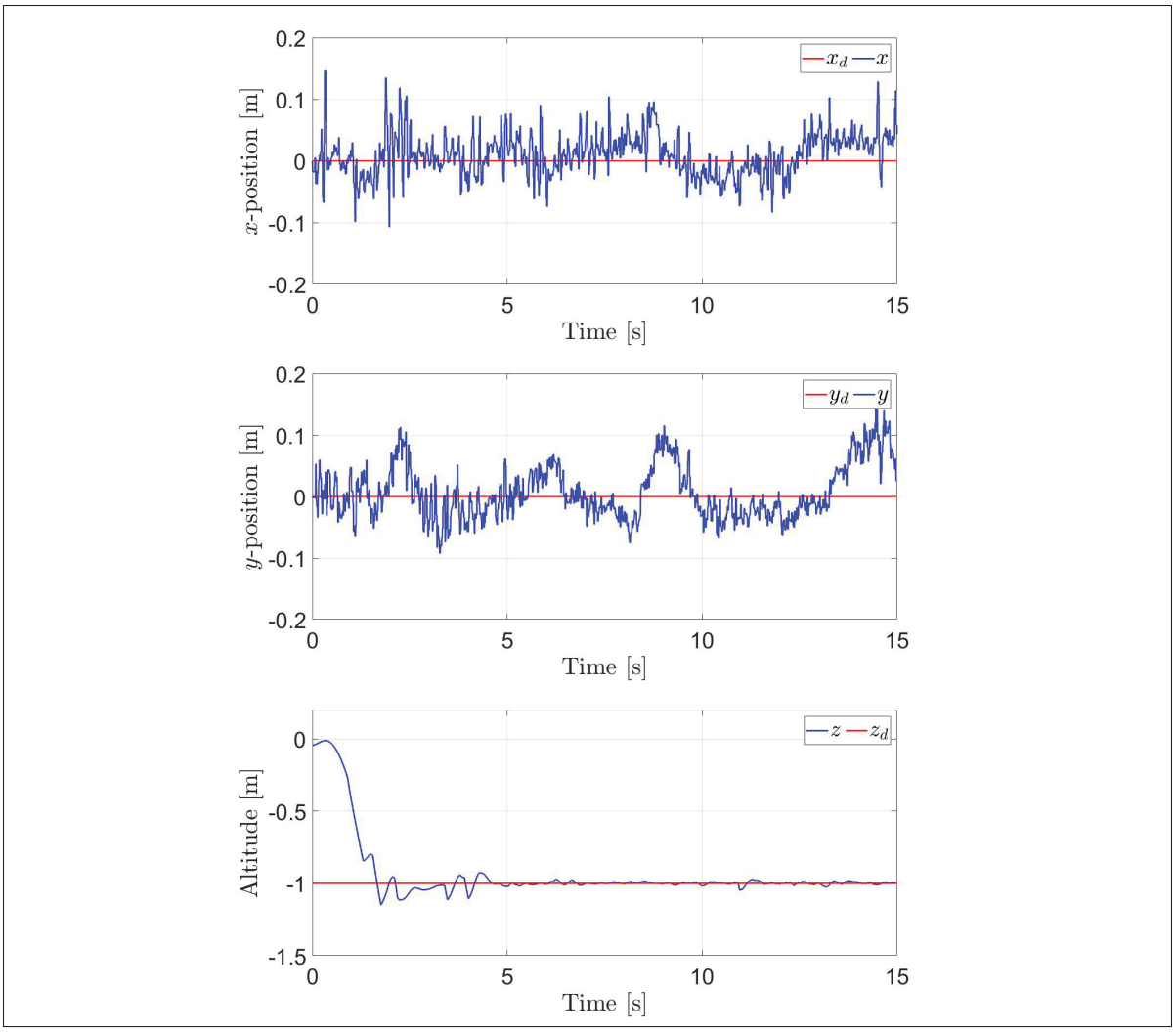

Figure 4.5 Spatial setpoint Position Tracking Performance

where R is the matrix of rotation defined in (Castillo et al., 2004), F represents the applied forces in the quadrotor's body, $\dot{P}_B$ is the velocity in the body frame and Ω is the body-fixed frame angular velocity vector.

Table 4.3 Position setpoint error peak and RMS values

Position	**RMS Error (m)**	**Peak Error (m)**
x	0.035	0.13
y	0.047	0.16
z	0.01	0.05

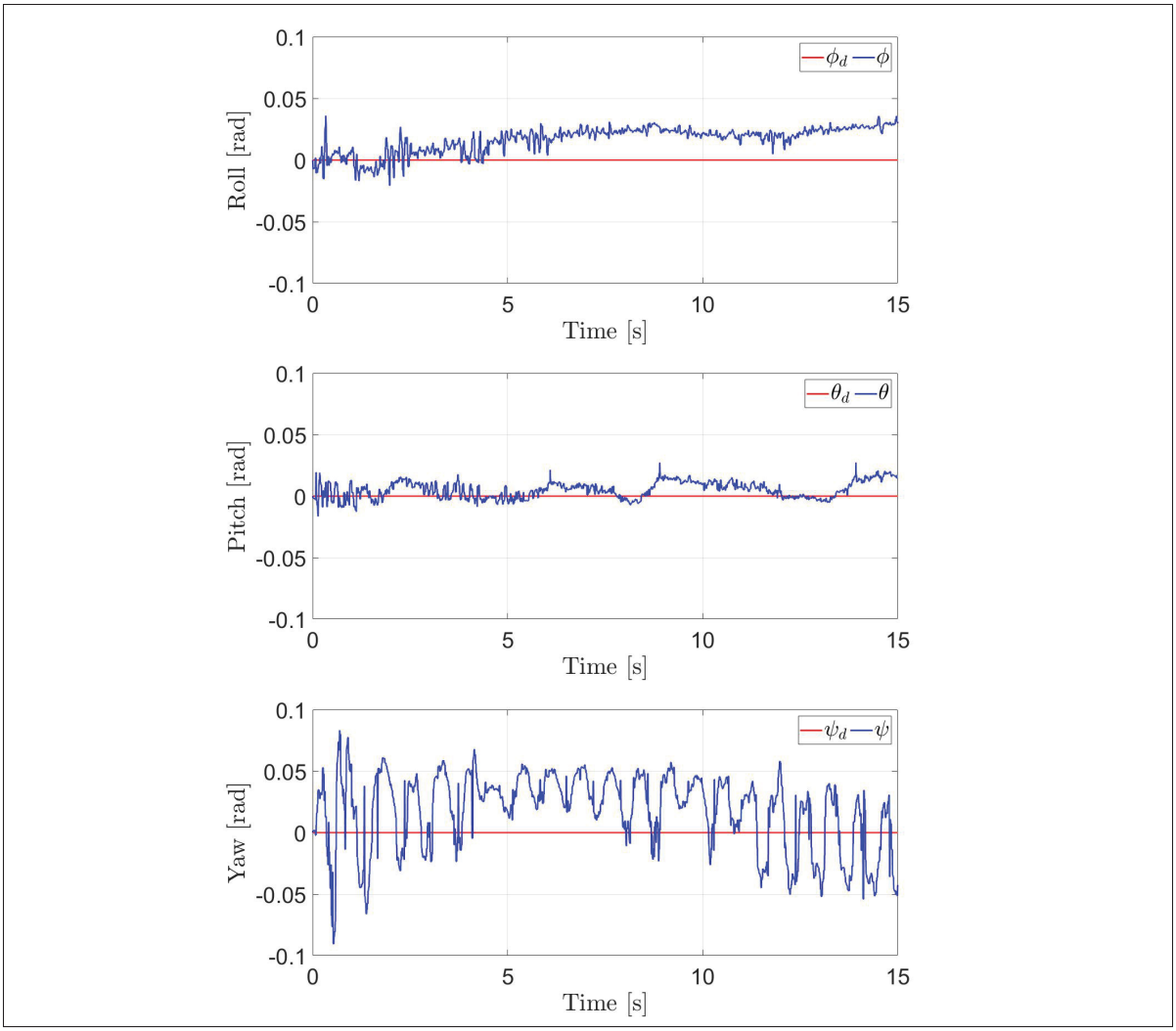

Figure 4.6 Attitude setpoint Tracking Performance

Table 4.4 Attitude Setpoint Error Peak and RMS Values

Attitude	**RMS Error (rad)**	**Peak Error (rad)**
ϕ	0.02	0.03
θ	0.009	0.027
ψ	0.034	0.058

Experimental results are shown in figures 4.5 to 4.7, as it can be seen that the stabilization of the hovering setpoint of the quadcopter has been achieved with a good level of precision on the

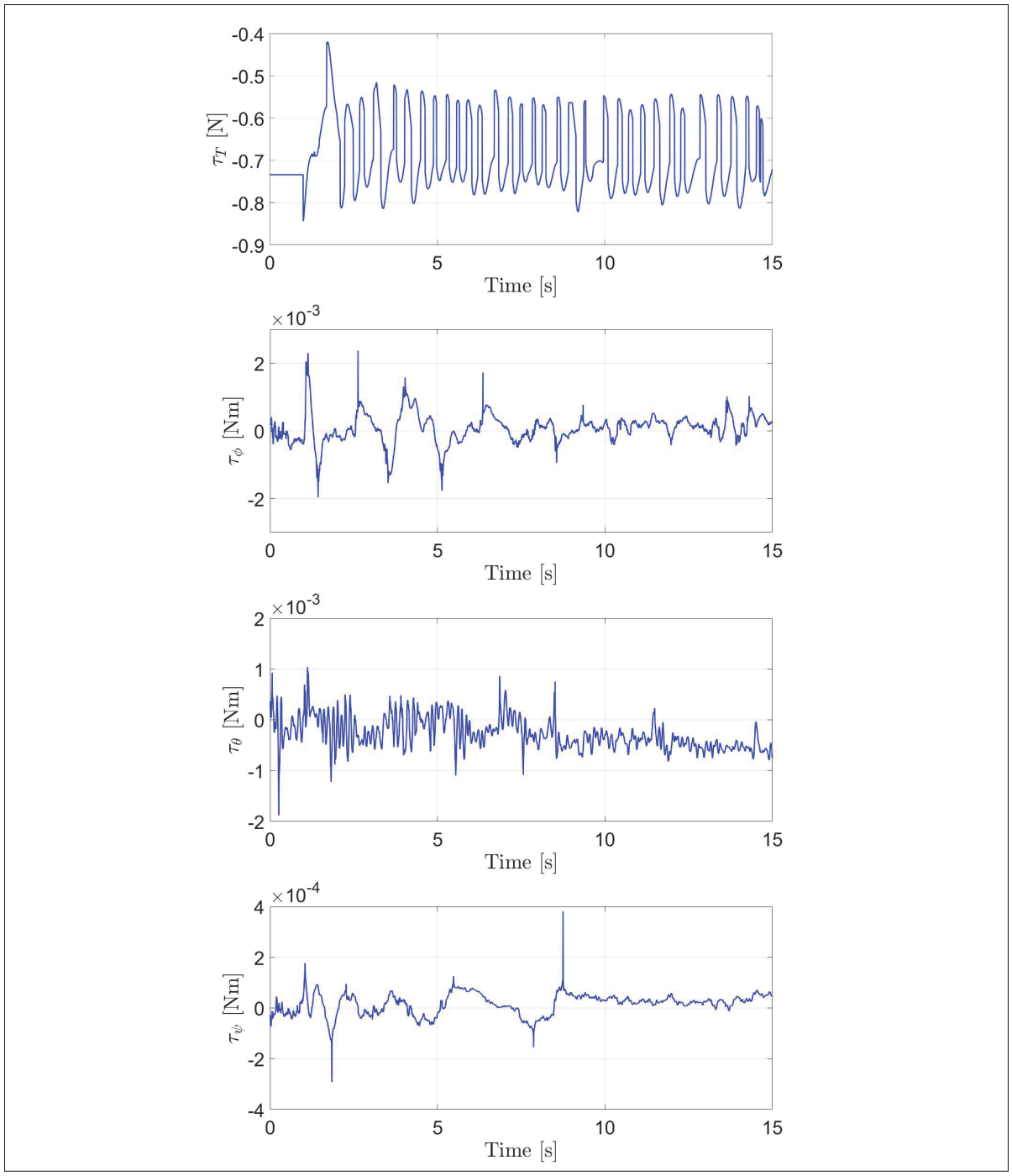

Figure 4.7 Torques Control Inputs for Thrust and Attitude Control

position and attitude as per figures 4.5 and 4.6. Notice that in this experimental case, the z_B of the reference is facing down, that is why the z^d is -1 and the total thrust is negative. Tables 4.3

and 4.4 display the setpoint peak and RMS errors for the position and attitude, respectively. This shows that the setpoint tracking is achievable with a good level of precision and with minimal control torque variation, especially for the inner-loop torques τ_ϕ, τ_θ and τ_ψ. Indeed, as per Figure 4.7, the variation of τ_ϕ is between $[-2\,10^{-3}, 2\,10^{-3}]$ Nm, τ_θ is between $[-1\,10^{-3}, 1\,10^{-3}]$ Nm, and τ_ψ is between $[-4\,10^{-4}, 4\,10^{-4}]$ Nm. This therefore experimentally validates the model-based switching functions approach in terms of torques simplification while keeping the required tracking performance of the attitude and position of the quadcopter.

4.6 Conclusion

In this paper, an experimental validation of a sliding mode controller using model-based switching functions has been successfully achieved on a quadcopter UAV. The experimental results have shown very good stabilization performance for a hovering position setpoint, while maintaining low activity levels on the inner-loop torques inputs. Future work on the quadcopter will include an experimental implementation of trajectory tracking sliding mode control with the model-based switching functions and performance comparison with a conventional sliding mode controller.

CHAPTER 5

SLIDING MODE CONTROL WITH MODEL-BASED SWITCHING FUNCTIONS APPLIED ON A 7-DOF EXOSKELETON ARM

Charles Fallaha[1] , Maarouf Saad[1] , Jawhar Ghommam[2] , Yassine Kali[1]

[1] Department of electrical engineering, École de Technologie Supérieure,
1100 Notre-Dame Ouest, Montréal, Québec, Canada H3C 1K3
[2] Department of computer and electrical engineering, Sultan Quaboos University
Muscat 123, Oman

Article published in the journal « IEEE/ASME Transactions on Mechatronics »
in November 2020.

5.1 Abstract

This paper features a novel sliding mode controller for robotic arms using nonlinear model-based switching functions. The new controller is experimentally validated on a 7-DOF exoskeleton arm used for upper-limb rehabilitation applications. The proposed approach features a novel concept using model-based switching functions in the sliding mode controller, which leads to considerable simplifications on the torque control inputs. Compared to conventional linear switching functions, model-based switching functions show substantial control performance improvements on the torque inputs, such as transient constraints reduction and enhanced robustness, while maintaining a very good tracking performance. Moreover, model-based switching functions design ensures a complete decoupling of chattering effect between joint axes. Furthermore, this approach can be combined with existing chattering reduction techniques to ensure proper control of chattering levels on the torque inputs. These advantages make the practical implementation of the model-based switching functions approach particularly desirable for wearable robotics, where smooth movements and high accuracy are important requirements for patients' comfort and security.

Sliding Mode Control, Exoskeleton, upper-limb, Robot, Model-Based Switching Functions, Chattering, Robust Control.

5.2 Introduction

The last decade has known a tremendous growth and diversification in robotics systems, which has been mainly supported by recent advances, accessibility and affordability of robotics technology. CPU computing power is increasing, sensors are getting smaller and cheaper, and robotic applications programming is becoming easier and more accessible. By the end of 2025, the global robotics market is expected to reach 87 billion US dollars (Wolfgang et al., 2017). The commercial robotics market, including services and healthcare applications, will be valued by then at approximately 23 billion dollars, in which biomedical robotics will take an important part.

Within the biomedical robotics segment, the wearable robotics market, and more specifically exoskeleton devices market, is expected to undergo a steady growth during the next decade. In 2019, the global exoskeleton market was valued at 626.3 million US dollars, in which healthcare exoskeletons took the largest share (Grand View Research, 2020). This valuation had almost quintupled from 2017 (BIS research, 2018). This is therefore triggering extensive research for exoskeleton design optimization and control.

Upper-limb exoskeletons are a very popular type of exoskeletons that are widely studied in literature. They are mainly used for upper-limb sports injuries or to treat patients that have undergone stroke incidents resulting in upper-limb impairments. Scientific literature presents various upper-limb exoskeleton structures, control strategies and technologies integration. The authors in (Perry et al., 2007) have designed a cable-actuated exoskeleton arm. In (Tsagarakis and Caldwell, 2003), pneumatic actuators are used for the upper-limb exoskeleton structure to emulate the mechanical and dynamic structure of human upper-limb muscles. Recent advances in virtual reality (VR) and augmented reality (AR) also allow for an effective integration of these technologies for human-in-the-loop exoskeleton controllers (Frisoli et al., 2009). Haptic feedback and dynamic admittance control (Li et al., 2018) are also control strategies that give patients realistic interactions and contact sensations and need to follow specific mechanical structures requirements (Gupta and O'Malley, 2006). Biological signals such as measured

Electromyogram (EMG) signals can be used as well to control actuator movements of the exoskeleton arm (Lucas et al., 2004).

Although simple linear control strategies such as PIDs can be used for upper limb exoskeleton control (Yu and Rosen, 2010), they lack overall robustness in practical implementations (Incremona et al., 2017). This paper proposes a robust nonlinear control strategy study on an experimental upper-limb 7-DOF exoskeleton prototype named Motion Assistive Robotic-Exoskeleton for Superior Extremity (ETS-MARSE) (Rahman et al., 2012, 2014*a*,*b*; Ochoa Luna et al., 2015). ETS-MARSE has been designed to provide effective rehabilitation therapy for patients that have suffered upper-limb impairment and is currently being used for this purpose. ETS-MARSE comprises a shoulder motion support part, an elbow and forearm motion support part, and a wrist motion support part. All these parts are directly driven by electrical actuators and rigid gearing systems.

The nonlinear control strategy of ETS-MARSE presented in this paper is based on the sliding mode control approach, which has been widely used for controlling nonlinear systems. The inherent robustness properties of sliding mode control remove the need of adding adaptive algorithms to the control loop (Slotine and Li, 1991). Sliding mode control can be applied to a wide range of dynamic SISO or MIMO systems and has been recently applied on numerous robotic and mechatronic systems (Roy et al., 2019; Wang et al., 2019; Temporelli et al., 2019). Sliding mode control can also be combined with other nonlinear control techniques for robotic arms control (Incremona et al., 2017).

The main downside of conventional sliding mode control is the chattering phenomenon existing on the control input signals. This chattering effect is due to a discontinuous term used in the construction of the control law input. Numerous approaches have been proposed to address this problem. the boundary layer approach (Slotine and Li, 1991) smoothens the discontinuous term by replacing the signum function with a saturation function. Gao and Hung (1993); Camacho et al. (1999) and more recently Fallaha et al. (2011) have explored nonlinear reaching laws that reduce the discontinuous gain when the system approaches the sliding surface. Levant (1993)

have used higher-order sliding mode (HOSM) to eliminate chattering. This approach requires however the implementation of higher order observers in its traditional implementation. Several authors (Hamerlain et al., 2007; Bartolini et al., 2000; Parra-Vega and Hirzinger, 2001) have explored a particular case of HOSM, namely second-order sliding mode. Sivaramakrishnan et al. (2015) proposed a third order sliding mode control. More recently, a variant of HOSM, the super-twisting algorithm, has been proposed by Moreno and Osorio (2008) and studied further by Floquet and Barbot (2007) and Gonzalez et al. (2012).

Conventional sliding mode control forces the system's closed loop dynamics to vary on a linear switching surface that guarantees the convergence of the tracking error to 0. Some developments can be found in literature in which nonlinear switching functions such as Terminal Sliding Mode (TSM) control (Tang, 1998) are used mainly to improve the dynamic performance of the tracking error. This paper introduces therefore a novel concept in sliding mode control applied to robotic systems, whereby traditional linear switching functions are replaced by nonlinear model-based switching functions. Model-based switching functions substantially simplify the expression of the torque control inputs, while ensuring trajectory tracking asymptotic convergence on the switching surface. This leads to transient constraints reduction on the control input, as well as a complete chattering decoupling on all joint axes. This improvement prevents against premature failures of actuating components in the system, and avoids unaccounted for fast dynamics behaviour in the closed-loop system. Experimental results on ETS-MARSE show that the proposed approach leads to an improved tracking performance with lower torque control inputs variance compared to conventional sliding mode approach. The proposed approach can furthermore be combined with known chattering reduction techniques and optimal control strategies such as Model Predictive Control (MPC) for practical implementation (Dai et al., 2020; Incremona et al., 2017).

To the best knowledge of the authors, the original contributions of this paper are summarized into the following points:

1. A novel approach for designing nonlinear switching functions based on any robotic structure model and focuses on the design of trajectory tracking switching functions. This ensures

considerable simplifications on the torques control law, while providing asymptotic stability of the state error. These simplifications lead to a linear relationship of the torque inputs with regards to the joints errors and error rates. This approach reduces control inputs activity while keeping excellent tracking performance and robustness, as shown in the experimental results. Moreover, the proposed approach ensures a complete decoupling of the chattering on all joint axes, which represents an important advantage compared to typical sliding mode control.

2. A novel general expression of a relationship on the gravity term of the robot's dynamic model ((5.12), (5.33)). This relationship leads to the formulation of a stability criterion on the controller's parameters. This relationship is also useful into extending the validation of the robot's dynamic model to the gravity term.

The paper is structured as follows: In section 5.3 the ETS-MARSE Exoskeleton structure, kinematic and inertial parameters are presented. In section III, conventional sliding mode control is applied on robotic systems and the problem statement is formulated. Section IV details model-based switching functions design for both the set point and the trajectory tracking problems and highlights the contributions of the proposed approach. Section V describes the experimental setup of ETS-MARSE and presents real-time results of the proposed approach. Section VI concludes the paper.

5.3 ETS-MARSE 7-DOF Exoskeleton Characterization

ETS-MARSE is a redundant 7-DOF robot prototype designed to ease upper-limb movement of physically disabled individuals with impaired upper-limb function. ETS-MARSE could be used for rehabilitation therapies of patients who have experienced sports injuries or stroke incidents that left their upper-limbs impaired. Fig. 5.1 shows the 7 actuation joints with the joint axes assignation following the modified Denavit-Hartenberg (DH) convention (Craig, 2005). The correspondent modified DH parameters can be derived as shown in Table 5.1 below. The design of ETS-MARSE emulates the anatomy of the human's upper-limb with the known 7 degrees of

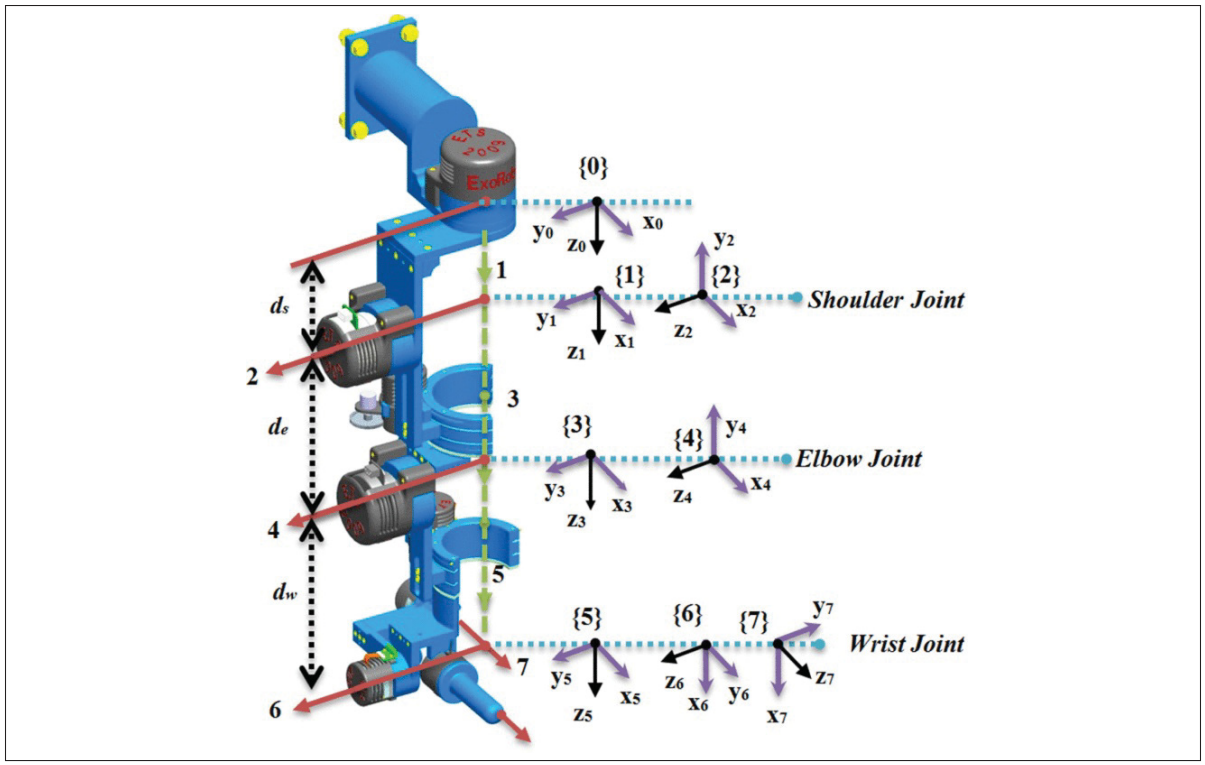

Figure 5.1 ETS-MARSE Structure and Reference Frames Assignation

movement, with the objective of providing the user a representative and ergonomic experience during therapy sessions.

Table 5.1 Modified DH Parameters of ETS-MARSE

Joint (i)	α_{i-1} **(rad)**	a_{i-1} **(m)**	d_i **(m)**	θ_i **(rad)**
1	0	0	d_s	θ_1
2	-$\pi/2$	0	0	θ_2
3	$\pi/2$	0	d_e	θ_3
4	-$\pi/2$	0	0	θ_4
5	$\pi/2$	0	d_w	θ_5
6	-$\pi/2$	0	0	$\theta_6 - \pi/2$
7	-$\pi/2$	0	0	θ_7

As depicted in Fig. 5.1, the shoulder motion consists of three joints, the elbow motion comprises one joint, and finally the wrist motion consists of three joints.

Table 5.2 characterizes the total workspace of ETS-MARSE by detailing the motion intervals of each joint. ETS-MARSE has a relatively small footprint structure and a remarkably high-power density with regards to weight, which considerably eases its installation, handling and operation. The measured weight and inertial parameters of ETS-MARSE are displayed in Table 5.3. ETS-MARSE can operate in passive motion mode (supports entirely the subject's upper-limb motion) and in active motion mode (uses force sensors (Rahman et al., 2014*a*; Ochoa Luna et al., 2015), or EMG (Rahman et al., 2014*b*) feedback signals to accompany and assist the subject's upper-limb motion).

Table 5.2 Physical workspace limits of ETS-MARSE

Joint (i)	**Motion**	**Workspace**
1	Shoulder joint horizontal flexion/extension	$0^o/140^o$
2	Shoulder joint vertical flexion/extension	$140^o/0^o$
3	Shoulder joint internal/external rotation	$-85^o/75^o$
4	Elbow joint flexion/extension	$120^o/0^o$
5	Forearm joint pronation/supination	$-85^o/85^o$
6	Wrist joint ulnar/radial deviation	$-30^o/20^o$
7	Wrist joint flexion/extension	$-50^o/60^o$

Table 5.3 Inertial parameters of ETS-MARSE

Joint (i)	**Mass** (kg)	**Center of mass** (m)	**Link length** (m)
1	3.475	0.0984	0.145
2	3.737	0.1959	0
3	0	0	0.25
4	2.066	0.163	0
5	0	0	0.267
6	0.779	0.121	0
7	0.496	0.0622	0

5.4 Nonlinear Control Design for ETS-MARSE

The control design for ETS-MARSE is based on the sliding mode control approach which forces the dynamics of the closed-loop system to remain or "slide" on a linear surface $S = 0$. Fig. 5.2 depicts the process in the phase plane for the case of a two-dimensional state vector system.

The sliding mode control process includes two phases. The first phase, also referred to as the reaching phase, is ensured by a discontinuous control term (u_{disc}) that allows the state error to reach the sliding surface. The second phase, or sliding phase, is ensured by a continuous equivalent term (u_{eq}) and keeps the error dynamics on the sliding surface and ultimately leads the error vector towards to the zero-equilibrium point (Fallaha et al., 2011).

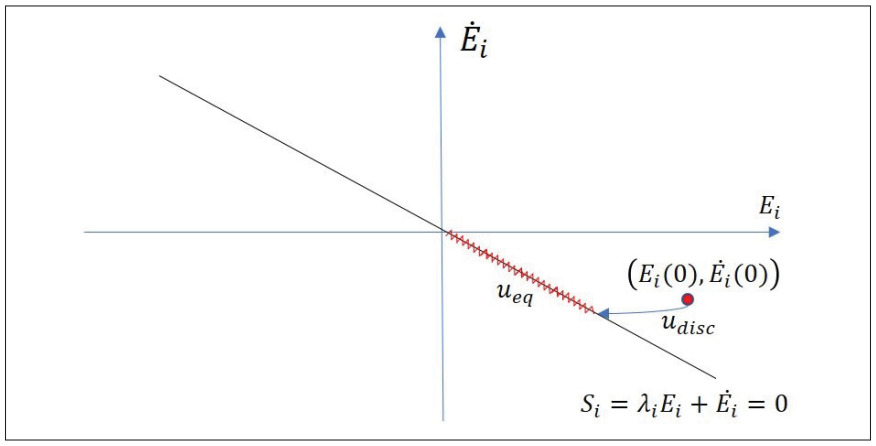

Figure 5.2 Asymptotic Convergence on a linear sliding surface depicted in the phase plane

5.4.1 Conventional Sliding Mode Control Applied to Robotic Systems

The general free dynamics of a multi-joint friction less robot without external constraints follows the nonlinear second-order differential equation in the joint angle space of the robot (Craig, 2005):

$$\tau = M(\theta)\ddot{\theta} + V_m(\theta, \dot{\theta})\dot{\theta} + G(\theta) \tag{5.1}$$

where $\tau \in R^n$ is the torque control input vector, $\theta \in R^n$ is the robot joint angles and/or displacements vector, $M(\theta) \in R^{n\times n}$ is the inertia matrix, and is positive definite, $V_m(\theta, \dot{\theta}) \in R^{n\times n}$ is the centrifugal and Coriolis matrix and $G(\theta) \in R^n$ is the gravity term vector.

With conventional sliding mode control associated with second-order MIMO systems, a typical first order linear switching function vector is chosen in terms of the tracking error and its time derivative:

$$S = \Lambda E + \dot{E},\ \Lambda = diag(\lambda_i),\ \lambda_i > 0 \tag{5.2}$$

where $E = \theta - \theta_R$ is the state tracking error vector defined as the difference between the measured joint angles/displacements and reference joint angles/displacements vector. The torque control law is then designed to force the tracking error vector E to reach and stay on the surface $S = 0$. As per (5.2), this leads the error vector to reach the zero-equilibrium point following first order convergence dynamics. The convergence rate of each differential equation is controlled by the values of λ_i. To ensure $S = 0$ is reached, the control law is designed to practically force the following relationship, often referred to as reaching law:

$$\dot{S} = -Ksign(S),\ K = diag(k_i),\ k_i > 0 \tag{5.3}$$

where $sign(S) = [sign(S_1), \cdots, sign(S_n)]^T$ with $sign(S_i)$ for $i = 1, \cdots, n$ is defined as follows:

$$sign(S_i) = \begin{cases} 1, & if\ S_i > 0 \\ -1, & if\ S_i < 0 \\ 0, & if\ S_i = 0 \end{cases} \tag{5.4}$$

Equation (5.3) allows the error state vector to reach the surface $S = 0$ in a finite time that is dependent upon the values of k_i. Substituting (5.1) and the time derivative of (5.2) in (5.3) gives the following torque vector control law:

$$\tau = \underbrace{V_m(\theta, \dot{\theta})\dot{\theta} + G(\theta) - M(\theta)(\Lambda\dot{E} - \ddot{\theta}_R)}_{u_{eq}} - \underbrace{M(\theta)Ksign(S)}_{u_{disc}} \tag{5.5}$$

Control law (5.5) is composed of the two terms u_{eq} and u_{disc} depicted in Fig. 5.2.

5.4.2 Problem Statement

From (5.5), the expression of u_{eq} and u_{disc} is complex and highly nonlinear. This complexity leads to transient and steady-state constraints on the torque control inputs. u_{eq} contains the robot's dynamic matrices for model compensation. For fast trajectory tracking applications, this implies higher dynamic constraints on the global torque control law. Analog or digital

noise from sensing systems are also amplified through these nonlinear matrices. On the other hand, the discontinuous term u_{disc} includes the robot's inertia matrix that multiplies the signum term $sign(S)$. In the general case, $M(\theta)$ is a non-constant and non-diagonal positive definite matrix that leads to a coupling effect between torque input signals when a chattering condition exists on one or more axes. Moreover, the inertia matrix has a direct modulating impact on the chattering amplitudes on the torque input signals. Control law (5.5) can be simplified by transferring model-based terms from the equivalent torque model-compensation term u_{eq} into the switching functions inside of the discontinuous term u_{disc}. The resultant switching functions become nonlinear, model-dependent and coupled differential functions. Fig. 5.3 depicts such nonlinear switching functions in the phase plane.

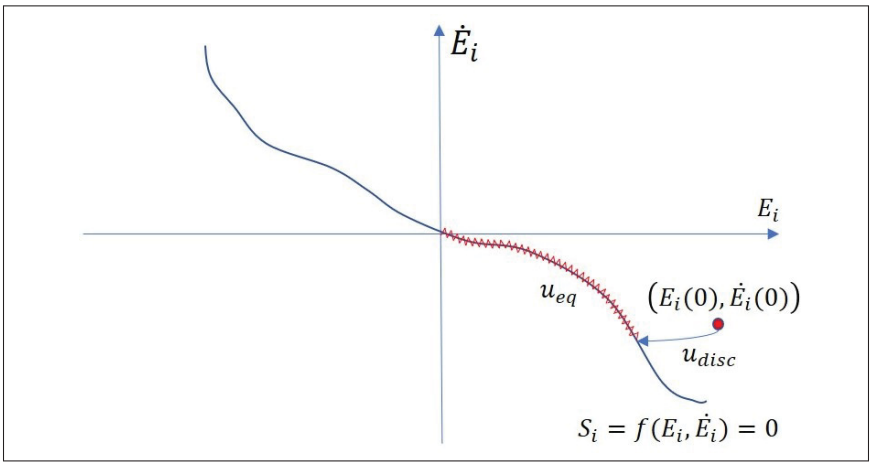

Figure 5.3 Asymptotic convergence with model-based switching functions in the phase plane

5.5 Model-Based Switching Functions Design Applied to Robotic Manipulators

This section details the design of model-based switching functions for any robot arm, and can be generalized to any second order mechanical system which dynamic differential equations can be formalized into relationship (5.1). The corresponding sliding surfaces are proved to be asymptotically stable, and the torque control law is shown to have a much simpler structure compared to (5.5). This approach is first introduced for a setpoint convergence problem, and its

main results are summarily covered in sub-section 5.5.1 below. This sets the framework basis for the generalized tracking error convergence problem covered in sub-section 5.5.2.

5.5.1 Model-Based Switching Functions Design for the Zero Setpoint Convergence Problem

For zero setpoint convergence using sliding mode control, consider the following switching function (Fallaha and Saad, 2018):

$$\begin{aligned} S(\theta,\dot{\theta}) =& M(\theta)\dot{\theta} + \Gamma\theta + \Xi\int_{t_0}^{t}\theta dt + \int_{t_0}^{t}\left(G(\theta) - G(0)\right)dt \\ &- \int_{t_0}^{t}\left(\sigma(\theta,\dot{\theta}) + V_m(\theta,\dot{\theta})\right)\dot{\theta}dt \end{aligned} \tag{5.6}$$

where $\sigma(\theta,\dot{\theta})$ is a skew-symmetric matrix binding matrix $M(\theta)$ and $V_m(\theta,\dot{\theta})$ into the following well-known relationship (Spong et al., 2005):

$$\sigma(\theta,\dot{\theta}) = \dot{M}(\theta) - 2V_m(\theta,\dot{\theta}) \tag{5.7}$$

Γ and Ξ are symmetrical positive definite constant matrices chosen to achieve the required dynamics performance when the system reaches the sliding surface $S = 0$. Note from (5.6) that $S(\theta,\dot{\theta})$ has integral terms that can directly place the system on the sliding surface with adequate choice of initial conditions of the integrators. The time derivative of $S(\theta,\dot{\theta})$ can be deduced from (5.6):

$$\begin{aligned} \dot{S}(\theta,\dot{\theta}) =& M(\theta)\ddot{\theta} + \dot{M}(\theta)\dot{\theta} + \Gamma\dot{\theta} + \Xi\theta + G(\theta) - G(0) \\ &- \left(\sigma(\theta,\dot{\theta}) + V_m(\theta,\dot{\theta})\right)\dot{\theta} \end{aligned} \tag{5.8}$$

Using (5.7) in (5.8) gives the following:

$$\dot{S}(\theta,\dot{\theta}) = M(\theta)\ddot{\theta} + V_m(\theta,\dot{\theta})\dot{\theta} + \Gamma\dot{\theta} + \Xi\theta + G(\theta) - G(0) \tag{5.9}$$

Using (5.1) in (5.9):

$$\dot{S}(\theta,\dot{\theta}) = \tau + \Gamma\dot{\theta} + \Xi\theta - G(0) \tag{5.10}$$

Therefore from (5.10) the torque control law that ensures the reaching law (5.3) is:

$$\tau = \underbrace{-\Gamma\dot{\theta} - \Xi\theta + G(0)}_{u_{eq}} - \underbrace{Ksign(S(\theta, \dot{\theta}))}_{u_{disc}} \tag{5.11}$$

Remark 1. Compared to the torque control law (5.5) given by conventional sliding mode control, (5.11) shows a much simpler torque control input structure with simplified expressions u_{eq} and u_{disc}. Control law (5.11) shows moreover the torque inputs are linear in terms of joint angles and rates with a decoupling of the chattering effect on the axes, provided that K is chosen to be a diagonal matrix.

The next step is to prove that the sliding surface $S(\theta, \dot{\theta}) = 0$ ensures asymptotic convergence of the joint angles towards the zero-equilibrium point. This is shown in proposition 1 below and uses the following lemma (Fallaha and Saad, 2018).

Lemma 1. The difference $G(\theta) - G(0)$ can be written as:

$$G(\theta) - G(0) = -\Psi_G(\theta)\theta \tag{5.12}$$

where $\Psi_G(\theta)$ is a symmetric matrix defined as follows:

$$\Psi_G(\theta) = -\int_0^1 J_G(h.\theta)dh \tag{5.13}$$

where J_G is the square Jacobian of G defined as follows:

$$J_G = \left[\frac{\partial G_i}{\partial \theta_j}\right] \tag{5.14}$$

Proof: Using the mean value theorem applied to differentiable vector functions, the following holds (Comenetz, 2002):

$$G(\theta) - G(0) = \left(\int_0^1 J_G(h.\theta)dh\right)\theta \tag{5.15}$$

where J_G is the square Jacobian of G defined by (5.14).

Using the fact that G is derived from a potential energy U, namely:

$$G_i = \frac{\partial U}{\partial \theta_i} \tag{5.16}$$

Then the Jacobian matrix can be written as:

$$J_G = \left[\frac{\partial}{\partial \theta_j} \frac{\partial}{\partial \theta_i} U \right] \tag{5.17}$$

Under the assumption that the second partial derivatives of U are continuous, then Schwarz' theorem yields the following:

$$\frac{\partial}{\partial \theta_j} \frac{\partial}{\partial \theta_i} U = \frac{\partial}{\partial \theta_i} \frac{\partial}{\partial \theta_j} U \tag{5.18}$$

Therefore J_G is symmetric.

Noting $\Psi_G(\theta) = -\int_0^1 J_G(h.\theta)dh$, $\Psi_G(\theta)$ is also symmetric as it is the integral of a symmetric matrix, which completes the proof of Lemma1. Note that since $\Psi_G(\theta)$ is symmetric, it is diagonalizable, and all its eigenvalues are real.

Proposition 1. (Fallaha and Saad, 2018), the sliding surface $S(\theta, \dot{\theta}) = 0$, where $S(\theta, \dot{\theta})$ is given by (5.6), ensures the asymptotic stability of θ to 0 provided that the eigenvalues of matrix Ξ verify the following constraint:

$$Min_i(Eig_i \Xi) > Max_i(Eig_i \Psi_G(\theta)) \tag{5.19}$$

Proof: Relationship (5.19) implies that the difference $\Xi - \Psi_G(\theta)$ is positive definite. When the sliding surface $S(\theta, \dot{\theta}) = 0$ is reached, (5.11) becomes:

$$\tau = -\Gamma\dot{\theta} - \Xi\theta + G(0) \tag{5.20}$$

Consider now the following Lyapunov candidate function:

$$L(\theta, \dot{\theta}) = \frac{1}{2}\dot{\theta}^T M(\theta)\dot{\theta} + P(\theta) - P(0) \tag{5.21}$$

with P a scalar function defined as (Tomei, 1991):

$$P(\theta) = U(\theta) + \frac{1}{2}\theta^T \Xi\theta - \theta^T G(0) \tag{5.22}$$

U is the potential energy term from which is derived $G(\theta)$. Differentiating $P(\theta)$ with respect to θ and noting that $\dfrac{\partial U(\theta)}{\partial \theta} = G(\theta)$ (Spong et al., 2005), then using Lemma 1, the following relation can be obtained:

$$\frac{\partial P(\theta)}{\partial \theta} = G(\theta) + \Xi\theta - G(0) = (\Xi - \Psi_G(\theta))\,\theta \tag{5.23}$$

Since $\Xi - \Psi_G(\theta)$ is positive definite, then $\dfrac{\partial P(\theta)}{\partial \theta} = 0$ only for $\theta = 0$, and therefore $P(\theta)$ is absolute minimum for $\theta = 0$ (Tomei, 1991), which implies $P(\theta) - P(0) > 0$ for $\theta \neq 0$. Thus, from (5.21) it can be deduced that $L(\theta, \dot{\theta})$ is a Lyapunov function. Differentiating $L(\theta, \dot{\theta})$ with respect to time gives:

$$\dot{L}(\theta, \dot{\theta}) = \dot{\theta}^T M(\theta)\ddot{\theta} + \frac{1}{2}\dot{\theta}^T \dot{M}(\theta)\dot{\theta} + \dot{\theta}^T G(\theta) + \dot{\theta}^T \Xi\theta - \dot{\theta}^T G(0) \tag{5.24}$$

The above equation can also be written as:

$$\dot{L}(\theta, \dot{\theta}) = \dot{\theta}^T \tau + \dot{\theta}^T \Xi\theta - \dot{\theta}^T G(0) \tag{5.25}$$

Using relationship (5.20), (5.25) simplifies into:

$$\dot{L}(\theta, \dot{\theta}) = -\dot{\theta}^T \Gamma\dot{\theta} \tag{5.26}$$

Therefore $\dot{L}(\theta, \dot{\theta})$ is negative semi-definite. Applying Barbalat's lemma (Slotine and Li, 1991), $\dot{\theta}$ converges to 0. Using (5.1) and (5.20) it comes that:

$$\Xi\theta + (G(\theta) - G(0)) = (\Xi - \Psi_G(\theta))\,\theta \underset{\text{t}}{\rightarrow} 0 \tag{5.27}$$

Since $\Xi - \Psi_G(\theta)$ is positive definite, this implies that θ converges to 0, which completes the proof of Proposition 1.

Remark 2. Note that one can choose to compensate the gravity term in the torque control law rather than in the switching functions. In this case, constraint (5.19) is not necessary anymore, and the switching function (5.6) becomes:

$$S(\theta, \dot{\theta}) = M(\theta)\dot{\theta} + \Gamma\theta + \Xi \int_{t_0}^{t} \theta dt - \int_{t_0}^{t} \left(\sigma(\theta, \dot{\theta}) + V_m(\theta, \dot{\theta})\right) \dot{\theta} dt \tag{5.28}$$

However, the torque control law becomes:

$$\tau = -\Gamma\dot{\theta} - \Xi\theta + G(\theta) - Ksign(S(\theta, \dot{\theta})) \tag{5.29}$$

5.5.2 Switching Functions Design for the Trajectory Tracking Problem

Trajectory tracking development in the robot's joint space is a generalization of the above set point development whereby model-based switching functions are designed such that the error $E = \theta - \theta_R$ asymptotically converges to 0. Consider the following model-based sliding function for the trajectory tracking problem:

$$\Sigma = S(\theta, \dot{\theta}) - S(\theta_R, \dot{\theta}_R) \tag{5.30}$$

Where S is defined by (5.6).

Remark 3. Note that the design of switching function Σ defined by (5.30) is not equivalent to replacing θ with the tracking error E in (5.6) and forming $S(E, \dot{E})$, since S is a nonlinear function. This specific choice of Σ ensures similar levels of simplifications of the torques control inputs as for the set-point tracking problem, and therefore is completely novel and remains different from the set-point convergence problem in (Fallaha and Saad, 2018).

It can be shown that the torque control law that allows the system to reach $\Sigma = 0$ is given by:

$$\tau = \underbrace{\tau_R - \Gamma\dot{E} - \Xi E}_{u_{eq}} - \underbrace{Ksign(\Sigma)}_{u_{disc}} \tag{5.31}$$

where

$$\tau_R = M(\theta_R)\ddot{\theta}_R + V_m(\theta_R, \dot{\theta}_R)\dot{\theta}_R + G(\theta_R) \tag{5.32}$$

Note that τ_R is exclusively composed of constructed reference signals and doesn't include any measured or estimated signal. Fig. 5.4 below shows the block diagram of the proposed general control algorithm with model-based switching functions design. This block diagram shows that the control strategy simplifies essentially to a proportional and derivative controller for the feedback loop, with a feedforward term τ_R solely dependent upon the reference, and the robust switching *signum* term that ensures the reaching condition on the model-based switching surfaces.

Remark 4. The torque control law (5.31) shows again that the torque inputs become linear in terms of the error vector and its time derivative when using model-based switching functions. Note again from (5.31) the discontinuity decoupling between joint axes. It remains to prove that $\Sigma = 0$ ensures asymptotic convergence of the error vector E towards 0. Similarly to the set point approach, consider the following lemma.

Lemma 2. The difference $G(\theta) - G(\theta_R)$ can be written as:

$$G(\theta) - G(\theta_R) = -\Psi_G(\theta, \theta_R)(\theta - \theta_R) \tag{5.33}$$

Where $\Psi_G(\theta, \theta_R)$ is a symmetric matrix defined as follows:

$$\Psi_G(\theta, \theta_R) = -\int_0^1 J_G(\theta_R + h(\theta - \theta_R))dh \tag{5.34}$$

where J_G is the same square Jacobian of G defined by (5.14). The proof of Lemma 2 is closely based on that of Lemma 1.

Proposition 2. The sliding surface $\Sigma = 0$ where Σ is given by (5.30), ensures the asymptotic convergence of θ to θ_R provided that the eigenvalues of matrix Ξ verify the following constraint:

$$Min_i(Eig_i\Xi) > Max_i(Eig_i\Psi_G(\theta, \theta_R)) \tag{5.35}$$

Proof: Relationship (5.35) implies that the difference $\Xi - \Psi_G(\theta, \theta_R)$ is positive definite. When $\Sigma = 0$, (5.31) leads to the following:

$$\tau = \tau_R - \Gamma\dot{E} - \Xi E \tag{5.36}$$

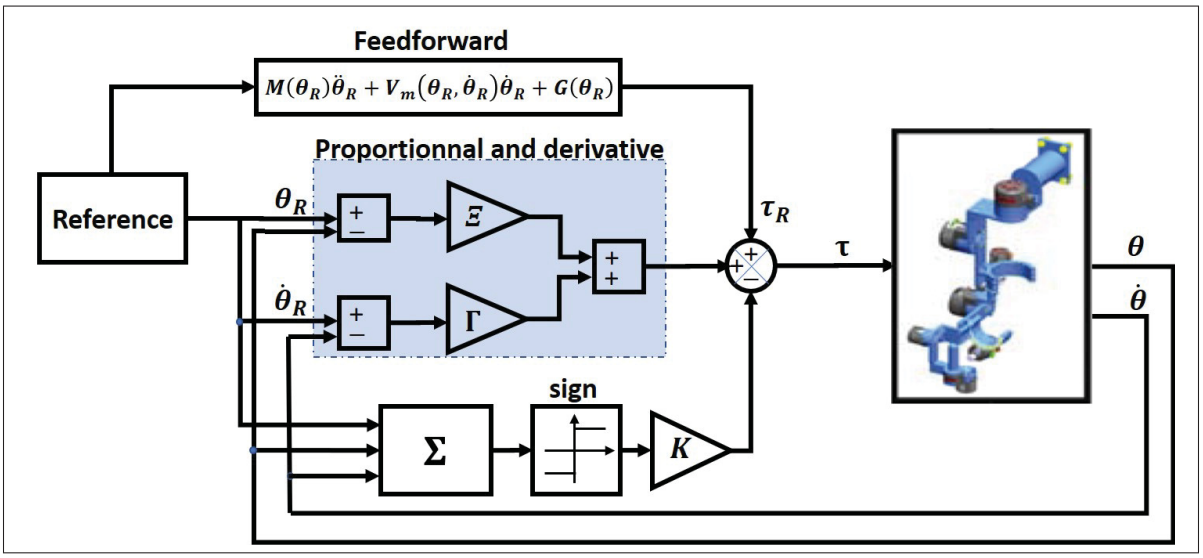

Figure 5.4 Block Diagram of sliding mode control algorithm with model-based switching functions

Consider now the following Lyapunov-like candidate function:

$$L = \frac{1}{2}\dot{\theta}^T M(\theta)\dot{\theta} + P(\theta) - \frac{1}{2}\dot{\theta_R}^T M(\theta_R)\dot{\theta_R} - P(\theta_R) \tag{5.37}$$

Where similarly to Proposition 1, P is a scalar function defined as follows:

$$P(\theta) = U(\theta) + \frac{1}{2}\theta^T \Xi\theta - \int_0^\theta \left(\tau_R - \Gamma\dot{\theta}_R + \Xi\theta_R\right)^T d\theta \tag{5.38}$$

Note that (5.22) becomes a particular case of (5.38) for $\theta_R = 0$. Differentiating $P(\theta)$ in terms of θ gives:

$$\begin{aligned} \frac{\partial P(\theta)}{\partial \theta} &= G(\theta) + \Xi\theta - G(\theta_R) + \Xi\theta_R - F_R \\ F_R &= M(\theta_R)\ddot{\theta}_R + V_m(\theta_R, \dot{\theta}_R)\dot{\theta}_R - \Gamma\dot{\theta}_R \end{aligned} \tag{5.39}$$

Therefore

$$\frac{\partial P(\theta)}{\partial \theta} = (\Xi - \Psi_G(\theta, \theta_R))E - F_R \tag{5.40}$$

Since $\Xi - \Psi_G(\theta, \theta_R)$ is positive definite, it can be shown that P has an absolute minimum $P(\theta_{minR})$, function of the reference trajectory and given by $\frac{\partial P(\theta)}{\partial \theta} = 0$. θ_{minR} verifies the following:

$$\theta_{minR} = \theta_R + (\Xi - \Psi_G(\theta, \theta_R))^{-1} F_R \tag{5.41}$$

Therefore $P(\theta) \geq P(\theta_{minR})\ \forall\theta$. Thus from (5.37), the Lyapunov-like function L has a lower bound (not necessarily positive) given by:

$$L \geq P(\theta_{minR}) - \frac{1}{2}\dot{\theta}_R^T M(\theta_R)\dot{\theta}_R - P(\theta_R) \tag{5.42}$$

Differentiating L with respect to time gives the following:

$$\dot{L} = \dot{\theta}^T\tau - \dot{\theta}_R^T\tau_R + \theta^T\Xi\dot{\theta} - \theta_R^T\Xi\dot{\theta}_R - \left(\tau_R - \Gamma\dot{\theta}_R + \Xi\theta_R\right)^T \dot{E} \tag{5.43}$$

Using equation (5.36) in (5.43) when the sliding surface is reached:

$$\begin{aligned}\dot{L} =&\dot{\theta}^T\left(\tau_R - \Gamma\dot{E} - \Xi E\right) - \dot{\theta}_R^T\tau_R + \theta^T\Xi\dot{\theta} - \theta_R^T\Xi\dot{\theta}_R \\ &- \left(\tau_R - \Gamma\dot{\theta}_R + \Xi\theta_R\right)^T\dot{E}\end{aligned} \tag{5.44}$$

Simplifying (5.44) gives finally:

$$\dot{L} = -\dot{E}^T\Gamma\dot{E} \tag{5.45}$$

$\dot{L}$ is therefore negative semi-definite. Since L has a lower bound, then as per Slotine and Li (1991), applying Barbalat's lemma implies that $\dot{L}$ converges to 0, which then implies that $\dot{E}$ converges to 0. Since $\Xi - \Psi_G(\theta, \theta_R)$ is positive definite, it can be proved that E converges to 0, which completes the proof of Proposition 2.

Note that constraint (5.35) is dependent on the reference trajectory θ_R. It is however possible to formulate a constraint with an absolute lower bound for $Min_i(Eig_i\Xi)$ that is independent of the trajectory as per Proposition 3 below:

Proposition 3. The following holds:

$$Max_i(Eig(\Psi_G(\theta, \theta_R))) \leq Max_i(Eig(-J_G(\theta))) \tag{5.46}$$

Proof: Note $\lambda_{Max} = Max_i(Eig(-J_G(\theta)))$. In other words, λ_{Max} is a constant absolute maximum of all varying eigenvalues of $-J_G(\theta)$. The following then holds:

$$\begin{aligned}\lambda_{Max}I_n - \Psi_G(\theta, \theta_R) =&\lambda_{Max}I_n \\ &- \left(-\int_0^1 J_G(\theta_R + h(\theta - \theta_R))dh\right) \\ =&\int_0^1 \lambda_{Max}I_n - \left(-J_G(\theta_R + h(E))\right)dh\end{aligned} \tag{5.47}$$

By construction, $\lambda_{Max}I_n - (-J_G(\theta_R + h(E)))$ is positive definite. Therefore $\int_0^1 \lambda_{Max}I_n - (-J_G(\theta_R + h(E)))\,dh$ is positive definite, then (5.47) implies $\lambda_{Max}I_n - \Psi_G(\theta, \theta_R)$ is positive definite, and thus (5.46) is straightforward.

From Proposition 3, a sufficient condition to meet constraint (5.35) can therefore be formulated as follows:

$$Min_i(Eig\Xi) > Max_i(Eig(-J_G(\theta))) \tag{5.48}$$

Remark 5. Note that the new constraint (5.48) represents a sufficient absolute condition on eigenvalues of Ξ for any trajectory tracking within the robot's working space. The advantage of constraint (5.48) is that it is independent of the reference trajectory and holds for any trajectory within the robot's work-space. The disadvantage however is that the choice of the eigenvalues of matrix Ξ might be overdimensioned to ensure constraint (5.48) is met. Also, as per Remark 2, one can choose as well in this case to compensate the gravity term in the torque control law rather than in the switching functions, which then removes the need of constraint (5.35).

5.5.3 Robustness Against Uncertainties

In this section, model uncertainties are introduced with the model-based switching functions design approach. It is shown that the proposed approach compensates for uncertainties with the discontinuous gain in a similar way conventional sliding mode control does. The additional advantage of using model-based switching functions is that only matched uncertainties are required to be compensated. Consider uncertainties on all the matrix terms of the robot model given by (5.1), and consider the following notations:

$\hat{M}(\theta)$, $\hat{M}(\theta_R)$ (noted $\hat{M}$ and $\hat{M}_R$) are estimates of $M(\theta)$ and $M(\theta_R)$; $\hat{V}_m(\theta,\dot{\theta})$, $\hat{V}_m(\theta_R,\dot{\theta}_R)$ (noted $\hat{V}_m$ and $\hat{V}_{mR}$) are estimates of $V_m(\theta,\dot{\theta})$, $V_m(\theta_R,\dot{\theta}_R)$); $\hat{G}(\theta)$, $\hat{G}(\theta_R)$ (noted $\hat{G}$ and $\hat{G}_R$) are estimates of $G(\theta)$ and $G(\theta_R)$.

The switching function Σ defined in (5.30) is then constructed by using the estimate matrices above as follows:

$$\begin{aligned}\Sigma =& \hat{M}\dot{\theta} - \hat{M}_R\dot{\theta}_R + \Gamma E + \Xi\int_{t_0}^{t} E\,dt + \int_{t_0}^{t}\left(\hat{G} - \hat{G}_R\right)dt \\ &- \int_{t_0}^{t}\left(\left(\hat{\sigma} + \hat{V}_m\right)\dot{\theta} - \left(\hat{\sigma}_R + \hat{V}_{mR}\right)\dot{\theta}_R\right)dt\end{aligned} \tag{5.49}$$

The time derivative of Σ gives:

$$\dot{\Sigma} = \hat{M}\ddot{\theta} + \hat{V}_m\dot{\theta} + \hat{G} - \hat{M}_R\ddot{\theta}_R - \hat{V}_{mR}\dot{\theta}_R - \hat{G}_R + \Gamma\dot{E} + \Xi E \tag{5.50}$$

Introducing the torque input in $\dot{\Sigma}$ gives:

$$\dot{\Sigma} = \tau + \tilde{M}\ddot{\theta} + \tilde{V}_m\dot{\theta} + \tilde{G} - \hat{\tau}_R + \Gamma\dot{E} + \Xi E \tag{5.51}$$

with $\hat{\tau}_R = \hat{M}_R\ddot{\theta}_R + \hat{V}_{mR}\dot{\theta}_R + \hat{G}_R$, $\tilde{M} = \hat{M} - M(\theta)$, $\tilde{V}_m = \hat{V}_m - V_m(\theta, \dot{\theta})$ and $\tilde{G} = \hat{G} - G(\theta)$. Similarly to (5.31), choose the following control law:

$$\tau = \hat{\tau}_R - \Gamma\dot{E} - \Xi E - Ksign(\Sigma) \tag{5.52}$$

This leads to the following reaching law:

$$\dot{\Sigma} = \tilde{M}\ddot{\theta} + \tilde{V}_m\dot{\theta} + \tilde{G} - Ksign(\Sigma) \tag{5.53}$$

From (5.53), note that the term $\tilde{M}\ddot{\theta} + \tilde{V}_m\dot{\theta} + \tilde{G}$ exists because of the introduced uncertainties. Assuming this term is bounded, it is then possible to choose matrix K elements larger than the upper bound of that term in order to ensure reaching the sliding surface. This uncertainty compensation is also a known procedure in conventional sliding mode control (Slotine and Li, 1991).

5.6 Experimental Application on ETS-MARSE

This section describes the experimental setup of ETS-MARSE exoskeleton prototype shown in the Fig. 5.7 (adapted from Rahman et al. (2014*b*)). The real-time controller using the model-based switching functions algorithm was implemented on a National Instrument (NI) processing platform as detailed in Fig. 5.5. The NI processing platform comprises a NI-PXI 8081 dual-core controller card and a NI-PXI 7813-R FPGA card. Both cards are enclosed in a PXI-1031 chassis. As shown in Fig. 5.6, the NI-PXI 8081 controller executes at a time step of

5 ms the top-level sliding mode control algorithm with the model-based switching functions along with the inverse kinematics logic. The NI PXI-7813R FPGA card executes, on the other hand, the low-level current PI control loop at the faster sample time of 50 us. The NI PXI-7813R processes as well the joints position feedback via Hall-effect sensors. Finally, user-defined commands are sent to the robot through a host HMI PC using a LabView interface in which it is possible to select the controller type and perform online controller gain adjustments. The joints of ETS-MARSE are actuated by brushless DC motors Maxon EC-45 and EC-90 using harmonic drives to ensure high gear ratios while maintaining very good accuracy positioning [gear ratio for motor 1, 2 and 4: 120:1; gear ratio for motor 3, 5, 6 and 7: 100:1].

5.6.1 Experimental Real-Time Results

The experimental test cases that were executed on ETS-MARSE are divided into two sets. The first set was executed without load and compares the model-based switching functions approach to conventional sliding mode control. The second set was performed by subject 1 (weight:83 kg, height: 1.83 m) using the model-based switching functions approach, in order to test its robustness under normal loading conditions. The reference trajectory of ETS-MARSE tool tip in the Cartesian space for both sets was chosen to have a rectangle-like shape, which is representative of an actual arm mobility exercise performed by patients. The reference trajectory is depicted in dashed black in Fig. 5.8. The correspondent reference joint angles for the 7

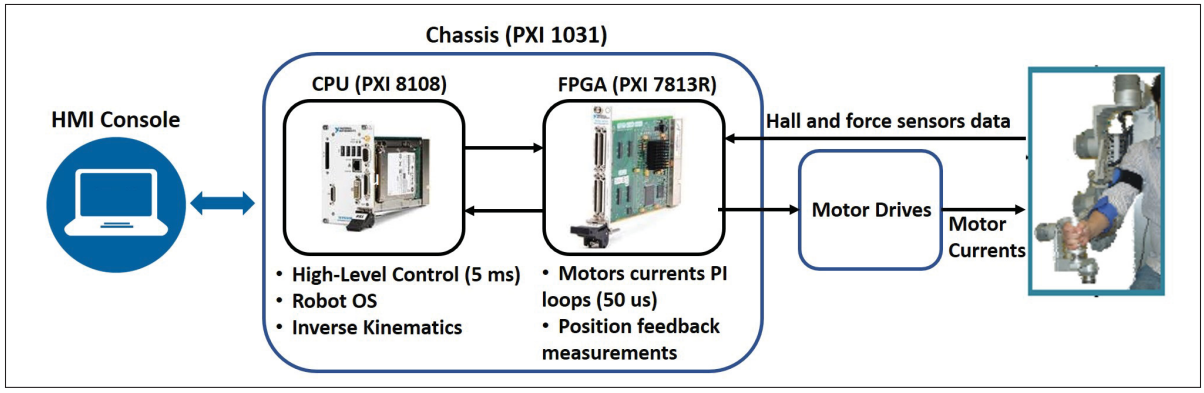

Figure 5.5 Hardware Control Architecture Setup for ETS-MARSE

axes in the joint space are shown in dashed black in Fig. 5.9. Numerical values of the sliding mode controller gains using conventional and model-based switching functions are shown in Table 5.4. For linear switching functions design, K was tuned to ensure an acceptable level of robustness against disturbances. The relatively high values of K were obtained as a result of low numerical values of M, which orders of magnitude are bounded to 10^{-3}. For the model-based switching functions approach, since M is eliminated in the discontinuous term of the torque control inputs, the values of K are expected to be three orders of magnitude lower to ensure a similar level of robustness. For simplification purposes, the diagonal values of K were therefore set at 0.25. From the joint space reference trajectories, $\Psi_G(\theta, \theta_R)$ was symbolically derived for ETS-MARSE and its upper eigenvalue limit numerically computed offline for the duration of the reference trajectory and showed to be inferior to 10 throughout this duration. Therefore by choosing all the eigenvalues of matrix Ξ to be higher than 10 will guarantee as per (5.35) asymptotic stability of the tracking error to 0 for this particular trajectory. However, as Table 5.4 shows, the diagonal elements numerical values of Ξ were chosen to be 25, which gives a good margin compared to the maximum eigenvalue limit of $-J_G(\theta)$ (numerically computed to be 21.32). The purpose of this choice is to ensure asymptotic convergence within the global work-space of ETS-MARSE regardless of the programmed reference trajectory, and to account as well for parameter uncertainties on the gravity matrix. Finally, the diagonal elements of

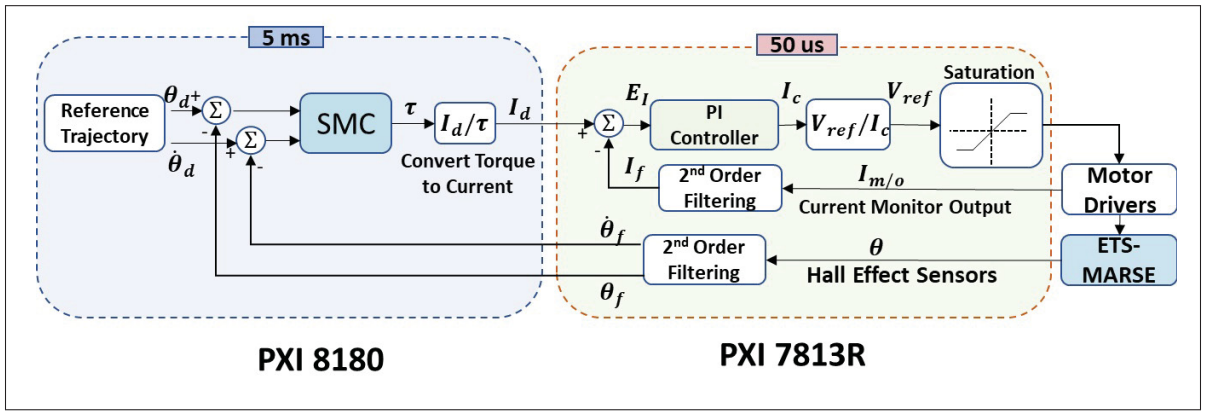

Figure 5.6 Block Diagram of Control Algorithm Loops for ETS-MARSE

Figure 5.7 ETS-MARSE Exoskeleton Prototype

matrix Γ were set to 12.2, which places a dominant pole in closed-loop varying between -2 and -2.5, given the values of Ξ and the numerical variation of M along the trajectory.

Table 5.4 Experimental Control Parameters of ETS-MARSE

	Parameter	**Matrix Numerical Value**
Model-Based switching functions (proposed)	Ξ	Diag7(25)
	Γ	Diag7(12.2)
	K	Diag7(0.25)
Linear switching functions	Λ	Diag7(15)
	K	10*diag(36, 30, 80, 55, 22, 30, 37)

Figures 5.10 and 5.11 display the results for the first set, and show the overlay of real-time performance of both model-based and linear switching functions approaches on joint error tracking performance and joint torque inputs. From Figure 5.10 it can be seen that the proposed model-based switching functions approach features a better overall tracking accuracy on the joint angles. Table 5.5 gives a quantitative overview of the Peak and RMS tracking errors in

the joint space. The model-based switching functions yield an overall improvement of peak and RMS error compared to linear switching functions. The RMS improvement is particularly important for joints 2 and 4 (resp. 63.6% and 87.44%), which is visually supported by the tracking superiority of the model-based switching functions approach over the conventional linear functions in the Cartesian space displayed in Fig. 5.8 . Table 5.6 shows the measured total variation computed as per Mondal and Mahanta (2014) on all torque control inputs. The total torque inputs variation is reduced by 20% up to 80% for axes 1 to 6 with the model-based switching functions approach, while staying comparable for wrist joint 7. The torque inputs variation reduction is an important requirement for control design. Indeed, the practical implementation of a controller requires constraints reduction on the control inputs to help against premature failures of actuating components in the system, as well as avoiding non-modeled fast dynamics behaviour in the closed-loop setup. Additionally, for the exoskeleton application, having reduced transient activity on the torques control inputs reduces the vibration cues felt by the patient, and therefore ensures improved comfort and ergonomic requirements.

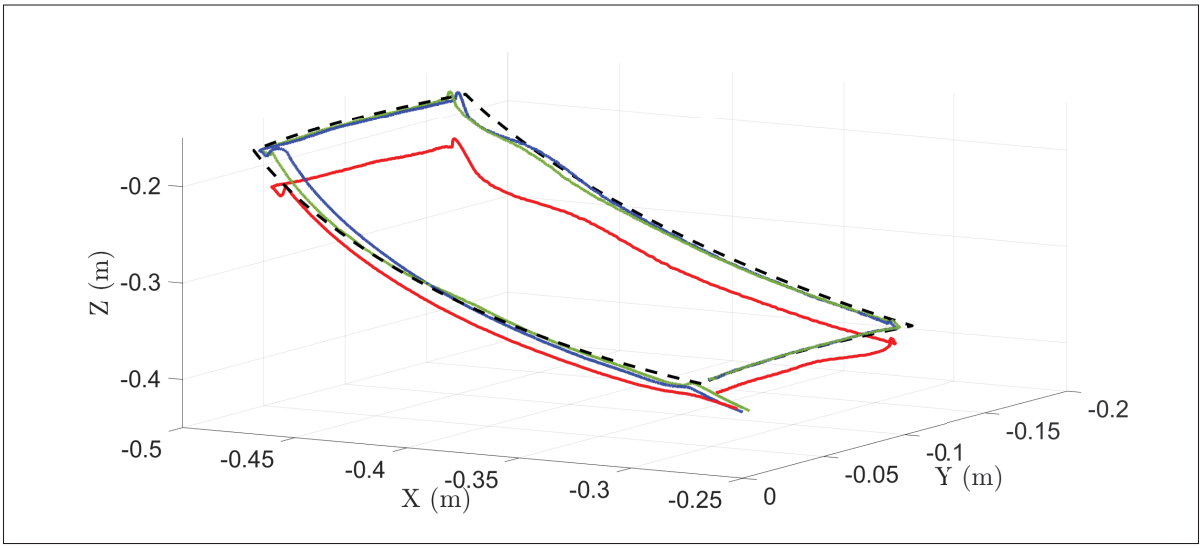

Figure 5.8 Cartesian space reference trajectory (dashed black), no-load tracking performance for proposed method (blue), no-load conventional SM (red), loaded tracking performance for proposed method (green)

Figure 5.12 shows a zoomed-in time section of control torque input for axis 1. Although the primary objective of the model-based switching functions approach is not to address the chattering

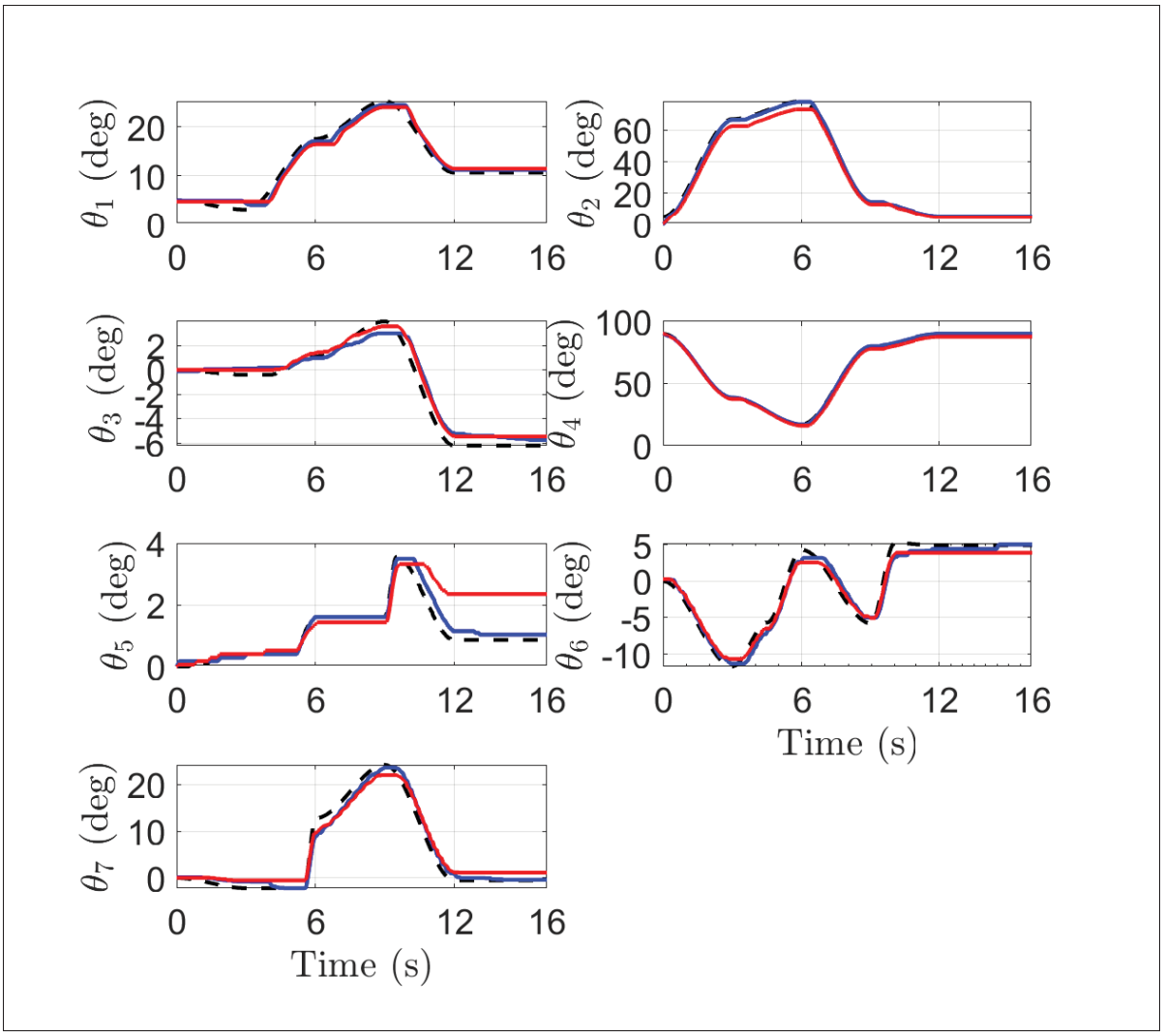

Figure 5.9 Joint space reference trajectory (dashed black) and no-load tracking performance for proposed method (blue) and no-load conventional SM (red)

problem, the zoomed-in square of Figure 5.12 shows at least 30% chattering level reduction on the torque control inputs due mainly to the inertia matrix compensation by the switching function, which leads to chattering decoupling on the control inputs. Transient dynamics with a 6 to 9 Hz frequency pattern also appears on the torque control input with conventional sliding mode control. These frequencies are caused by non-compensated model-based terms in the equivalent control input for the conventional approach.

Figures 5.13, 5.14 and 5.15 present the experimental results performed by subject-1 and feature the tracking performance and the torque inputs for the model-based switching functions approach under normal loading conditions. The tracking performance in this case is very good and remains within the boundaries of the no-load results, which demonstrates the robustness of the proposed approach under uncertain/non-modeled loading conditions. The torques inputs variations are also comparable to the no-load results, with levels slightly higher especially for joints 1 to 4, reflecting the addition of the arm weight of subject-1.

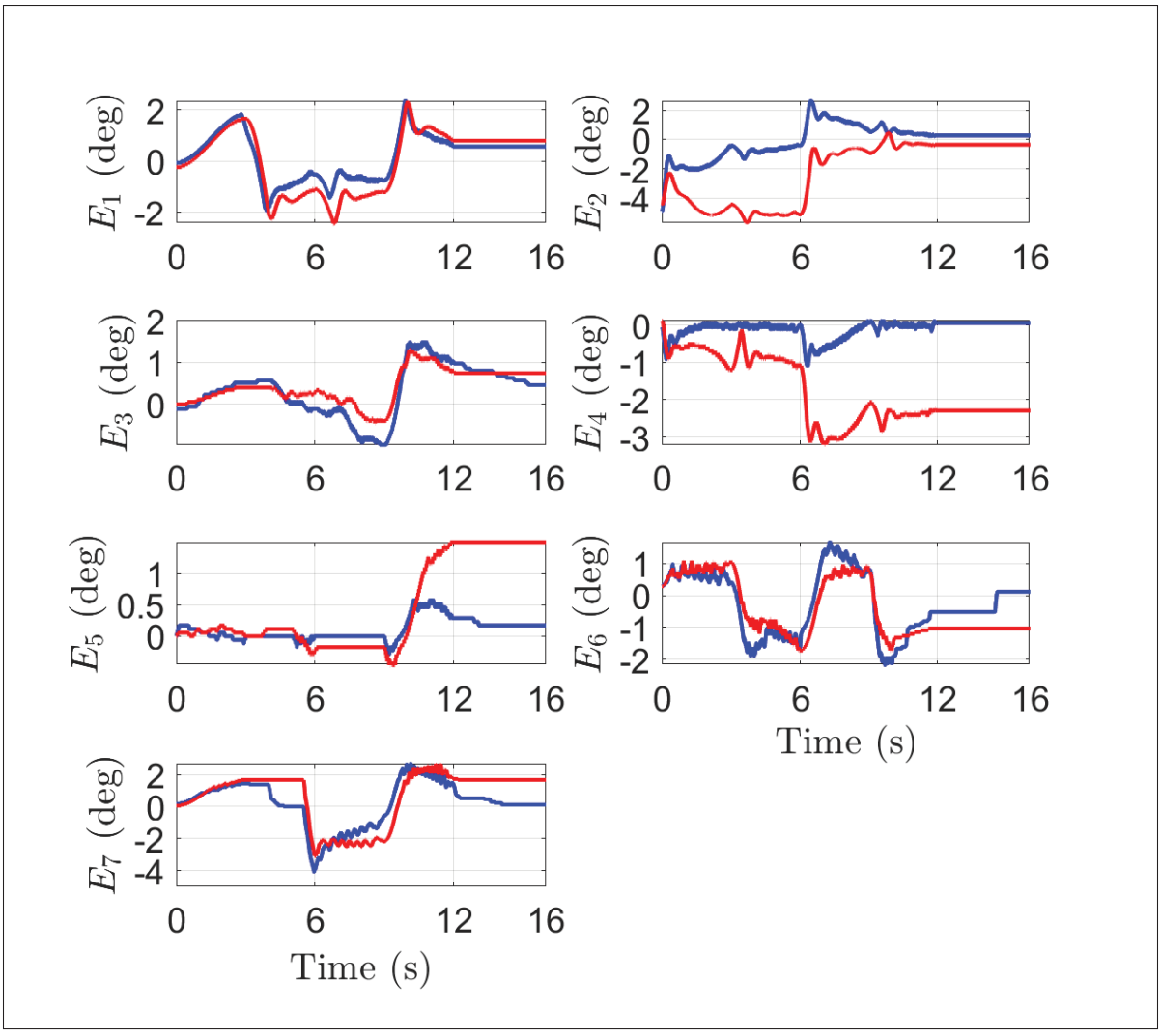

Figure 5.10 No-load joint tracking errors for proposed method (blue) and no-load conventional SM (red)

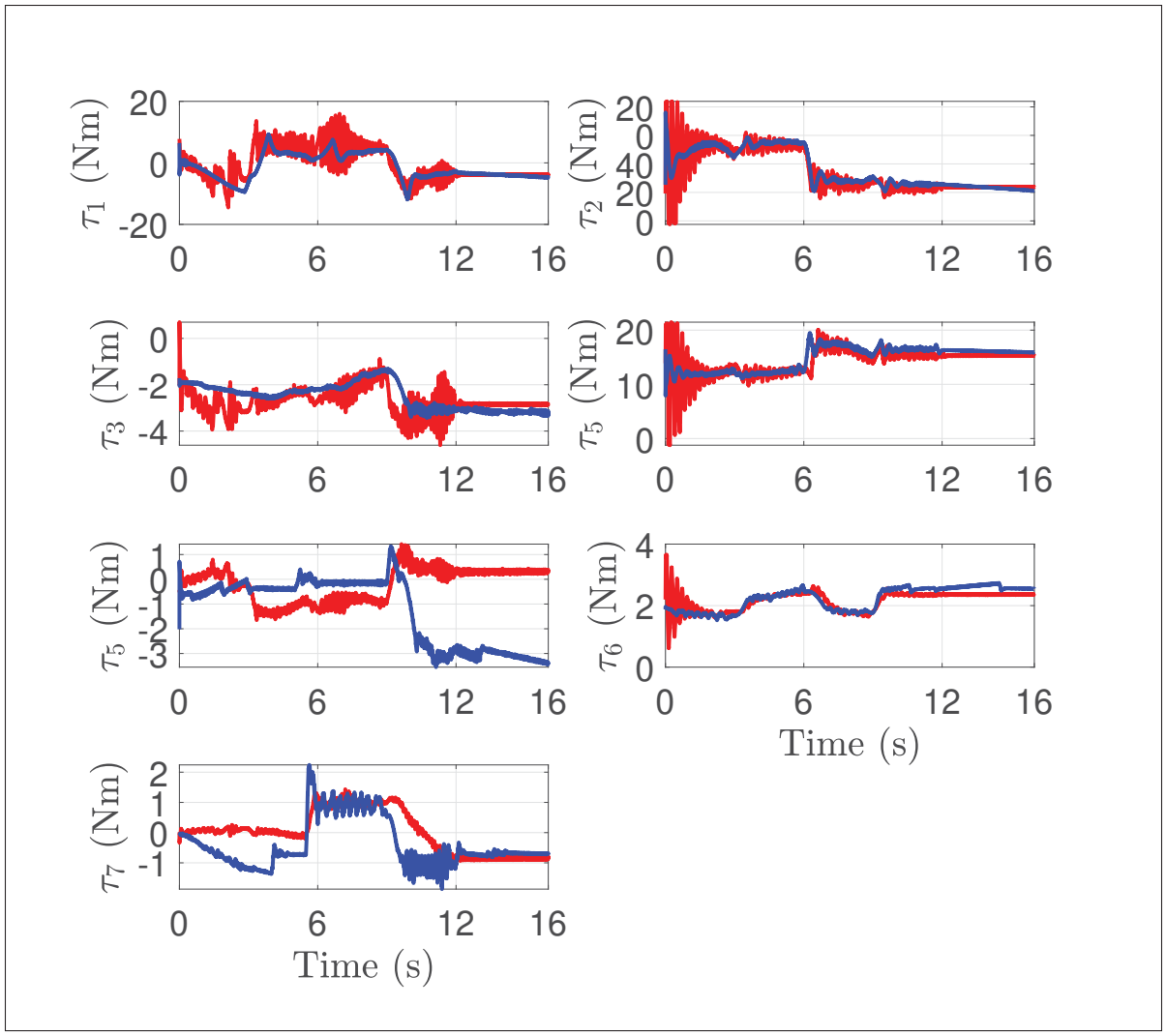

Figure 5.11 No-load joint torque for proposed method (blue) and no-load conventional SM (red)

5.7 Conclusion

In this paper, a novel sliding mode approach with model-based switching functions design was developed and experimentally tested on a 7-DOF exoskeleton robotic arm for trajectory tracking control. The main advantages of the model-based switching functions design were highlighted. These advantages include a complete decoupling of chattering and transient constraints reduction on the torque control inputs, as well as increased robustness compared to conventional linear

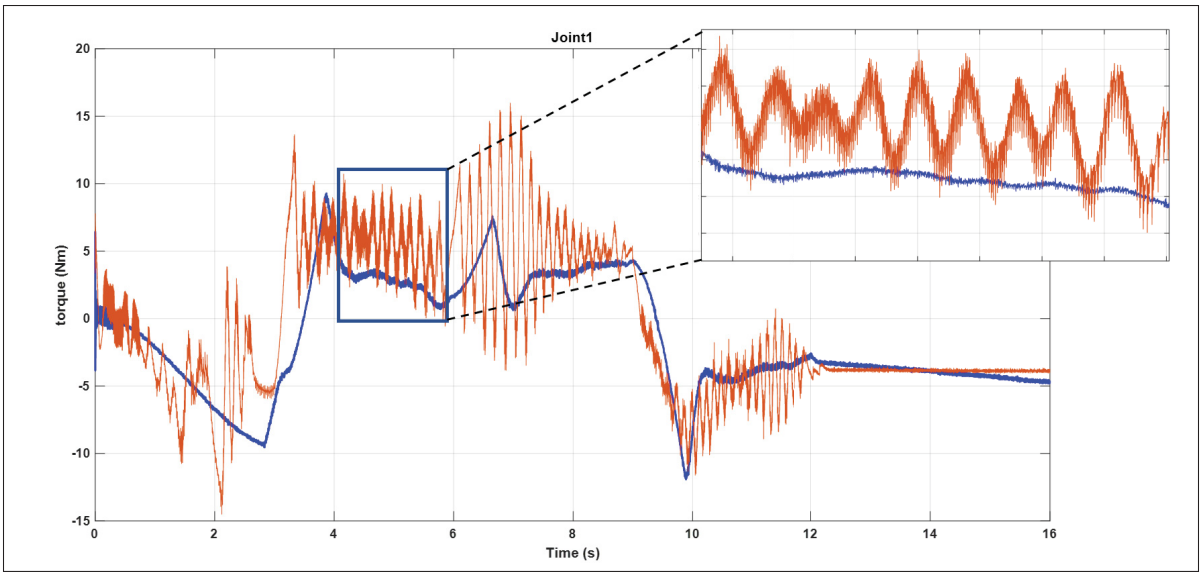

Figure 5.12 Zoomed-in performance for axis 1 joint torque input, proposed method (blue) and conventional SM (red)

Table 5.5 Improvements of proposed model-based switching functions in tracking error peak and RMS values

	Peak Error Value (degrees)			RMS Error value (degrees)		
Joint (i)	**Conventional SMC**	**Proposed Approach**	**improvement (%)**	**Conventional SMC**	**Proposed Approach**	**improvement (%)**
1	2.46	2.29	6.98	1.2	0.92	23.53
2	5.73	4.92	14.01	3.02	1.10	63.60
3	1.32	1.49	-13.05	0.59	0.69	-16.98
4	3.21	1.09	66.06	2.01	0.25	87.44
5	1.49	0.57	61.54	0.85	0.20	76.59
6	1.72	2.12	-23.33	1.01	0.99	1.17
7	3.09	4.01	-29.64	1.77	1.40	20.98

sliding functions, while ensuring better tracking performance. Future work will combine the use of model-based switching functions with existing chattering reduction techniques.

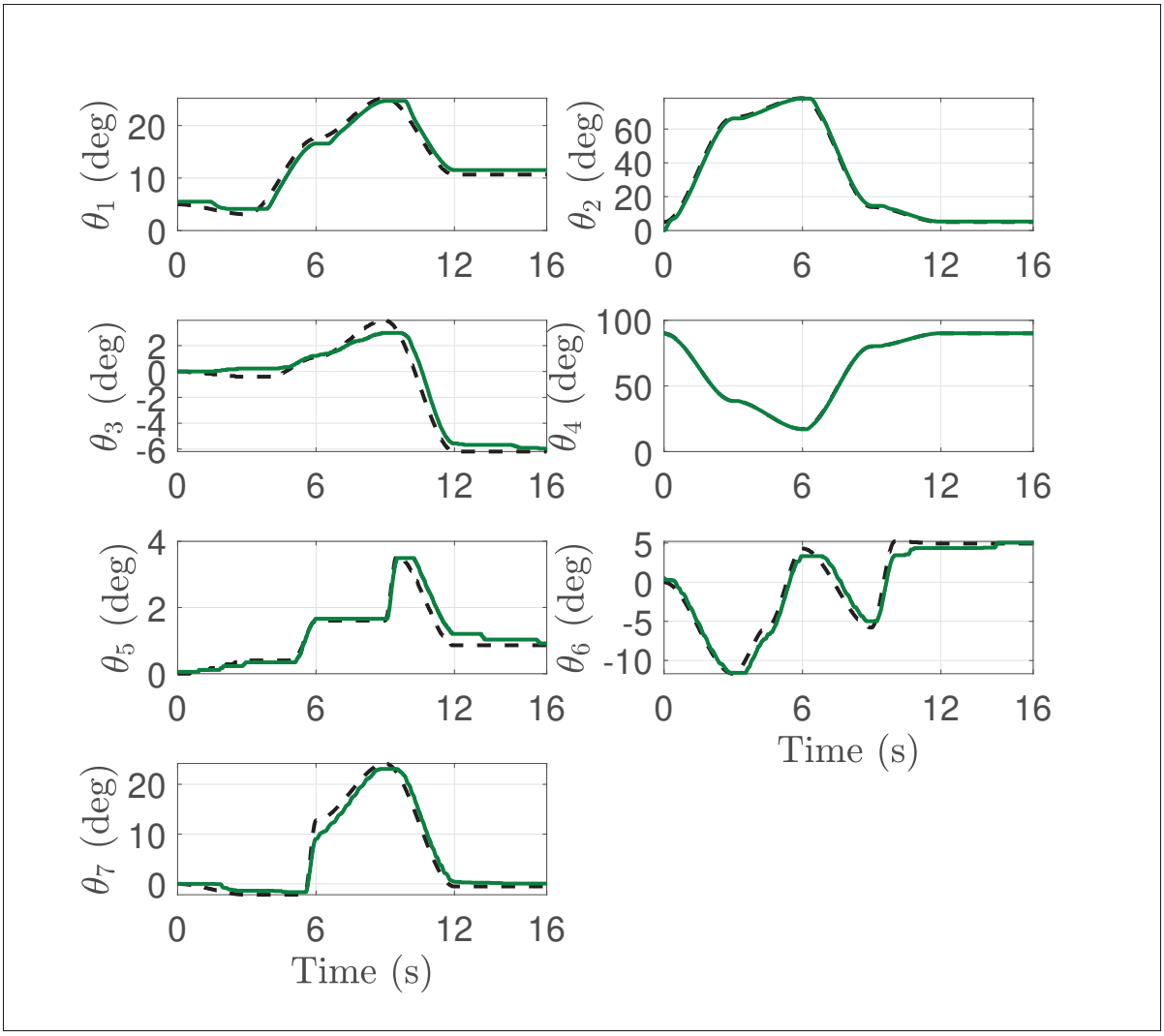

Figure 5.13 Joint space reference trajectory (dashed black) and loaded tracking performance for proposed method (green)

Table 5.6 Improvements of proposed model-based switching functions in torque inputs total variation

	Measured Torques Control Input Total Variance (Nm)		
Joint (*i*)	**Conventional SMC**	**Proposed Approach**	**improvement (%)**
1	1572.0	334.5	78.72
2	2766.0	894.8	67.65
3	492.7	212.8	56.81
4	1315.0	566.6	56.91
5	152.6	121.1	20.64
6	233.6	113.1	51.58
7	80.24	84.19	-4.92

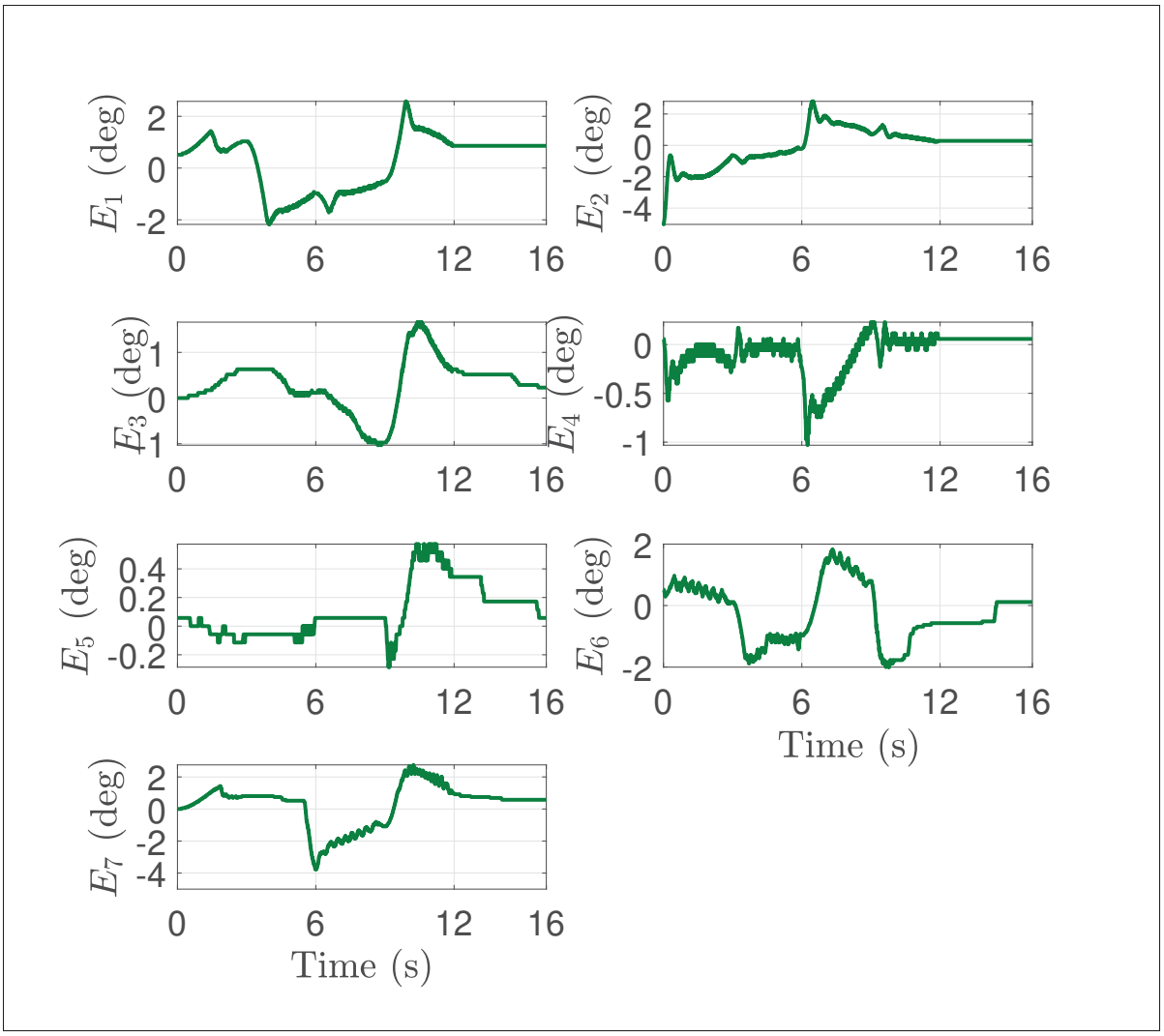

Figure 5.14 Loaded joint tracking errors for proposed method

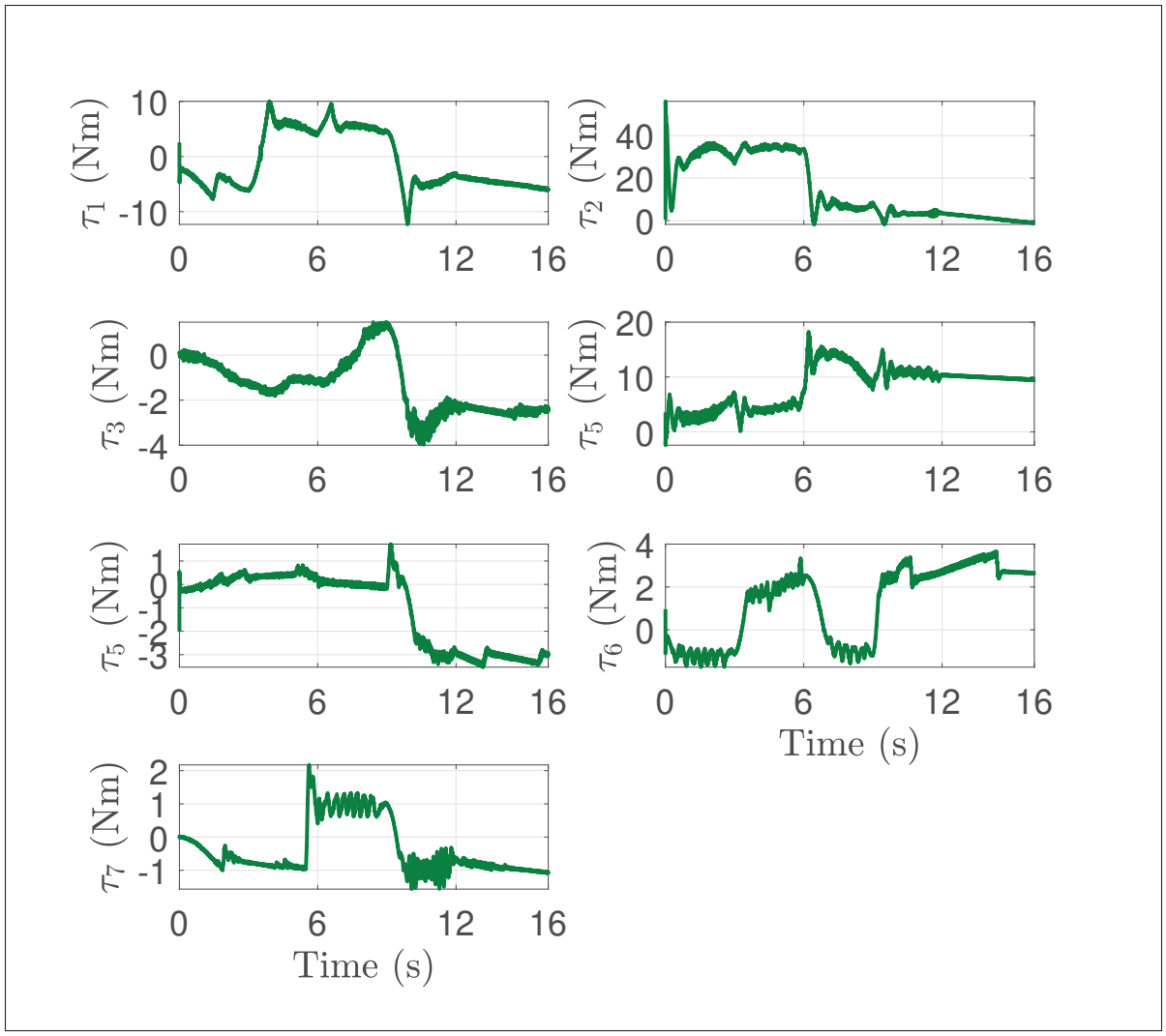

Figure 5.15 Loaded joint torque for proposed method

CONCLUSION AND RECOMMENDATIONS

The research subject presented by this thesis covered the theoretical development and the practical application of a new approach with regards to sliding mode control, by presenting the design of sliding functions based on the dynamic model of robotic systems.

Through this research thesis, the following main contributions have been highlighted:

1. From a theoretical point of view, it has been shown that the design of model-based switching functions makes it possible to compensate for the dynamic terms which appear in the control law. This compensation leads to a significant simplification of the torque control law, which leads to a reduction in the transient constraints, as well as a total decoupling of the chattering effect on each of the joints torque inputs. It has also been shown that these functions ensure overall asymptotic stability of the system when the sliding phase is reached.
2. A new formulation involving the gravity term has also been introduced to form a constraint on the proportional gain matrix of the controller to ensure the overall asymptotic convergence of the system with gravity compensation in the sliding functions. It has also been highlighted that the mathematical properties of this new formulation may also be used to push further the validation of the robot's dynamic model by extending it to the gravity matrix of the robot.

In terms of experimental validation, the proposed approach has been first implemented and validated for trajectory tracking on a prototype of an exoskeleton robot with 7 degrees of movement. The experimental results demonstrated that while maintaining very good trajectory tracking performance, the model-based sliding function controller exhibits a marked improvement in torque input signals over the conventional sliding mode controller, thereby reducing transient stresses on the torque inputs. The new controller also demonstrated a reduction in the chattering levels on the torque inputs, due to the elimination of the discontinuous term coupling effect of the inertia matrix on the robot axes. In order to demonstrate the applicability of the approach

to wider robotic systems, the proposed approach has been also applied to a quadcopter drone system in which a sliding mode controller using model-based switching functions has also been experimentally validated on the internal attitude loop of a quadcopter-type drone system for a setpoint tracking problem. Thus, the generalization of the approach has demonstrated from an experimental point of view.

As further research steps and continuation of this present work, the following recommendations on key lead research points are proposed:

1. As a first step, consider the implementation and experimental validation of the model-based switching functions approach for the trajectory tracking problem of the quadcopter-type drone, which represents the logical continuation of the setpoint tracking problem already validated experimentally.
2. As a second step, the combination of the model-based approach with chattering reduction or elimination techniques such as the ERL and the STA can be explored. This could be experimentally validated on the exoskeleton prototype and on the quadcopter-type drone setup. An adaptive algorithm can also be considered to reduce the constraints on gain matrix K.
3. As a third step, explore the combination of the use of model-based switching functions with the TSM approach, which consists of designing nonlinear sliding functions to ensure the convergence of the error towards 0 in a finite time. In this case, however, the combination of these two approaches requires further analysis, and demonstrations of the stability of the resulting sliding functions will therefore be necessary.
4. As a fourth step, extend the application of model-based switching functions to the dynamic model of the robot expressed in the Cartesian space.
5. Finally, it would be interesting to explore the possibility of having time-varying positive definite control matrices for the proportional and derivative terms of the error in the control input, in order to adapt to the variation of the eigenvalues of matrix Ψ_G along any trajectory

in the robot's work environment. This will avoid the over dimensioning of these matrices to account for all possible trajectories in the cartesian workspace. This will however require the theoretical development of stability proof with these varying matrices. From a practical point of view, it will also require the real-time computation of the eigenvalues of matrix Ψ_G, and this might also require increased CPU performance at execution time. Alternatively, a discrete mapping of the workspace could be performed to compute offline the eigenvalues of matrix Ψ_G, however this might require on the other hand additional memory resources.

APPENDIX I

EXPLANATION OF THE COMPENSATION OF THE GRAVITY TERM THROUGH A SIMPLE SISO EXAMPLE

The development in this appendix is intended to explain the theoretical development in section 2.3 of Chapter 2 through a simple SISO system example, and more precisely tackling the explanation of the gravity vector relationship (2.36). Function $f(x)$ in the following example will be a simple scalar representation of the gravity vector for MIMO robot systems.

1. Application Example on a SISO Nonlinear Second-Order System

Consider the following second-order nonlinear differential equation

$$\ddot{x} + k\dot{x} + bx - f(x) = 0 \tag{A I-1}$$

Where k and b are positive constants, and $f(x)$ is a nonlinear function, and x is assumed to vary within a closed subset ζ. For the sake of the example, consider that $f(x) = 6x^2$

Note that $f(x)$ can be written as:

$$f(x) = f(0) + \left(\int_0^1 f'(x \cdot h) dh \right) \cdot x \tag{A I-2}$$

Where $f'(x)$ is the derivative of f with respect to x. Therefore:

$$\int_0^1 f'(x \cdot h) dh = \int_0^1 12x \cdot h \cdot dh = 6x \tag{A I-3}$$

(A I-2) can therefore be written as:

$$f(x) = f(0) + (6x) \cdot x \tag{A I-4}$$

Where $f(0) = 0$ in this case. Thus the term $\int_0^1 f'(x \cdot h)dh$ is the slope of the segment (0,0):(x,f(x)) as shown in figure

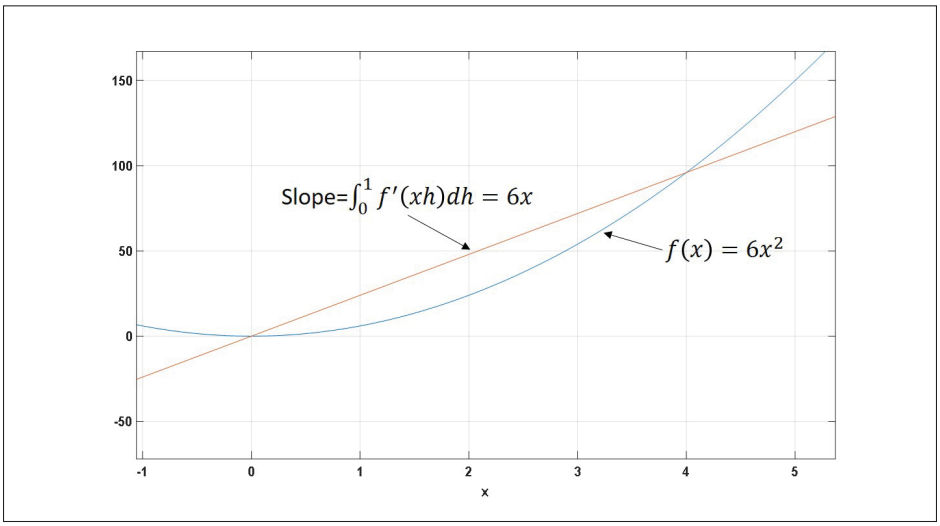

Figure-A I-1 Depiction of $f(x)$ and $\int_0^1 f'(x \cdot h)dh = 6x$ for $x = 4$

Note that when x is in the neighborhood of 0, then the following approximation is valid

$$\int_0^1 f'(x \cdot h)dh \approx f'(0) \tag{A I-5}$$

And therefore (A I-2) becomes

$$f(x) \approx f(0) + f'(0) \cdot x \tag{A I-6}$$

(A I-6) represents the first order Taylor approximation of f(x) in the neighborhood of 0. Hence, (A I-6) is a particular case of (A I-2) whereby it is approximated by the first-order Taylor development of function f(x). Note that (A I-1) can then be written as

$$\ddot{x} + k\dot{x} + \left(b - \int_0^1 f'(x \cdot h)dh\right)x - f(0) = 0 \qquad \text{(A I-7)}$$

Using $f(x) = 6x^2$, (A I-7) simplifies into:

$$\ddot{x} + k\dot{x} + (b - 6x)\,x = 0 \qquad \text{(A I-8)}$$

In order to ensure that (A I-8) implies the asymptotic convergence of x towards 0, then $b - 6x$ has to be strictly positive for x varying within ζ. Indeed, consider the following Lyapunov candidate:

$$L(x, \dot{x}) = \frac{1}{2}\dot{x}^2 + P(x) - P(0) \qquad \text{(A I-9)}$$

Where $P(x) = \frac{1}{2}bx^2 - \int f(x)dx$

Differentiating P(x) with respect to x gives:

$$\frac{dP}{dx} = bx - f(x) = (b - 6x)\,x \qquad \text{(A I-10)}$$

Since $b - 6x$ is chosen to be strictly positive, therefore $\frac{dP}{dx}$ is of the same sign as x, and $\frac{dP}{dx} = 0$ only for x=0. Then this implies that P has a unique minimum at x=0, which then leads to $P(x) - P(0) \geq 0$, which finally implies that L is a valid Lyapunov candidate.

Differentiating L with respect to time gives:

$$\dot{L}(x,\dot{x}) = \dot{x}\ddot{x} + bx\dot{x} - f(x)\dot{x} \qquad \text{(A I-11)}$$

Using (A I-8) in (A I-11) finally gives $\dot{L} = -k\dot{x}^2$

Applying here Barbalat's Lemma and reminding that $b - 6x > 0$ finally implies the asymptotic convergence of x towards 0.

BIBLIOGRAPHY

Abbasi, E., Ghayour, M. and Danesh, M. (2017), Virtual leader-follower formation control of multi quadrotors by using feedback linearization controller, *in* '2017 5th RSI International Conference on Robotics and Mechatronics (ICRoM)', pp. 614–619.

Aboulem, S., Boufounas, E.-m. and Boumhidi, I. (2019), 'Intelligent proportional-integral sliding mode control of wind turbine systems based particle swarm optimisation', *International Journal of Automation and Control* **13**(3), 347–373.

Akhrif, O. and Blankenship, G. (1988), Robust stabilization of feedback linearizable systems, *in* 'Proceedings of the 27th IEEE Conference on Decision and Control', IEEE, pp. 1714–1719.

Al-Hiddabi, S. A. (2009), Quadrotor control using feedback linearization with dynamic extension, *in* '2009 6th International Symposium on Mechatronics and its Applications', pp. 1–3.

Alqaisi, W., Kali, Y., Ghommam, J., Saad, M. and Nerguizian, V. (2020), 'Position and attitude tracking of uncertain quadrotor unmanned aerial vehicles based on non-singular terminal super-twisting algorithm', *Proceedings of the Institution of Mechanical Engineers, Part I: Journal of Systems and Control Engineering* **234**(3), 396–408.

Ardjal, A., Mansouri, R. and Bettayeb, M. (2019), 'Hybrid petri network super twisting sliding mode control of wind turbine for maximum power point tracking', *International Journal of Automation and Control* **13**(6), 698–716.

Barikbin, B. and Fakharian, A. (2019), 'Trajectory tracking for quadrotor uav transporting cable-suspended payload in wind presence', *Transactions of the Institute of Measurement and Control* **41**(5), 1243–1255.

Bartolini, G., Ferrara, A. and Usai, E. (1998), 'Chattering avoidance by second-order sliding mode control', *IEEE Transactions on Automatic Control* **43**(2), 241–246.

Bartolini, G., Ferrara, A., Usai, E. and Utkin, V. I. (2000), 'On multi-input chattering-free second-order sliding mode control', *IEEE Transactions on Automatic Control* **45**(9), 1711–1717.

Basri, M. A. M., Husain, A. R. and Danapalasingam, K. A. (2015), 'Intelligent adaptive backstepping control for mimo uncertain non-linear quadrotor helicopter systems', *Transactions of the Institute of Measurement and Control* **37**(3), 345–361.

BIS research (2018), *Global Wearable Robotic Exoskeleton Market, by Value and Volume: Focus on Mode of Operation, End User, Application, Material Type, and Limb Type*, Analysis Forecast 2018-2028, BIS research.

Camacho, O., Rojas, R. and Garcıa, W. (1999), 'Variable structure control applied to chemical processes with inverse response', *ISA Transactions* **38**(1), 55 – 72.

Cao, Q., Li, S. and Zhao, D. (2015), 'A framework of terminal sliding mode for force/position control of constrained manipulators', *International Journal of Modelling, Identification and Control* **24**(4), 332–341.

Castillo, P., Dzul, A. and Lozano, R. (2004), 'Real-time stabilization and tracking of a four-rotor mini rotorcraft', *IEEE Transactions on Control Systems Technology* **12**(4), 510–516.

Chen, H., Song, S. and Li, X. (2019), 'Robust spacecraft attitude tracking control with integral terminal sliding mode surface considering input saturation', *Transactions of the Institute of Measurement and Control* **41**(2), 405–416.

Choi, S.-B., Park, D.-W. and Jayasuriya, S. (1994), 'A time-varying sliding surface for fast and robust tracking control of second-order uncertain systems', *Automatica* **30**(5), 899–904.

Comenetz, M. (2002), *Calculus: The Elements*, World Scientific.

Craig, J. J. (2005), *Introduction to Robotics Mechanics and Control*, 3 edn, Pearson Education, Inc.

Dai, L., Yu, Y., Zhai, D., Huang, T. and Xia, Y. (2020), 'Robust model predictive tracking control for robot manipulators with disturbances', *IEEE Transactions on Industrial Electronics* pp. 1–1.

DeCarlo, R. A., Zak, S. H. and Matthews, G. P. (1988), 'Variable structure control of nonlinear multivariable systems: a tutorial', *Proceedings of the IEEE* **76**(3), 212–232.

Emelyanov, S. V. (1967), *Variable Structure Control Systems*, Nauka, Moscow.

Fallaha, C. J., Saad, M., Kanaan, H. Y. and Al-Haddad, K. (2011), 'Sliding-mode robot control with exponential reaching law', *IEEE Transactions on Industrial Electronics* **58**(2), 600–610.

Fallaha, C. and Saad, M. (2016), *Étude du terme gravitationnel dans le modèle d'état d'un bras robotique*, École de technologie supérieure.

Fallaha, C. and Saad, M. (2018), 'Model-based sliding functions design for sliding mode robot control', *International Journal of Modelling, Identification and Control* **30**, 48.

Feng, Y., Yu, X. and Man, Z. (2002), 'Non-singular terminal sliding mode control of rigid manipulators', *Automatica* **38**(12), 2159 – 2167.
URL: *http://www.sciencedirect.com/science/article/pii/S0005109802001474*

Fessi, R. and Bouallègue, S. (2019), 'Lqg controller design for a quadrotor uav based on particle swarm optimisation', *International Journal of Automation and Control* **13**(5).

Filippov, A. F. (1988), *Differential Equations with Discontinuous Righthand Side*, Dordrecht [Netherlands] ; Boston : Kluwer Academic Publishers.

Floquet, T. and Barbot, J. P. (2007), 'Super twisting algorithm-based step-by-step sliding mode observers for nonlinear systems with unknown inputs', *International Journal of Systems Science* **38**(10), 803–815.

Floquet, T., Barbot, J.-P. and Perruquetti, W. (2003), 'Higher-order sliding mode stabilization for a class of nonholonomic perturbed systems', *Automatica* **39**(6), 1077–1083.

Fnaiech, M. A., Betin, F., Capolino, G.-A. and Fnaiech, F. (2009), 'Fuzzy logic and sliding-mode controls applied to six-phase induction machine with open phases', *IEEE Transactions on Industrial Electronics* **57**(1), 354–364.

Frisoli, A., Salsedo, F., Bergamasco, M., Rossi, B. and Carboncini, M. C. (2009), 'A force-feedback exoskeleton for upper-limb rehabilitation in virtual reality', *Applied Bionics and Biomechanics* **6**(2), 115–126.

Gao, W. and Hung, J. C. (1993), 'Variable structure control of nonlinear systems: a new approach', *IEEE Transactions on Industrial Electronics* **40**(1), 45–55.

Gonzalez, T., Moreno, J. A. and Fridman, L. (2012), 'Variable gain super-twisting sliding mode control', *IEEE Transactions on Automatic Control* **57**(8), 2100–2105.

Grand View Research (2020), *Exoskeleton Market Size, Share Trends Analysis Report By Technology Type (Mobile, Stationary), By Technology Drive Type, By End User, By Region, And Segment Forecasts*, Grand View Research.

Gupta, A. and O'Malley, M. K. (2006), 'Design of a haptic arm exoskeleton for training and rehabilitation', *IEEE/ASME Transactions on Mechatronics* **11**(3), 280–289.

Hamerlain, F., Achour, K., Floquet, T. and Perruquetti, W. (2007), Trajectory tracking of a car-like robot using second order sliding mode control, *in* '2007 European Control Conference (ECC)', pp. 4932–4936.

Hashimoto, H., Maruyama, K. and Harashima, F. (1987), 'A microprocessor-based robot manipulator control with sliding mode', *IEEE Transactions on Industrial Electronics* (1), 11–18.

Hosseinabadi, P. A. and Abadi, A. S. S. (2019), 'Adaptive terminal sliding mode control of high-order nonlinear systems', *International Journal of Automation and Control* **13**(6), 668–678.

Incremona, G. P., Ferrara, A. and Magni, L. (2017), 'Mpc for robot manipulators with integral sliding modes generation', *IEEE/ASME Transactions on Mechatronics* **22**(3), 1299–1307.

Isidori, A. (1995), *Nonlinear Control Systems*, Springer-Verlag, Berlin.

Jiang, T., Lin, D. and Song, T. (2018), 'Finite-time backstepping control for quadrotors with disturbances and input constraints', *IEEE Access* **6**, 62037–62049.

Jin, M., Lee, J., Chang, P. H. and Choi, C. (2009), 'Practical nonsingular terminal sliding-mode control of robot manipulators for high-accuracy tracking control', *IEEE Transactions on Industrial Electronics* **56**(9), 3593–3601.

Kali, Y., Rodas, J., Gregor, R., Saad, M. and Benjelloun, K. (2018), Attitude tracking of a tri-rotor uav based on robust sliding mode with time delay estimation, *in* '2018 International Conference on Unmanned Aircraft Systems (ICUAS)', pp. 346–351.

Kali, Y., Saad, M., Benjelloun, K. and Khairallah, C. (2018), 'Super-twisting algorithm with time delay estimation for uncertain robot manipulators', *Nonlinear Dynamics* **93**, 557–569.

Kawasaki, H., Ito, S., Ishigure, Y., Nishimoto, Y., Aoki, T., Mouri, T., Sakaeda, H. and Abe, M. (2007), Development of a hand motion assist robot for rehabilitation therapy by patient self-motion control, *in* '2007 IEEE 10th International Conference on Rehabilitation Robotics', IEEE, pp. 234–240.

Khalil, H. (2002), *Nonlinear Systems*, Upper Saddle River, NJ: Prentice Hall.

Khosla, P. and Kanade, T. (1989), 'Real-time implementation and evaluation of the computed-torque scheme', *IEEE Transactions on Robotics and Automation* **5**(2), 245–253.

Krstic, M., Kanellakopoulos, I. and Kokotovic, P. (1995), *Nonlinear and Adaptive Control Design*, John Wiley, New-York.

Levant, A. (1993), 'Sliding order and sliding accuracy in sliding mode control', *International Journal of Control* **58**(6), 1247–1263.

Li, Z., Huang, B., Ye, Z., Deng, M. and Yang, C. (2018), 'Physical human–robot interaction of a robotic exoskeleton by admittance control', *IEEE Transactions on Industrial Electronics* **65**(12), 9614–9624.

Liang, Y.-W., Xu, S.-D., Liaw, D.-C. and Chen, C.-C. (2008), 'A study of t–s model-based smc scheme with application to robot control', *IEEE Transactions on Industrial Electronics* **55**(11), 3964–3971.

Lin, C.-M. and Hsu, C.-F. (2005), 'Recurrent-neural-network-based adaptive-backstepping control for induction servomotors', *IEEE Transactions on industrial electronics* **52**(6), 1677–1684.

Lucas, L., DiCicco, M. and Matsuoka, Y. (2004), 'An emg-controlled hand exoskeleton for natural pinching', *Journal of Robotics and Mechatronics* **16**(5), 482 – 488.

Modirrousta, A. and Khodabandeh, M. (2017), 'Adaptive non-singular terminal sliding mode controller: new design for full control of the quadrotor with external disturbances', *Transactions of the Institute of Measurement and Control* **39**(3), 371–383.

Mondal, S. and Mahanta, C. (2014), 'Adaptive second order terminal sliding mode controller for robotic manipulators', *Journal of the Franklin Institute* **351**(4), 2356 – 2377.

Moreno, J. A. and Osorio, M. (2008), A lyapunov approach to second-order sliding mode controllers and observers, *in* '2008 47th IEEE Conference on Decision and Control', pp. 2856–2861.

Narendra, K. S. (1996), 'Neural networks for control theory and practice', *Proceedings of the IEEE* **84**(10), 1385–1406.

Nguyen, H. T., Quyen, T. V., Nguyen, C. V., Le, A. M., Tran, H. T. and Nguyen, M. T. (2020), 'Control algorithms for uavs: A comprehensive survey', *EAI Endorsed Transactions on Industrial Networks and Intelligent Systems* **7**(23).

Ochoa Luna, C., Rahman, M. H., Saad, M., Archambault, P. S. and Ferrer, S. B. (2015), 'Admittance-based upper limb robotic active and active-assistive movements', *International Journal of Advanced Robotic Systems* **12**(9), 117.

Orlowska-Kowalska, T., Dybkowski, M. and Szabat, K. (2009), 'Adaptive sliding-mode neuro-fuzzy control of the two-mass induction motor drive without mechanical sensors', *IEEE Transactions on Industrial Electronics* **57**(2), 553–564.

Park, C.-W. and Cho, Y.-W. (2007), 'Robust fuzzy feedback linearisation controllers for takagi-sugeno fuzzy models with parametric uncertainties', *IET Control Theory & Applications* **1**(5), 1242–1254.

Parra-Vega, V. and Hirzinger, G. (2001), 'Chattering-free sliding mode control for a class of nonlinear mechanical systems', *Intl. Jnrl. of Robust and Nonlinear Control* **11**(12), 1161–1178.

Perry, J. C., Rosen, J. and Burns, S. (2007), 'Upper-limb powered exoskeleton design', *IEEE/ASME Transactions on Mechatronics* **12**(4), 408–417.

Pranayanuntana, P. and Vanchai, R. (2000), Nonlinear backstepping control design applied to magnetic ball control, *in* '2000 TENCON Proceedings. Intelligent Systems and Technologies for the New Millennium (Cat. No. 00CH37119)', Vol. 3, IEEE, pp. 304–307.

Pratap, B. and Purwar, S. (2019), 'Real-time implementation of nonlinear state and disturbance observer-based controller for twin rotor control system', *International Journal of Automation and Control* **13**(4).

Rahman, M., Kittel-Ouimet, T., Saad, M., Kenne, J.-P. and Archambault, P. (2012), 'Development and control of a robotic exoskeleton for shoulder, elbow and forearm movement assistance', *Applied Bionics and Biomechanics* **9**, 275–292.

Rahman, M., Ochoa Luna, C., Saad, M. and Archambault, P. (2014*a*), 'Force-position control of a robotic exoskeleton to provide upper extremity movement assistance', *International Journal of Modelling, Identification and Control* **21**, 390–400.

Rahman, M., Ochoa Luna, C., Saad, M. and Archambault, P. (2014*b*), 'Motion control of an exoskeleton robot using electromyogram signals', *Advances in Robotics, Mechatronics and Circuits* pp. 27–33.

Roy, S., Roy, S. B., Lee, J. and Baldi, S. (2019), 'Overcoming the underestimation and overestimation problems in adaptive sliding mode control', *IEEE/ASME Transactions on Mechatronics* **24**(5), 2031–2039.

Shieh, H.-J. and Hsu, C.-H. (2008), 'An adaptive approximator-based backstepping control approach for piezoactuator-driven stages', *IEEE Transactions on Industrial Electronics* **55**(4), 1729–1738.

Sivaramakrishnan, J., Agwan, M. and Dewan, L. (2015), 'A smart higher order sliding mode control of rigid articulated robotic manipulator with passive joints', *International Journal of Modelling Identification and Control* **23**, 260–266.

Slotine, J.-J., Hedrick, J. K. and Misawa, E. A. (1987), 'On sliding observers for nonlinear systems'.

Slotine, J. and Li, W. (1991), *Applied Nonlinear Control*, NJ, Englewood Cliffs: Prentice-Hall.

Spong, M. W., Hutchinson, S. and Vidyasagar, M. (2005), *Robot Modeling and Control*, John Wiley and Sons, Inc.

Spurgeon, S. K. (2008), 'Sliding mode observers: a survey', *International Journal of Systems Science* **39**(8), 751–764.

Stepanenko, Y. and Su, C.-Y. (1993), 'Variable structure control of robot manipulators with nonlinear sliding manifolds', *International Journal of Control* **58**(2), 285–300.

Tang, Y. (1998), 'Terminal sliding mode control for rigid robots', *Automatica* **34**(1), 51 – 56.

Temporelli, R., Boisvert, M. and Micheau, P. (2019), 'Control of an electromechanical clutch actuator using a dual sliding mode controller: Theory and experimental investigations', *IEEE/ASME Transactions on Mechatronics* **24**(4), 1674–1685.

Thomas, D. E. and Armstrong-Helouvry, B. (1995), 'Fuzzy logic control-a taxonomy of demonstrated benefits', *Proceedings of the IEEE* **83**(3), 407–421.

Tomei, P. (1991), 'Adaptive pd controller for robot manipulators', *IEEE Transactions on Robotics and Automation* **7**(4), 565–570.

Tsagarakis, N. and Caldwell, D. G. (2003), 'Development and control of a 'soft-actuated' exoskeleton for use in physiotherapy and training', *Autonomous Robots* **15**(1), 21–33.

Tsypkin, Y. Z. (1984), *Relay Control Systems*, Cambridge University Press, UK.

Utkin, V. (1981), *Sliding Modes and Their Applications in Variable Structure systems*, MIR, Moscow.

Utkin, V., Guldner, J. and Shijun, M. (1999), *Sliding mode control in electro-mechanical systems*, Vol. 34, CRC press.

Valavanis, K. P. and Vachtsevanos, G. J. (2015), *Handbook of unmanned aerial vehicles*, Vol. 1, Springer.

Venkataraman, S. and Gulati, S. (1991), Terminal sliding modes: a new approach to nonlinear control synthesis, *in* 'Fifth International Conference on Advanced Robotics' Robots in Unstructured Environments', IEEE, pp. 443–448.

Voos, H. (2009), Nonlinear control of a quadrotor micro-uav using feedback-linearization, *in* '2009 IEEE International Conference on Mechatronics', pp. 1–6.

Wang, L., Chai, T. and Zhai, L. (2009), 'Neural-network-based terminal sliding-mode control of robotic manipulators including actuator dynamics', *IEEE Transactions on Industrial Electronics* **56**(9), 3296–3304.

Wang, Y., Zhou, W., Luo, J., Yan, H., Pu, H. and Peng, Y. (2019), 'Reliable intelligent path following control for a robotic airship against sensor faults', *IEEE/ASME Transactions on Mechatronics* pp. 1–1.

Wolfgang, M., Lukic, V., Sander, A., Martin, J. and Kupper, D. (2017), 'Gaining robotics advantage', *The Boston Consulting Group* .

Yang, Z.-J., Miyazaki, K., Kanae, S. and Wada, K. (2004), 'Robust position control of a magnetic levitation system via dynamic surface control technique', *IEEE Transactions on Industrial Electronics* **51**(1), 26–34.

Yu, S., Yu, X., Shirinzadeh, B. and Man, Z. (2005), 'Continuous finite-time control for robotic manipulators with terminal sliding mode', *Automatica* **41**(11), 1957–1964.

Yu, W. and Rosen, J. (2010), A novel linear pid controller for an upper limb exoskeleton, *in* '49th IEEE Conference on Decision and Control (CDC)', pp. 3548–3553.

Yu, X. and Zhihong, M. (2002), 'Fast terminal sliding-mode control design for nonlinear dynamical systems', *IEEE Transactions on Circuits and Systems I: Fundamental Theory and Applications* **49**(2), 261–264.

Zuo, Z. (2015), 'Non-singular fixed-time terminal sliding mode control of non-linear systems', *IET Control Theory Applications* **9**(4), 545–552.